University of Leoben

Dissertation

Fracture behavior of tungsten

Bernd Gludovatz

Leoben, October 2010

This work was financially supported by the Christian Doppler Society.

Erich Schmid Institute of Materials Science
Austrian Academy of Sciences
Jahnstrasse 12
A–8700 Leoben

This thesis was typeset by the use of KOMA-Script and LaTeX 2_ε.

Affidavit

I declare in lieu of oath, that I wrote this thesis and performed the associated research myself, using only literature cited in this volume.

Leoben, October 2010

Danksagung

Mein aufrichtiger Dank gilt Prof. Dr. Reinhard Pippan, erstens für die Übertragung und Betreuung dieser Dissertation, seine fachliche Hilfestellung und seine bemerkenswerte Art und Weise, auch kompliziertere Aufgabenstellungen zu verdeutlichen. Zweitens jedoch auch für seine Geduld und sein Entgegenkommmen, sowohl in fachlicher als auch in menschlicher Hinsicht, ohne dabei je an Professionalität oder die Ruhe zu verlieren. Für die Betreuung seitens unseres Industriepartners darf ich mich bei Dr. Andreas Hoffmann und Dr. Wolfram Knabl bedanken. Die zahlreichen Diskussionen waren stets eine Bereicherung und Hilfestellung zur eigenen Sichtweise und haben sehr geholfen, den Blick zur Industriewelt beizubehalten. Neben der finanziellen Unterstützung der Plansee Metall GmbH sei an dieser Stelle auch der Christian Doppler Forschungsgesellschaft gedankt.

Mein außerordentlicher Dank gilt der gesamten Belegschaft des Erich Schmid Instituts, an der Spitze Prof. Dr. Gerhard Dehm, für das ausgesprochen angenehme Arbeitsklima sowie jegliche Hilfestellung, die ich erfahren durfte. Besonders zu nennen sei hier das Werkstättenteam, Herr Franz Hubner und der inzwischen pensionierte Günter „Aschi“ Aschauer, deren unkomplizierte und rasche Zusammenarbeit vieles erleichtert hat. Den Männern der Prüfhalle, Peter Kutleša und dem ins Lehrgenre gewechselten Hannes Schlager, danke ich herzlich für ihre handwerkliche, ideenreiche und humorvolle Unterstützung. Der gewissenhafte und bereitwillige Einsatz unserer Metallographiedamen hat bedeutend zum Gelingen dieser Arbeit beigetragen - danke Traudi, Gabi und Silke. Anerkennung gebührt auch Herwig Felber, der sich einfach überall auskennt und man daher sehr viel von ihm lernen kann. Ein großes Dankeschön haben auch Marianne Fliesser und Doris Schrutt für ihren administrativen Support verdient.

Eine besondere Gruppe von Mitarbeitern, mit denen man sicherlich am meisten zu tun hat - sei es zum Diskutieren oder sich gegenseitig weiter zu helfen - sind studentische Hilfskräfte, Diplomanden, Dissertationskollegen, sowie bereits promovierte Kollegen. Erwähnen darf ich hier zu allererst meinen Weggefährten und hoch geschätzten Freund Toni Hohenwarter, mit dem mich neben fachlichen Problemstellungen, auch viele private Dinge verbinden. Durch sein wissenschaftliches Verständnis und seinen Einsatz löst er technische Probleme mit gleicher Bravour wie alles an-

dere mit Weitblick. Stefan Wurster, der als Bürokollege sämtliche Höhen und Tiefen hautnah miterleben durfte (bzw. musste), bin ich für seine Ruhe, Gelassenheit, unzählige Debatten und seine Unterstützung zu großem Dank verpflichtet. Einen besseren "Nachbarn" kann man sich nicht wünschen. Der *smarteste* mir bekannte Engländer, Aidan Taylor, war eine große Hilfe beim Korrigieren der Papers und eine Bereicherung bei unzähligen wissenschaftlichen sowie nicht wissenschaftlichen Diskussionen. Seine Geduld und Ausdauer sind schlichtweg bewunderswert - Thanks „'Idan"! Weiters möchte ich auch Bo Yang, Christian Rehrl, Wolfgang Grosinger, Stephan Scheriau, Christoph Kammerhofer, Daniel Kiener und Christian Motz für die gute und nette Zusammenarbeit, sowie für den regen Gedankenaustausch während der Kaffeepausen Dank aussprechen. Mein großer Respekt gilt Wolfgang Schiller und Bernhard Völker, die als studentische Mitarbeiter schier Unglaubliches geleistet haben. Alles Gute möchte ich Daniel Rupp vom Forschungszentrum Karlsruhe wünschen, der an Wolfram genauso lange „genagt" hat wie ich.

Zusätzlich ist es mir ein Anliegen, hier meine Mitbewohner und Freunde zu nennen, dere Zuspruch stets positiv war und unterstützend wirkte.

Am Ende möchte ich mich bei meiner Familie für ihren Rückhalt, Optimismus und die schönen, erholsamen Aufenthalte daheim bedanken. Autumn, „thank you" für die wunderbaren Jahre, die wir miteinander verbracht haben und hoffentlich noch lange gemeinsam verbringen werden.

Abstract

Tungsten-based materials are candidates for various high temperature applications such as future fusion reactors due to their excellent high temperature properties, however, the fracture behavior of polycrystalline tungsten and tungsten alloys is not well understood. These materials show the typical change in fracture behavior of body-centered cubic (bcc) metals - from ductile at elevated temperatures to brittle at low temperatures. This ductile-to-brittle transition (DBT) is well above room temperature and much higher compared to many other bcc metals like for example α-Fe. Grain size, grain shape, dislocation density, texture, chemical composition and grain boundary impurities are thought to have a large effect on the fracture toughness especially at temperatures below DBT. The limited ductility in the low temperature regime is one of the confining factors in the use of tungsten for structural applications.

In this thesis the fracture behavior of tungsten and tungsten alloys was investigated in a temperature range from room temperature up to 800°C. Main work was done on technically pure tungsten with a special focus on the fracture resistance of recrystallized and various deformed microstructures. Samples with different crack plane orientations were used to analyze the influence of grain shape. Furthermore, the effect of grain boundary impurities on the fracture behavior was investigated by Auger electron spectroscopy.

It will be shown that polycrystalline tungsten exhibits two coexisting types of fracture for most investigated samples - intergranular as well as transgranular. The varying amount of each type is mainly dependent on the grain shape and the crack propagation direction, therefore, the fracture toughness varies significantly with the testing direction. Impurities do not show a pronounced influence on the type of fracture while an increasing dislocation density due to deformation improves the fracture resistance. Furthermore, it will be shown that the fracture resistance increases with crack extension, known as R-curve behavior of a material. As a consequence the fracture toughness cannot be characterized solely by a single value, a resistance curve - R-curve - is necessary.

Kurzfassung

Aufgrund ihrer hervorragenden Eigenschaften bei erhöhten Temperaturen eignen sich wolframbasierende Werkstoffe besonders für Hochtemperaturanwendungen, wie sie etwa in speziellen Bereichen zukünftiger Fusionsreaktoren zu finden sind. Das Bruchverhalten polykristallinen Wolframs sowie von Wolframlegierungen ist jedoch weitgehend unverstanden. Die Werkstoffe zeigen den für kubisch-raumzentrierte (krz) Materialien typischen spröd-duktil Übergang, welcher im Vergleich zu anderen krz-Metallen, wie zum Beispiel α-Fe, viel höher und damit weit über Raumtemperatur liegt. Korngröße, Kornform, Versetzungsdichte, Textur, chemische Zusammensetzung, sowie Korngrenzenverunreinigungen spielen eine entscheidende Rolle für die Bruchzähigkeit, besonders unterhalb des spröd-duktil Übergangs. Die geringe Duktilität in diesem Temperaturbereich ist ein die Verwendung von Wolfram als Strukturwerkstoff limitierender Faktor.

In dieser Arbeit wurde das Bruchverhalten von Wolfram und Wolframlegierungen in einem Temperaturbereich von Raumtemperatur bis 800°C untersucht. Hauptaugenmerk wurde dabei auf den Risswiderstand von rekristallisiertem und unterschiedlich verformtem, technisch reinem Wolfram gelegt. Der Einfluss der Kornform wurde anhand von Proben mit unterschiedlichen Rissausbreitungsrichtungen analysiert. Weiters wurde mit Hilfe von Augeruntersuchungen der Einfluss von Verunreinigungen der Korngrenze auf das Bruchverhalten studiert.

Es wird gezeigt, dass der Bruch der meisten polykristallinen Wolframproben durch zwei Arten gekennzeichnet ist - interkristallinen und transkristallinen Bruch. Die unterschiedlichen Anteile der Brucharten variieren hauptsächlich mit der Kornform und der Rissausbreitungsrichtung. Die sich stark ändernden Bruchzähigkeitswerte sind abhängig von der Probenausrichtung bezüglich des Ausgangsmaterials. Verunreinigungen haben keinen großen Einfluss auf das Bruchverhalten, eine erhöhte Versetzungsdichte aufgrund von Verformung steigert jedoch den Risswiderstand. Weiters wird gezeigt, dass der Bruchwiderstand mit der Rissverlängerung ansteigt - diese Eigenschaft wird als R-Kurvenverhalten eines Werkstoffs bezeichnet. Die Bruchzähigkeit muss daher anstelle eines einzigen Werts mithilfe einer Risswiderstandskurve - R-Kurve - beschrieben werden.

Contents

1

Motivation and aim of the present work

Tungsten has the highest melting point of all pure metals; 3422°C. An excellent combination of high temperature properties, such as low vapor pressure, high erosion resistance and reasonable strength at elevated temperatures, qualifies the material for many high temperature applications, for example in future fusion reactors. However, due to a limited resistance against oxidation, its high temperature application is confined to vacuum or inert gas atmosphere. Despite the high strength, there remains a significant challenge in the practical application of tungsten, which is its low ductility at room temperature. Tungsten shows the typical change in fracture behavior of body-centered-cubic (bcc) metals, from ductile at elevated temperatures to brittle at low temperatures. As the ductile-to-brittle transition (DBT) is well above room temperature and because of the elastical isotropic properties, tungsten is often used as a model material to study the brittle fracture as well as the DBT.
Most studies related to the ductility of tungsten were performed in the fifties and sixties, see for example [1–4], at this time the field of fracture mechanics was not as developed as today. In the nineties, Riedle and Gumbsch started an extensive study on the fracture resistance of tungsten single crystals and the influence of crystallographic orientation, temperature and loading rate [5–7]. Experiments were performed in the temperature range of 77 K to 600 K and compared to dislocation simulations [8]. The investigations indicated the {100}-plane as the primary cleavage plane with ⟨110⟩ as preferred crack propagation direction. Together with the {110}-plane as the secondary cleavage plane, where ⟨110⟩ is also the preferred crack propagation direction, these two planes are reported to be the only true cleavage planes in tungsten. Tests were performed at 77 K to minimize the mobility of dislocations and to prevent plasticity. The obtained fracture toughness, K_{IC}, values at this testing temperature were $2.4\,\mathrm{MPa\,m^{0.5}}$ and $2.8\,\mathrm{MPa\,m^{0.5}}$ for the $\{100\}\langle 110\rangle$ crack system and the $\{110\}\langle 110\rangle$ crack system, respectively. At room temperature

experiments K_{IC} increased to 6.4 MPa m$^{0.5}$ for the $\{100\}\langle 110\rangle$ crack system and to 12.9 MPa m$^{0.5}$ for the $\{110\}\langle 110\rangle$ crack system. Additionally, the investigations exhibited a significant dependence of the DBT on the loading rate especially at higher temperature. The group of Roberts was able to show an Arrhenius relationship of the strain rate giving an activation energy for the process controlling the DBT. This was found to be equal to the activation energy for the double-kink formation on screw dislocations, suggesting their motion controlling the DBT [9, 10]. Comparing fracture experiments with simulations showed that the brittle fracture at low temperatures is governed by dislocation nucleation, whereas the dependence on loading rate in the semi-brittle regime is based on the dislocation mobility [11, 12]. From the experiments as well as from simulations it was obvious that the increasing fracture toughness with temperature can be related to an increasing plasticity. This became even clearer by testing pre-deformed samples which shifted the DBT to lower temperatures.

Despite the solid basis of the work of Riedle and Gumbsch on tungsten single crystals, significantly more work needs to be done for the understanding of fracture processes of more complex microstructures, like polycrystalline tungsten with elongated grains. Such microstructures with a strongly increased dislocation density are often a result of several deformation steps, which are necessary for the production of rods, sheets and wires. They are amongst the main influences on the fracture behavior of the material. Therefore, their study is essential for the application of tungsten as structural materials.

The aim of this work is to improve the understanding of the brittle fracture of tungsten materials and to investigate some of the influences on the fracture process. Hence, the fracture behavior of samples of technically pure tungsten as well as of tungsten alloys with different microstructures was investigated in the temperature range from room temperature up to 800°C. The crack resistance as a function of the crack extension was studied for technically pure tungsten samples with different crack plane orientations. Special focus was given to the comparison of recrystallized microstructures with deformed materials. Furthermore, a detailed study of grain boundary impurities was performed by Auger electron spectroscopy.

After a short discussion of the most important parameters and microstructural features affecting the fracture behavior of tungsten, some remarks on the term ductility are given. In the following section the results of the thesis are summarized and shortly discussed. Finally the publications originating from this work will be presented.

2 Introduction

2.1 Influences on the fracture of tungsten

The fracture of polycrystalline tungsten in the low temperature regime, where brittle fracture occurs, is mainly characterized by a mixture of fracture along the grain boundaries and cleavage fracture. The amount of both types of fracture can vary significantly and has a pronounced influence on the measured fracture toughness values. The occurrence of either intergranular or transgranular fracture is controlled by several factors; some of the most important are discussed below.

Since dislocation movement is thermally activated, **temperature** is the main factor controlling the fracture behavior of most bcc metals which exhibit a DBT. In the case of tungsten, this DBT temperature can vary widely since it is mainly dependent on microstructure and testing conditions and especially the applied strain rate [9, 13]. Aside from this transition, which can only be measured by testing samples which have a pre-crack, elevated temperatures are necessary for increasing the formability of tungsten materials.
Grain boundary impurities, e.g. carbon (C), oxygen (O), potassium (K) and phosphorous (P), have been thought to be one of the main causes of intergranular fracture of tungsten since the seventies [14–18]. Such elements lead to a change in the strength of the boundaries, however the amount of impurities must be considered when discussing their influence on the embrittlement of tungsten. Presently, tungsten materials contain a significantly lower quantity of impurities than a few decades ago. Impurities cannot be correlated with the fraction of intergranular fracture, as shown in paper B. However, the distribution of the impurities on the grain boundaries may influence the ductility of the material as in some cases there may be "islands" on the otherwise "clean" grain boundaries. These islands might cause

the nucleation of pores or cracks in deformation experiments and furthermore the initiation of a crack.
The **grain size** and the **grain shape** have a pronounced influence on the fracture resistance of tungsten which has been found in preliminary studies [19–21]. In the case of a recrystallized microstructure with equiaxed grains, the grain size, or rather the grain size distribution, governs the ratio of inter- and transgranular fracture. While smaller grain sizes lead to a more level, direct crack plane and a mainly intergranular propagating crack, larger grains tend to cause cleavage. Despite the somewhat smaller fracture resistance of the grain boundary, major crack deviations would be necessary for grain boundary fracture which would then increase the global fracture resistance. This makes intergranular fracture more unfavorable in the case of larger grains. A broad grain size distribution causes a relatively rough fracture surface. The crack deflection due to the large variation in grain size leads to both intergranular as well as transgranular fracture.
Elongated grains in the form of needles cause a pronounced anisotropy of the fracture toughness in tungsten [22–25]. Samples with crack propagation directions perpendicular to the major axis of elongated grains exhibit significantly higher fracture toughness values compared to the other two directions. Despite the lower fracture resistance of the grain boundaries, crack propagation along the boundaries would cause a significant increase in the global fracture resistance in this direction due to major crack deviations. It is thus transgranular crack propagation which is responsible for the higher fracture toughness values in this perpendicular direction. In the other two directions the crack can easily propagate along the grain boundaries (paper C and paper D).
Deformation is always associated with an increasing **dislocation density**. Predeformed samples cause an increased dislocation density and furthermore a shielding of the crack in pre-cracked samples which leads to improved fracture toughness values [11]. The arrangement of dislocations within a grain causes misorientations which additionally increase the intrinsic cleavage resistance of the grain, as the crack cannot follow a single cleavage plane. Both factors improve the resistance against fracture which is pointed out in paper D.
Rolling of tungsten rods is normally associated with the formation of a **texture** [26]. Such texture is an alignment of the orientation of the grains which can influence the fracture behavior significantly. In case of sheets, the rolling texture causes an extreme 45° embrittlement [27]. Tungsten wires normally vary in their texture over the diameter [20, 26, 28]. Different orientations at different radii therefore cause either an improved or degraded fracture toughness.
Alloying of tungsten does not show a pronounced effect on the fracture toughness at room temperature except for the element rhenium, which significantly increases the fracture toughness and shifts the DBT to lower temperatures [29, 30]. The use of potassium or lanthanum oxide stabilizes elongated microstructures for high temperature applications, however the fracture behavior of equivalent microstructures of technically pure tungsten may not be notably different at ambient temperatures.

The global fracture toughness of tungsten materials is mainly controlled by the crack path, or in other words the geometry of the crack, the intrinsic cleavage resistance and the grain boundary resistance. The parameters mentioned above have significant influences on these factors. Furthermore, one has to take into account that both, the grain cleavage resistance and the grain boundary resistance, can have a different temperature dependence.

2.2 Remarks on the term ductility

The terms brittle and ductile are often used in materials science, in mechanical and in civil engineering, however, often with very different meanings. In principle one has to distinguish between the ductility in fracture mechanics and the stress-strain approach. In fracture mechanics the ductility is described by the term fracture toughness which determines the "ductility" of a material in presence of a crack. In the classical stress-strain approach the tensile test is usually used to characterize the ductility. Such tests are performed sometimes on notched but usually on unnotched samples. Sometimes, impact experiments are also performed to quantify the ductility. An important question is usually: Is there a relation between fracture toughness and the other "ductility" parameters obtained in tensile or impact experiments. In general the answer is *no*.

Impact tests determine the toughness through the ability of a material to absorb energy during fracture. The tests are performed under very high strain rates and the results can only be compared relatively. It is a wide-spread method as it is easy to perform and data can be obtained quickly. The results also allow differentiation between a very brittle and a very ductile material, however, due to the extreme testing conditions, the values cannot be used for a description of a ductility.
Uniaxial tensile tests are mainly used to measure strength and deformation related parameters of a material. Figure 2.1 schematically shows a stress strain curve of a linear-elastic/plastic material. Aside from the ultimate tensile strength, R_{m}, the ultimate strain at uniform elongation, A_{g}, and the ultimate strain at rupture, A, can be measured. The reduction in area, Z, is given by

$$Z = \frac{S_0 - S}{S_0} \cdot 100\% \tag{2.1}$$

where S_0 is the starting cross section of the sample and S the cross section after fracture. The necking elongation A_{z} is defined by $A - A_{\mathrm{g}}$. The ultimate strain at uniform elongation, A_{g}, is independent of the specimen geometry and proportional to the strain hardening exponent, n. This property makes the parameter very attractive to compare different materials with different geometries, however, it is normally just used for ductile materials as A_{g} is often not measurable in case of brittle materials. Additionally, the flat plateau in the stress-strain curve in the region of A_{g} complicates its exact measurement. This restricts the usefulness of this parameter. In order

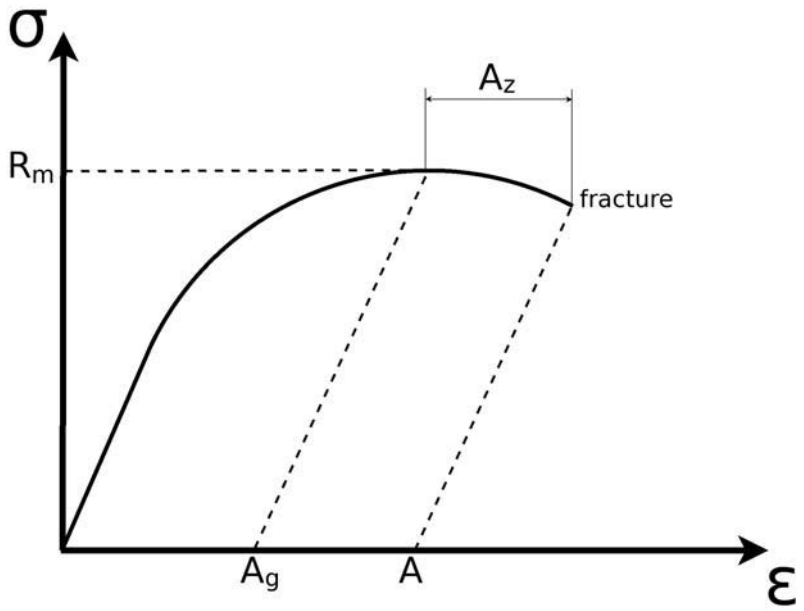

Figure 2.1 Schematic illustration of the stress-strain curve of a linear-elastic/plastic material. R_m is the ultimate tensile strength, A_g the ultimate strain at uniform elongation and A the ultimate strain at rupture.

to overcome this limitation most of the time in the material science community the ultimate strain at rupture, A, is measured. The measurement itself is very simple and can be automated, however, the parameter itself is size dependent which makes any kind of comparison difficult if no common standards are used. The necking elongation is another parameter which might be related to the term ductility. Up to R_m the microstructural damage processes are small and cannot be compared to processes related to a fracture mechanics experiment in which the crack tip experiences a high amount of tensile triaxiality. At the point where necking starts the uniaxial tensile stress state gradually changes into a multiaxial state where void growth and coalescence are the dominating damage mechanisms. These mechanisms are similar to the ones found ahead of the crack tip in a fracture mechanics experiment. Since the toughness and the ductility in terms of A_z are controlled by the same damage processes, they should be comparable. However, as A_g can hardly be measured for brittle materials like tungsten, it is almost impossible to determine A_z. It must also be taken into account that the damage mechanisms for brittle fracture are incomparable to void initiation, growth and coalescence. The most useful approach to evaluate toughness and ductility with a single parameter seems to be the reduction in area, Z. Similar to a tensile test the formability of a material is accounted in this parameter as well as the damage tolerance of a material, normally measured by the fracture toughness. As an example, assuming two materials with similar ductility

but different toughness the material with the higher fracture toughness will show the higher reduction in area and vice versa. Additionally, Z can be measured after testing, this is particularly useful for tests conducted at elevated temperatures where accurate measurement of load and elongation is technically challenging.

3
Summary of the results

Preliminary experiments on tungsten and tungsten alloys show the expected increase of fracture toughness with temperature [31]. Figure 3.1 emphasizes the excellent fracture toughness of WRe alloys at low temperatures, in comparison to the other tungsten materials. The tested samples were manufactured from the sintered materials. WRe was rolled and stress relieved.

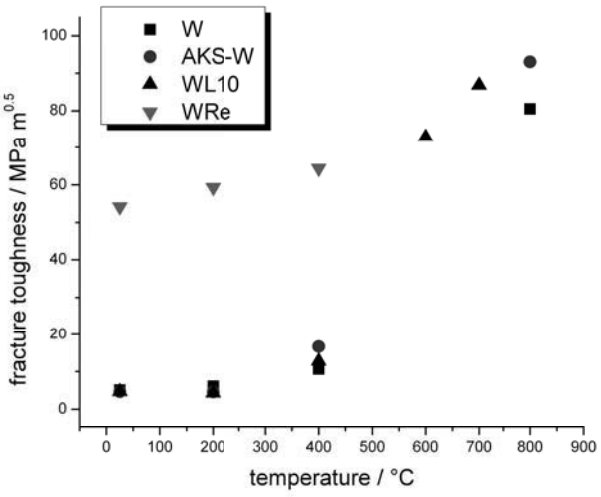

Figure 3.1 Fracture toughness, K_Q, of W, AKS-W, WL10 (sintered) and WRe26 (rolled and stress relieved) as a function of temperature, T.

Table 3.1 K_Q values of W and W-alloy specimens tested at room temperature.

Material	Condition	Rod ∅ [mm]	φ [%]	Tests performed	K_Q [MPa m$^{0.5}$]
W	As sintered	23	-	CT	5.1
	Rolled	9	84.7	CT (C-R)	4.7
	Forged	25	75.9	3PB (L-R)	8.0
	Rolled	9	84.7	3PB (L-R)	9.1
	Rolled	4	97.0	3PB (L-R)	5.4
	Rolled and drawn	1	99.8	3PB (L-R)	35.1
WL	As sintered	23	-	CT	4.7
	Rolled	9	84.7	CT (C-R)	6.0
	Forged	25	76.9	3PB (L-R)	16.6
	Rolled	9	84.7	3PB (L-R)	9.8
	Rolled	4	97.0	3PB (L-R)	9.7
AKS-W	As sintered	23	-	CT	6.4
	Rolled	9	84.7	CT (C-R)	4.5
	Rolled	9	84.7	3PB (L-R)	32.1
	Rolled	4	97.0	3PB (L-R)	13.5
	Rolled and drawn	1	99.8	3PB (L-R)	32.1
WRe (26%)	Forged	25		3PB (L-R)	54.2
	Recrystallized	18		CT (C-R)	22.8

Further investigations on the same materials, manufactured in subsequent steps of the production route to rods and wires, were performed at room temperature and compared to the results of the sintered samples. These materials therefore exhibited different microstructures leading to a large variation of the measured fracture toughness values between 5 - 30 MPa m$^{0.5}$ (table 3.1). The spread in these values is mainly dependent on the technical degree of deformation, φ, the propagation plane of the crack and the position of the samples with respect to the axis of the rods and wires. Referring to a rolling process, φ is given by $\Delta A/A_0$ where ΔA is the cross-sectional reduction in area and A_0 is the original area of the cross-section. Three-point bending (3PB) and compact tension, C(T), specimens were manufactured with *C-R* and *L-R* crack plane orientation according to ASTM standard E399 [32]. The first letter designates the *direction normal* to the crack plane, and the second letter the *expected direction of crack propagation*. *C* stands for *circumferential*, *R* for *radial* and *L* for *longitudinal*. In other words, samples with *C-R* orientation had the normal of the crack plane perpendicular to the rod axis and the crack front parallel to the axis of the rolled or forged materials. This orientation exhibits the lowest fracture toughness values. The other samples had the crack propagating perpendicular to the axis which leads to a significant increase in fracture toughness.

Preliminary experiments indicate a pronounced influence of the processing route

Table 3.2 Main impurity elements of the investigated technically pure tungsten (W > 99.97%).

Element	C	H	N	O	P	S	Si
Guaranteed analysis (max) / μg/g	30	5	5	20	20	5	20
Typical analysis / μg/g	10	2	<2	5	<10	<2	5

as well as of the sample position with respect to the rod or wire axis on the fracture toughness.
To separate some of the influences mentioned in 2.1, further investigations were performed with technically pure tungsten. The chemical composition of the material manufactured by Plansee Metall GmbH is given in table C.1.

3.1 Influence of impurities

All tested samples revealed intergranular as well as transgranular fracture surfaces although the fractions vary significantly. As the typical impurity elements, oxygen (O), phosphorous (P) and carbon (C), are not soluble in tungsten [33], a variation in the area of grain boundaries due to changing microstructures causes a changing fraction of impurity concentration on the grain boundaries. The fracture behavior of technically pure tungsten materials purchased as-is was therefore compared to the fracture behavior of materials processed to obtain different microstructures. A tungsten single crystal, with a significantly smaller impurity concentration, was severely plastically deformed (SPD) by a high pressure torsion (HPT) tool [34, 35] to generate an ultra-fine grained (UFG) polycrystal. Different grain sizes were generated by subsequent annealing of the UFG material, details are given in paper B. Together with the fracture behavior of these samples, the fracture behavior of sintered tungsten and hipped tungsten - this material has a significantly higher concentration of oxygen - was also taken into account.
The amount of both fracture types was analyzed by scanning electron microscopy (SEM) and impurity analyses were performed by Auger electron spectroscopy (AES). If there is an influence of the impurities on the fracture behavior, this should become obvious by a changing fraction of inter- and transgranular fracture.
The fracture surfaces of the investigated materials are shown in figure 3.2, details on the grain sizes, grain aspect ratios, the resulting grain boundary areas and the fraction of intergranular fracture are given in paper B. The SEM fractographs show grain boundary fracture as the major type of fracture for most microstructures except for the rolled material fractured perpendicular to the axis of the rod (figure 3.2-b) which is dominated by cleavage.

AES investigations of the different samples manufactured from the former single crystal did not show impurities at the grain boundaries within the resolution limit

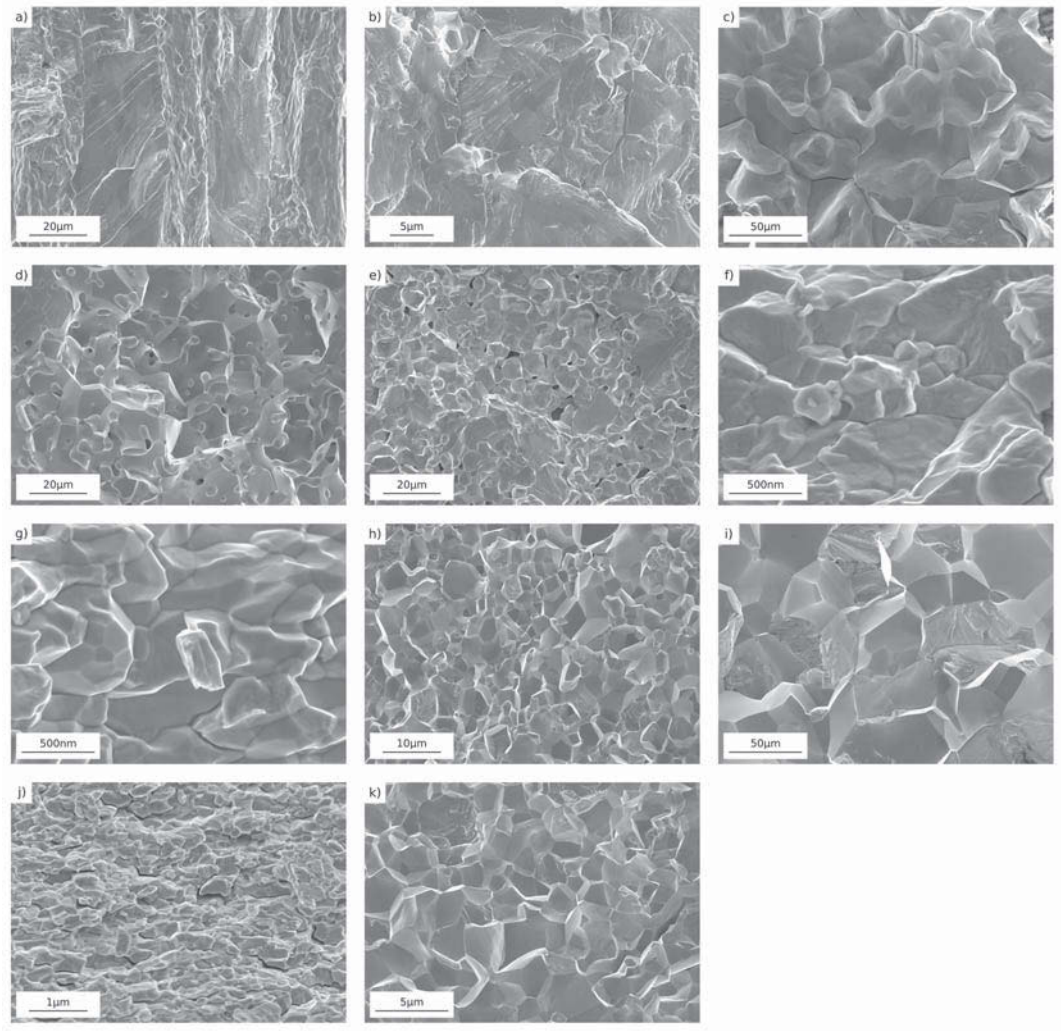

Figure 3.2 Fracture surfaces of tungsten materials with different microstructures investigated by Auger electron spectroscopy (AES). Rolled tungsten rod (W_{rolled}) with crack propagation front parallel to the axis of the rod (a) and perpendicular to the axis of the rod (b), recrystallized tungsten ($W_{recryst}$) (c) and sintered tungsten ($W_{sintered}$) (d) are technically pure tungsten materials with the average impurity concentration shown in table C.1. Other technically pure tungsten materials are shown in (j) and (k), where (j) was just severe plastically deformed (SPD) by high pressure torsion (HPT) (UFG-W) and (k) was deformed and additionally heat treated at 1200°C for an hour in a vacuum furnace (W_{1200}). Figure (e) depicts the fracture surface of hipped tungsten (W_{hipped}) which contains a much higher amount of oxygen. Figure (f)-(i) show fracture surfaces of tungsten materials produced from a single crystal by HPT. While (f) was just severe plastically deformed (UFG-W^{sc}), the other materials were subsequently recrystallized at 600°C (W^{sc}_{600}) (g), 800°C (W^{sc}_{800}) (h) or 1200°C (W^{sc}_{1200}) (i).

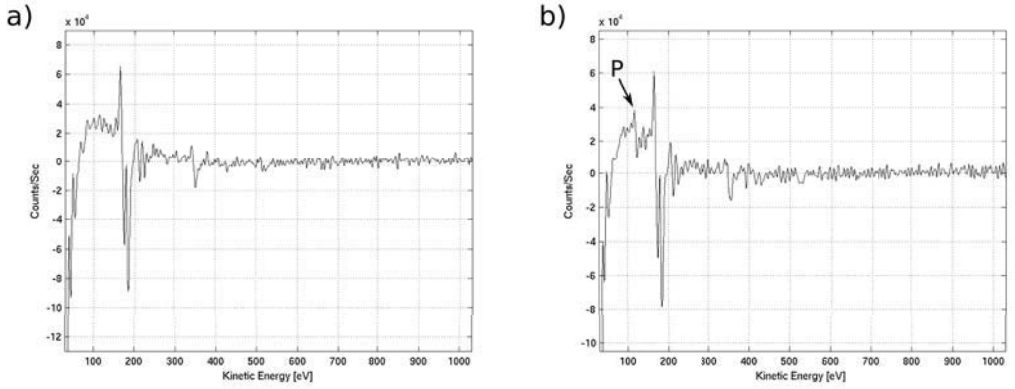

Figure 3.3 Auger electron spectroscopy analyses of investigated tungsten materials. (a) is showing the AES-spectrum of technically pure tungsten which was just severe plastically deformed. The spectrum shown in (b) represents technically pure tungsten rods where after a rolling deformation mainly phosphorous (123 eV) was found at the grain boundaries. Both spectra were taken at grain boundaries.

of AES. The very low impurity concentrations of such single crystals has little influence on the material with respect to the absolute impurity concentrations per grain boundary area.
Figure 3.3 shows spectra of technically pure tungsten. Impurities like O, P or C were not found on the grain boundaries of the UFG material (figure 3.3-a), therefore, the spectrum is clean and similar to the single crystalline samples with the low impurity content. Due to the shear deformation of the HPT process, impurities are widely distributed over the large amount of high angle grain boundaries resulting in an almost pure tungsten spectrum. The grain boundaries of technically pure tungsten with a rolled microstructure, however, were covered somewhat with P shown by the Auger-peak at 123 eV in figure 3.3-b. This material has significantly less grain boundary area than the UFG tungsten, however, the elongated grains still cause a high density of grain boundaries where impurities are widely distributed which decreases their weakening-effect. This should lead to cleavage being the preferred fracture mode. While cleavage was the minor fracture type along the axis of the rod (figure 3.2-a), transgranular fracture is the dominant type in the case of crack propagation perpendicular to the rolling direction (figure 3.2-b). Although P was found on several grain boundaries, which can be seen in the spectrum of figure 3.3-b, its weakening-effect on the grain boundaries is rather limited and does not force a crack to propagate strictly intergranularly although many grain boundaries are available in the rolling direction due to the elongated grain structure. Instead of propagating only along the grain boundaries, it is just as easy for a crack to cleave grains. Even in recrystallized technically pure tungsten, with a lower grain boundary density and therefore impurities covering most grain boundaries, transgranular fracture can be found alongside intergranular fracture, as shown in figure 3.4-a.

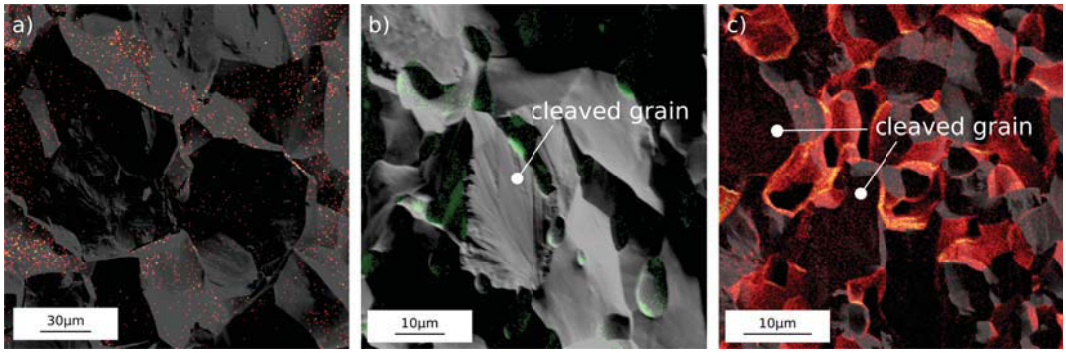

Figure 3.4 Fracture surfaces of different tungsten materials with impurity maps as overlay. (a) depicts the fracture surface of recrystallized tungsten with a P-mapping as an overlay showing P covering several grain boundaries. Sintered tungsten with a P-mapping as an overlay showing P concentrated in the sinter pores (b). The fracture surface of hipped tungsten with an overlaying O-mapping shows O covering most grain boundaries.

Sintered tungsten is a technically pure tungsten material, with P as the only detected major impurity, mainly to be found in the sinter pores and not covering the grain boundaries, as shown in figure 3.4-b. This material, however, is dominated by intergranular fracture. In comparison, hipped tungsten, the only material with a significantly higher O concentration, where most of the grain boundaries are covered by a certain amount of O (figure 3.4-c), is also dominated by intergranular fracture but shows a higher fraction of cleavage than the sintered tungsten. Although both materials have the same porosity and a similar grain size, their fracture behavior is quite different. This cannot be caused by impurities alone especially since hipped tungsten, the material with the higher impurity concentration, has a higher fraction of cleavage fracture. The reason for this behavior is most probably the grain size distribution. Sintered tungsten exhibits a well developed polycrystalline microstructure with a relatively unique grain size compared to the hipped material whose grains contain a higher dislocation density as a result of the HIP process as well as a larger variation in the grain size. In a material with small, equiaxed grains and small variation in grain size the crack can follow the grain boundaries without large deviations from the macroscopic crack plane. In the case of a bimodal distribution of grain size, the crack can deviate more from the ideal crack propagation plane. To avoid this, the larger grains are sometimes cleaved. This is similar for coarse grained recrystallized materials where cleaved grains are more frequently observed. The varying ratio of inter- and transgranular fracture in the different directions of the rolled material, which is similar for HPT deformed UFG tungsten as well as UFG iron [36], demonstrate an influence of the shape of the grains. For crack propagation perpendicular to the rolling direction an almost transgranular fracture behavior is observed (figure 3.2-b), while crack propagation along the rolling direction shows a mixture of both types of fracture (figure 3.2-a). Despite the fact

that most of the grain boundaries are partly covered with P, crack propagating in the rolling direction still occurs intergranularly as well as transgranularly fracture, although a larger number of grain boundaries are available for pure intergranular fracture. This indicates the small effect of impurities compared to other parameters. It is furthermore obvious from the fracture experiments in the rolling direction that the fracture resistance of the grain boundary at room temperature is only somewhat smaller than the resistance to cleave grains, because both fracture modes are present.

The observations indicate that grain boundary impurities do not influence the fracture behavior of technically pure tungsten as strongly as other factors. It is obvious that factors like size and shape of the grains play a more significant role in the fracture behavior of these tungsten materials than impurities.

3.2 Crack propagation resistance

The micrographs in figure 3.2 have shown that grain shape, grain size and grain size distribution have a large influence on the fracture behavior of tungsten. It is likely that these are also the dominating factors affecting the crack path as they have a pronounced influence on the fracture resistance of a propagating crack. This furthermore causes the varying ratio of inter- to transgranular fracture. To further investigate these influences on fracture resistance experiments were carried out with recrystallized tungsten, its microstructure is shown in figure 3.5. The inverse pole figure (IPF) map of the as-recrystallized material shows slightly elongated grains remaining from the rolling procedure after recrystallization. Specimens with different crack propagation directions were manufactured and fatigue pre-cracked in cyclic compression [37,38]. Advantages and disadvantages of this pre-cracking method are discussed in paper C and compared to other methods. Details on grain size, sample size as well as testing conditions are given in paper C and paper D.

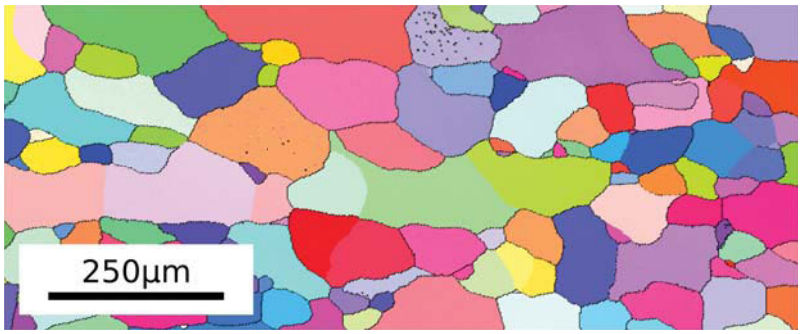

Figure 3.5 Microstructures of the tungsten sample investigated. The inverse pole figure, IPF, map shows the elongated grain structure of the recrystallized material.

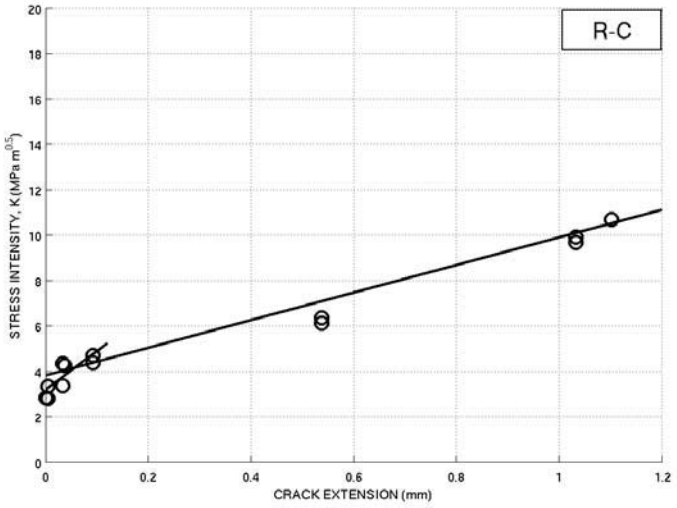

Figure 3.6 R-curve behavior of intergranularly fractured recrystallized tungsten. The sample was manufactured in *R-C* crack plane orientation out of a rod according to ASTM standard E399 [32]. The stress intensity K increases as a function of the crack extension Δa.

Figure 3.6 shows the R-curve behavior, i.e. the increasing fracture resistance with crack extension, of intergranularly fractured tungsten. The use of R-curves to analyze fracture resistance is well established in the field of ceramic materials [39]. The necessary stress intensity K to cause a crack propagation of this sample with *R-C* crack plane orientation (the normal of the crack plane is perpendicular to the rod axis and the crack propagation front is parallel to the axis) rises steeply with first crack extension Δa followed by a less pronounced increase.

The initial part of the R-curve originates from the primarily transgranularly arrested fatigue pre-crack cleaving the encountered grains, details are shown in paper C. Hereafter, the crack switches to mainly intergranular crack propagation. This indicates that the crack propagation resistance of the grain boundaries is somewhat smaller than the resistance to cleave grains. The remaining part of the R-curve is dominated by larger crack bridges which are formed by connecting grains. Bridging is often a result of crack branching, which might occur as a combination of geometric influences and small differences in the local crack propagation resistance of the grain boundaries. Such bridges can be found along the whole crack path, as shown in figure 3.7. IPF maps of a C(T) specimen with a crack in the *R-L* plane orientation show intergranular fracture with limited plastic deformation observed a few micrometers from the crack faces even at room temperature, depicted in detail in figure 3.7. More plastic deformation can sometimes be found at grains which form crack bridges or along the crack flanks at elevated temperatures [23].

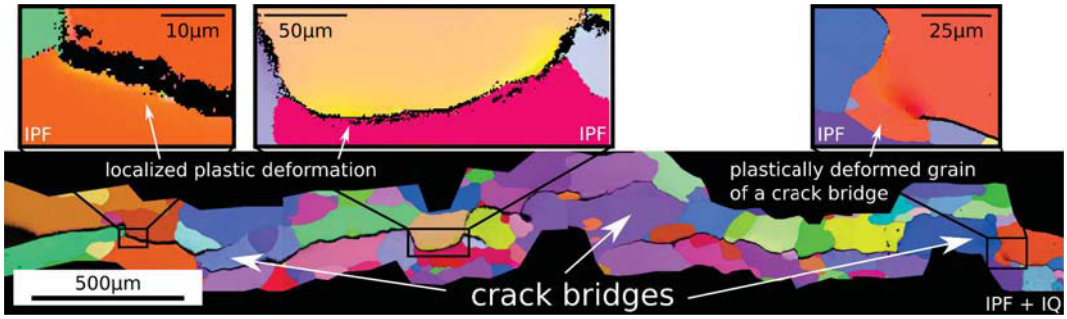

Figure 3.7 Electron backscatter diffraction (EBSD) scan of the crack path in a recrystallized C(T) specimen with *R-L* crack plane orientation. The IPF map is depicted as an overlay on the image quality (IQ) map to illustrate the crack path, showing that the crack propagates predominantly along the grain boundaries. (The IQ describes the quality of EBSD pattern and is dependent on the material and its condition [40].) The propagated crack exhibits a significant number of crack bridges. Plastic deformation, i.e. a change in the color within a single grain, is only very localized along the crack path and at grains which form crack bridges.

3.2.1 Influence of deformation and grain shape

Samples with different crack propagation directions were manufactured from the recrystallized material shown in figure 3.5 and compared to samples from materials deformed by compression resulting in different microstructures. Details of the applied degrees of deformation, the deformation temperatures and the resulting microstructures are given in paper D. Figure 3.8 shows the microstructure of one of these materials, the sample was deformed to 110% at 650°C. The EBSD scan clearly shows the compressed grains and the pronounced substructure.

The fracture surfaces of samples in as-recrystallized and one as-deformed condition, tested in three different crack propagation directions, are compared in figure

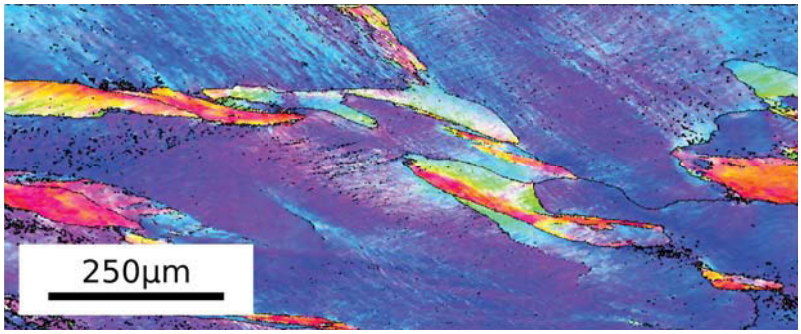

Figure 3.8 Electron backscatter diffraction (EBSD) scan from the tungsten material deformed to 110% at 650°C.

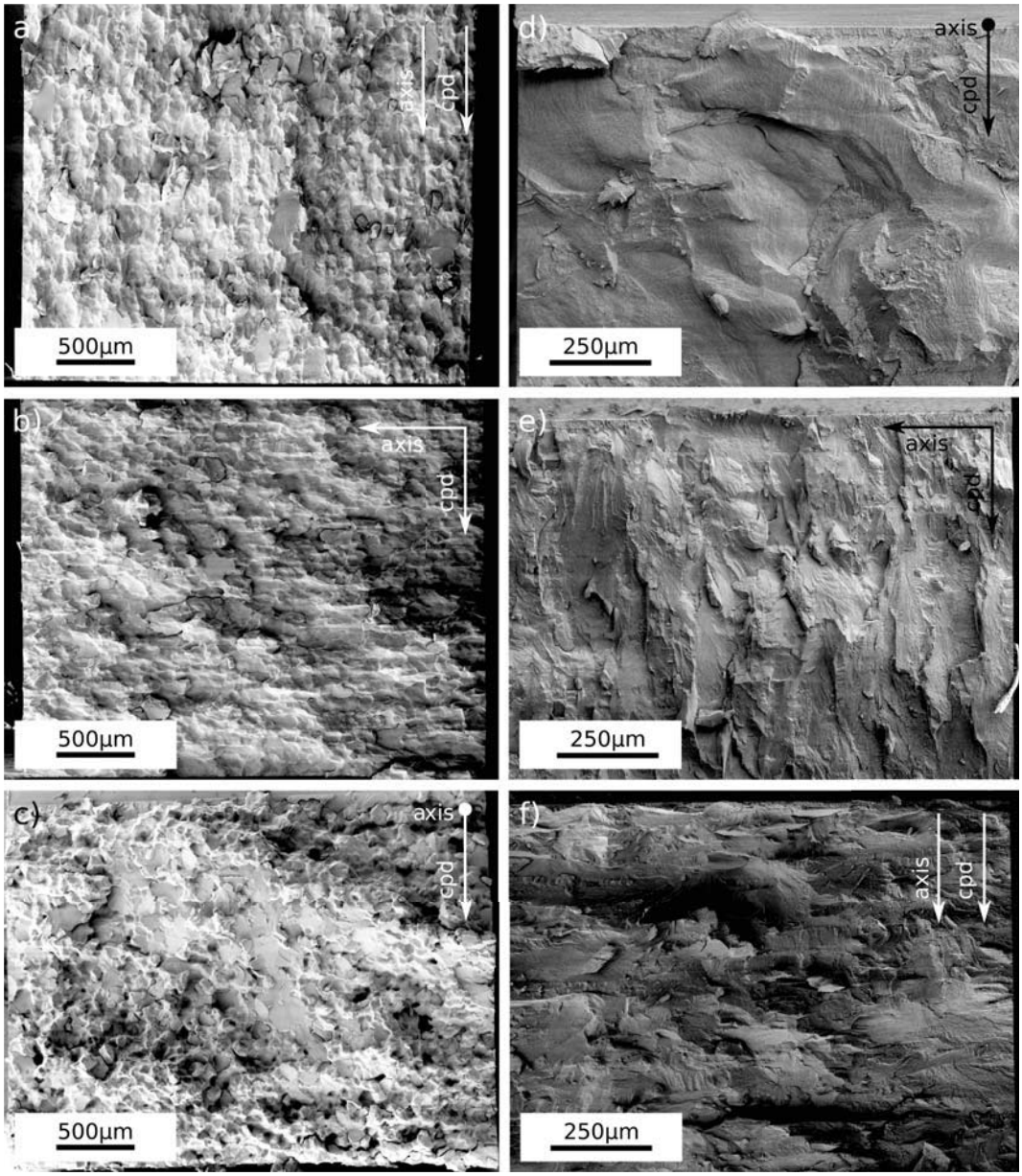

Figure 3.9 SEM fractographs of the fracture surfaces of recrystallized (a, b, c) and deformed (d, e, f) tungsten tested in three major crack propagation directions. The recrystallized material was dominated by intergranular fracture in two directions (a, b) and showed an increase fraction of transgranular fraction in the third direction (c). Intergranular fracture was found in just one direction of the deformed material (d), while transgranular fracture was dominant in the other two directions (e, f).

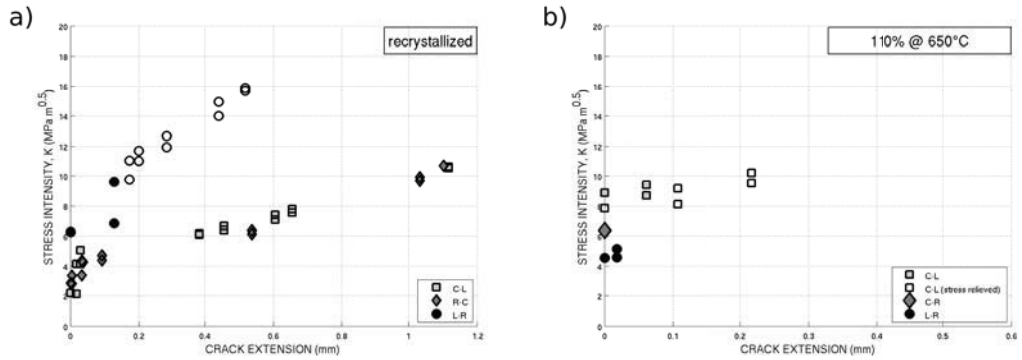

Figure 3.10 R-curves of the fracture resistance of recrystallized tungsten (a) and tungsten deformed to 110% at 650°C (b).

3.9. The compression to 110% along the axis leads to a pronounced flattening of the grains as shown in figure 3.8 and results in differences in the fracture surfaces when compared to the recrystallized material (figure 3.9). In the case of the recrystallized material, grain boundary dominated fracture occurs in two crack propagation directions: along the rod axis (figure 3.9-a) and the crack plane normal perpendicular and the propagation front parallel to the axis (figure 3.9-b). These two directions have many grain boundaries available for intergranular fracture. The third direction exhibits an increased fraction of cleaved grains (figure 3.9-c).
The deformed material shows intergranular dominated fracture in only one crack propagation direction. Because of the flattened grains, samples with a crack propagation front and crack plane normal to the rod axis are the only samples where crack propagation mainly occurs along the grain boundaries (figure 3.9-d). The other two orientations exhibit mainly transgranular fracture (figure 3.9-e/-f).
In both materials the fracture in each crack propagation direction is dominated by a single type of fracture. In general, in most fracture situations, intergranular fracture occurs due to the lower fracture resistance of the grain boundary. In the case of a crack propagating perpendicular to the major axis of elongated grains, the lower fracture resistance of the grain boundary is not significant enough to overcome the tortuous path the crack would need to follow. Very large crack deviations would be necessary for grain boundary fracture, which would result in a higher local fracture resistance than transgranular fracture, hence cleavage is preferred.

Figure 3.10 shows the R-curves of fracture resistance for both microstructures in three crack propagation directions. Figure 3.10-a depicts the data of the recrystallized and figure 3.10-b the deformed tungsten. In the case of the recrystallized material, the samples with intergranular dominated fracture (*C-L*, *R-C*) show first crack propagation at very low stress intensities between 2 - 4 $\mathrm{MPa\,m^{0.5}}$ (figure 3.10-a). The third direction (*L-R*), dominated by transgranular fracture, starts crack

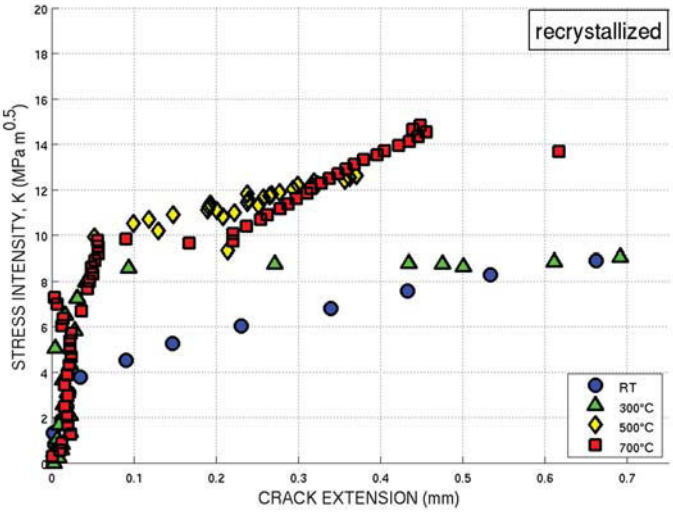

Figure 3.11 Fracture resistance of recrystallized tungsten as a function of the crack extension tested in the temperature range room temperature to 700°C.

propagation at significantly higher values of 6 MPa $m^{0.5}$. The crack of this sample kinked 90° into the rolling direction, further data points were calculated with the projected crack length and are shown as nonfilled symbols.
In the case of the deformed material, the increased dislocation density seems to have a positiv effect on the fracture resistance which can be seen in the higher stress intensities for first crack extension in all major crack propagation directions. The intergranular propagating crack of the *L-R* - sample starts crack propagation at about 4.5 MPa $m^{0.5}$. This is lower in comparison to both other directions dominated by transgranular fracture. The *C-R* direction failed catastrophically without increasing fracture resistance, however the samples with *C-L* crack plane orientation showed significantly increased stress intensities of 9 MPa $m^{0.5}$ at first crack propagation. Despite the short crack extension before catastrophic failure of this sample, it is clear from these data and the corresponding fracture surfaces (figure 3.9) that transgranular fracture exhibits an R-curve of fracture resistance as intergranular fracture does. While the R-curve in the case of grain boundary fracture is resulting mainly from crack bridges along the crack path, the R-curve for transgranular fracture is controlled by processes connecting the different cleavage planes. These interconnecting areas may be also considered as bridges, however they are not isolated from the crack front.

3.2.2 Influence of temperature

The influence of temperature has already been shown in figure 3.1. The fracture toughness increases as expected due to an increasing fracture resistance of both, the grain boundary and the grain.

In the case of recrystallized tungsten, samples with *R-C* crack plane orientation were tested in the temperature range from room temperature to 700°C. Details on the sample geometry are given in paper D. Crack extensions were measured with the DC potential drop method [41] and the obtained R-curves are shown in figure 3.11. Compared to the room temperature experiments, where first crack extension occurs at about 4 MPa $m^{0.5}$ and the stress intensity rises slowly with crack extension, elevated temperatures cause crack propagation starting at higher stress intensities and a much steeper increase of the fracture resistance. It has to be noted that the obtained crack lengths, calculated from the monitored potential, underestimate

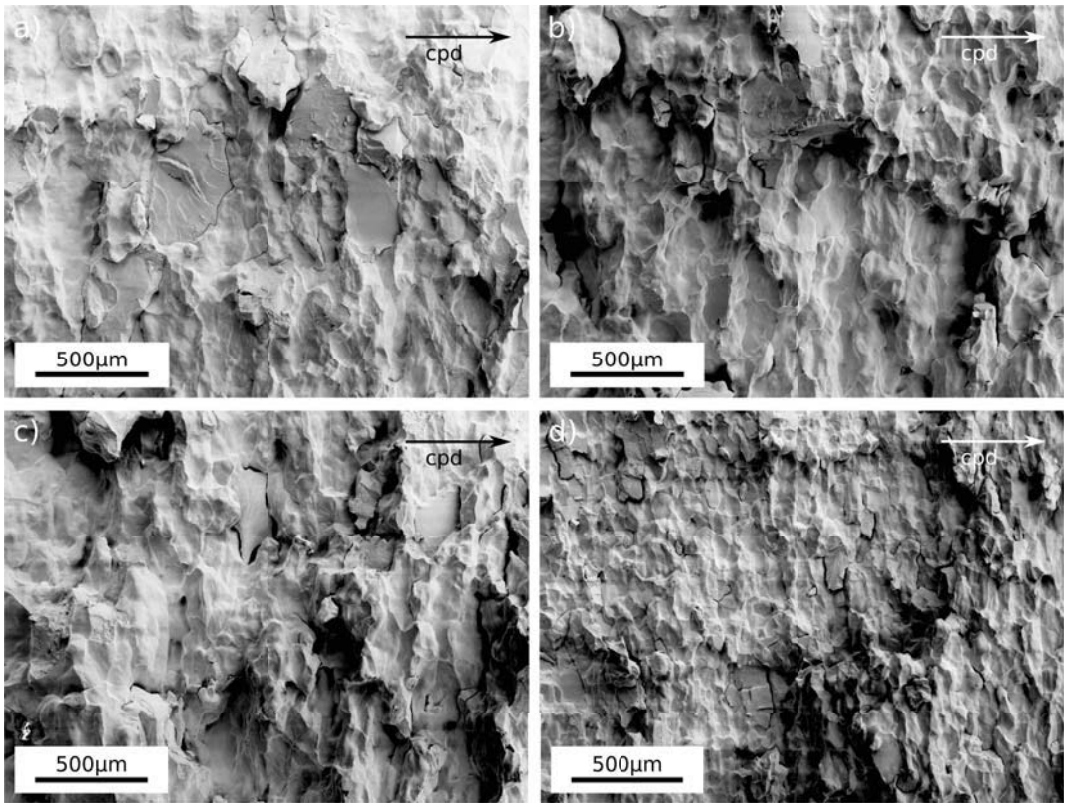

Figure 3.12 Recrystallized tungsten DC(T) samples with *C-R* crack propagation direction, tested at room temperature (a), 300°C (b), 500°C (c) and 700°C (d). The fracture surfaces show more cleaved grains at room temperature while elevated temperatures seem to cause more deviations from an even crack front.

the real crack lengths. This is caused by the large number of crack bridges found along the crack path which act as electrical contacts between the crack flanks [42]. The relative error induced by such bridges increases progressively with crack extension. The crack extension was measured by a potential drop technique. For larger crack extensions crack bridges may induce a significant underestimation of the crack length. The corresponding fracture surfaces of the tested samples are shown in figure 3.12. Despite intergranular fracture being the dominant type of fracture, cleaved grains occur but with a decreasing number with increasing temperature. This might be an effect of the changing fracture resistance of the grain boundary and the grain. While elevated temperatures increase both, it is still easier to propagate along the boundary than to cleave a grain. Much more plasticity is involved in the interior of a grain which can be seen around the crack path at higher temperatures [23]. Fewer cleaved grains are therefore found already starting from 300°C and the rougher fracture surface is a direct result of more crack deviations from a mode I level crack plane. The R-curves and the corresponding fracture surfaces indicate that the fracture resistance of grains raises more steeply in the investigated temperature window than the grain boundary fracture resistance does.

The experiments clearly show that the fracture of tungsten cannot solely be described by a single fracture toughness value. The fracture resistance increases with crack extension for both types of fracture - intergranular and transgranular. Deformation and temperature have a positive effect on the fracture resistance, however it is obvious that most improvements are possible by the grain shape, as also shown in [24, 25].

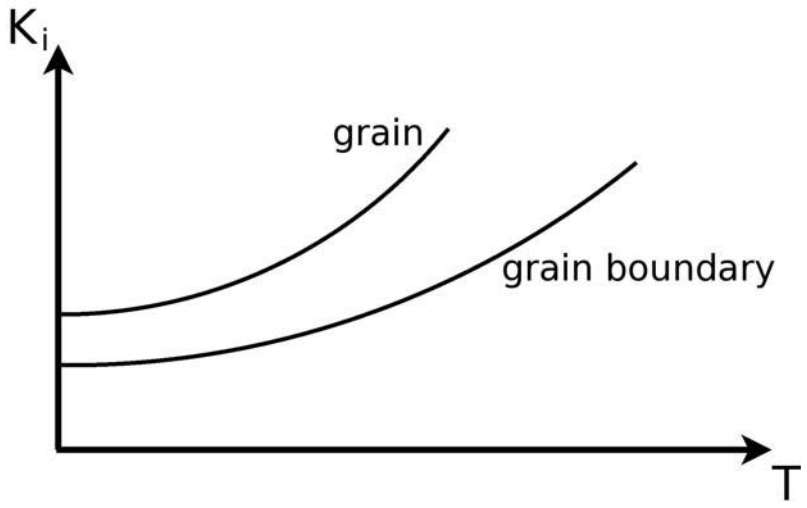

Figure 3.13 Schematic illustration of the intrinsic resistance to cleave a grain and a grain boundary.

In summary, it is evident that both, the intrinsic fracture resistance to cleave a grain and the intrinsic resistance to fracture the grain boundary, increase with temperature, as schematically shown in figure 3.13. Furthermore, the shielding contribution which causes the R-curve behavior also exhibits temperature dependence. This makes the interpretation of the literature data more complex because they usually consider only a single value for the fracture toughness and do not take into account the R-curve behavior. It is evident from this study that the grain structure has a dominant effect on the fracture behavior, however other factors such as crystallographic texture and dislocation substructure also affect the fracture resistance. Further detailed investigation is required for a better understanding of the fracture of tungsten and to design microstructures with better fracture resistance.

4 Conclusions

In this thesis the fracture behavior of tungsten and tungsten alloys was investigated with a focus on the fracture resistance of technically pure tungsten with recrystallized and various deformed microstructures. Samples with different crack plane orientations were used to analyze the influence of deformation, grain size and grain shape. In addition the influence of impurities on the fracture behavior was investigated by means of Auger electron spectroscopy.

Technically pure tungsten as well as tungsten alloys show the typical ductile-to-brittle transition, DBT, of body-centered cubic (bcc) materials. The obtained fracture toughness values in the low temperature regime vary over a wide range and the fracture surfaces show a changing ratio of inter- to transgranular fracture.
At the low-levels which impurities can be found in technically pure tungsten nowadays they do not have an influence on the fracture behavior. The amount of grain boundary fracture and cleavage fracture is much more related to the grain size, the grain shape and the deformation.
Cracks propagate in tungsten preferentially at the grain boundaries due to a somewhat lower fracture resistance of the boundary compared to the grain interior. The dominant fracture mode is, however, mainly dependent on the grain shape. Intergranular fracture is preferred as long as enough grain boundaries are available for a relatively plain mode I crack path. Instead of major deviations, the crack rather cleaves grains which furthermore causes the varying fractions of transgranular fracture with different microstructures.
The fracture resistance increases with crack extension for both - intergranular and transgranular fracture. This is called R-curve behavior. In the case of fracture along the grain boundaries, crack bridges can be found along the crack path, they are mainly responsible for the increasing fracture resistance with crack extension. The R-curve of transgranular dominated fracture is just dependent on the cleavage

process. Deformation and elevated temperature have a positive effect on the fracture resistance.

This work helped to clarify that the brittle fracture of tungsten is an intrinsic property of the material and cannot simply be caused by impurities. Despite deformation having a positive effect on the fracture resistance, most enhancements are possible by engineering the grain shape and the grain size. Considering the brittle nature of technically pure tungsten, even with improvements in two major crack propagation directions an extremely brittle material will remain in the third major direction.

Bibliography

[1] P. Beardmore, D. Hull, J. Less Common Met. 9 (1965) 168–180.

[2] D. Hull, P. Beardmore, A.P. Valintine, Phil. Mag. 12 (1965) 1021–1041.

[3] P.L. Raffo, J. Less Common Met. 17 (1969) 133–149.

[4] J. Liu, J.C. Bilello, Phil. Mag. 35 (1977) 1453–1472.

[5] Riedle J., *Bruchwiderstand in Wolfram-Einkristallen: Einfluss der kristallographischen Orientierung, der Temperatur und der Lastrate*, PhD-thesis, University of Stuttgart.

[6] J. Riedle, P. Gumbsch, H.F. Fischmeister, V.G. Glebovsky, V.N. Semenov, Mat. Res. Soc. Symp. Proc. 409 (1996) 23–28.

[7] J. Riedle, P. Gumbsch, H.F. Fischmeister, Phys. Rev. Lett. 76 (1996) 3594–3597.

[8] P. Gumbsch, J. Nucl. Mater. 323 (2003) 304–312.

[9] A. Giannattasio, S. G. Roberts, Phil. Mag. 87 (2007) 2589–2598.

[10] E. Tarleton, S.G. Roberts, Phil. Mag. 89 (2009) 2759–2769.

[11] P. Gumbsch, J. Riedle, A. Hartmaier, H.F. Fischmeister, Science 282 (1998) 1293–1295.

[12] A. Hartmaier, P. Gumbsch, Phys. Rev. B 71 (2005) 024108-1–024108-11.

[13] M. Rieth, A. Hoffmann, Int. J. Refract. Met. Hard Mater. 28 (2010) 679–686.

[14] A.W. Funkenbusch, F. Bacon, D. Lee, Met. Trans. A 10A (1979) 1085–1091.

[15] A. Joshi, D.F. Stein, Met. Trans. 1 (1970) 2543–2546.

[16] J.M. Liu, B.W. Shen, Acta Met. 30 (1982) 1197–1202.

[17] Tran-Huu-Loi, J.P. Morniroli, M. Gantois, M. Lahaye, J. Mater. Sci. 20 (1985) 199–206.

[18] H. Danninger, F. Knoll, B. Lux, P. Wilhartitz, M. Grasserbauer, Int. J. Refract. Met. Hard Mater. 4 (1985) 92–96.

[19] E. Pink, L. Bartha, *The Metallurgy of doped/non-sag Tungsten*, Elsevier Applied Science, London and New York, 1989.

[20] B. Gludovatz, *Bestimmung der Bruchzähigkeit an Wolframdrähten*, Diplomathesis, University of Leoben.

[21] D. Rupp, *Bruch und Spröd-duktil-Übergang in polykristallinem Wolfram: Einfluss von Mikrostruktur und Lastrate*, PhD-thesis, Karlsruhe Institute of Technology.

[22] D. Rupp, S.M. Weygand, J. Nucl. Mater. 386–388 (2009) 591–593.

[23] B. Gludovatz, S. Wurster, A. Hoffmann, R. Pippan, Int. J. Refract. Met. Hard Mater. 28 (2010) 674–678.

[24] D. Rupp, R. Mönig, P. Gruber, S.M. Weygand, Int. J. Refract. Met. Hard Mater. 28 (2010) 669–673.

[25] D. Rupp, S. Weygand, Phil. Mag. 90 (2010) 4055–4069.

[26] M.R. Ripoll, J. Očenášek, Eng. Fract. Mech. 76 (2009) 1485–1499

[27] J. Neges, B. Ortner, G. Leichtfried, H.P. Stüwe, Mat. Sci. Eng. A 196 (1995) 129–133.

[28] P.F. Browning, C.L. Briant, K.Rajan, B.A. Knudsen, Eng. Fail. Anal. 2 (1995) 105–115.

[29] Y. Mutoh, K. Ichikawa, K. Nagata, M. Takeuchi, J. Mater. Sci. 30 (1995) 770–775.

[30] S. Wurster, B. Gludovatz, R. Pippan, Int. J. Refract. Met. Hard Mater. 28 (2010) 692–697.

[31] M. Faleschini, *Severe Plastic Deformation of Tungsten Alloys and its Influence on Fracture Behavior*, PhD-thesis, University of Leoben.

[32] Annual Book of ASTM Standards - Standard Test Method for Plane-Strain Fracture Toughness of Metallic Materials (ASTM E 399-90), vol. 03.01. American Society for Testing and Materials; 1997. p. 413–43.

[33] B. Predel, *Landolt-Börnstein - Numerical Data and Functional Relationships in Science and Technology*; Group IV: Physical Chemistry; Thermodynamic Properties - Phase Equilibria, Crystallographic and Thermodynamic Data of Binary Alloys, vol. 5i, Springer-Verlag, Berlin Heidelberg, 1998.

[34] A. Vorhauer and R. Pippan, Scr. Mater. 51 (2004) 921–925.

[35] A.P. Zhilyaev and T.G. Langdon, Prog. Mater. Sci. 53 (2008) 893–979.

[36] A. Hohenwarter, R. Pippan, Mater. Sci. Eng. A 527 (2010) 2649–2656.

[37] S. Suresh, Engng. Fract. Mech. 21 (1985) 453–463.

[38] R. Pippan, Fatigue Fract. Engng. Mater Struct. 9 (1987) 319–328.

[39] R.O. Ritchie, Int. J. Fract. 100 (1999), 55–83.

[40] EDAX: Orientation Image Microscopy - Analysis Software v5.31.

[41] G.H. Aronson, R.O. Ritchie, J. Test. Eval. 7 (1979) 208–215.

[42] F.O. Riemelmoser, R. Pippan, H. Weinhandl, O. Kolednik, J. Test. Eval. 27 (1999) 42–46.

5
List of appended papers

Paper A
B. Gludovatz, S. Wurster, A. Hoffmann, R. Pippan
Fracture toughness of polycrystalline tungsten alloys
International Journal of Refractory Metals and Hard Materials 28 (2010) 674–678

Paper B
B. Gludovatz, S. Wurster, T. Weingärtner, A. Hoffmann, R. Pippan
Influence of impurities on the fracture behavior of tungsten
Accepted for publication in Philosophical Magazine

Paper C
B. Gludovatz, S. Wurster, A. Hoffmann, R. Pippan
A study into the crack propagation resistance of pure tungsten
Submitted for publication in Metallurgical and Materials Transactions A

Paper D
B. Gludovatz, S. Wurster, A. Hoffmann, R. Pippan
Influence of deformation, microstructure and temperature on the fracture resistance of tungsten
Will be submitted for publication in Philosophical Magazine

Remark

In the appended papers, I, Bernd Gludovatz, performed all experiments, data analyses and was the primary author with the following exceptions:

- In **paper A** S. Wurster performed the investigations on WRe.
- In **paper B** T. Weingärtner carried out the AES measurement. Additionally, E. Nold from KIT in Karlsruhe is thankfully acknowledged for his expert guidance.
- My supervisor, R. Pippan, contributed in all the papers by providing the basic ideas for publications with helpful discussions and support during their preparation.

A

Fracture toughness of polycrystalline tungsten alloys

B. Gludovatz[a,b], S. Wurster[a], A. Hoffmann[c], R. Pippan[a,b]

[a]Erich Schmid Institute of Materials Science, Austrian Academy of Sciences, A-8700 Leoben, Austria
[b]Christian Doppler Laboratory for Local Analysis of Deformation and Fracture, A-8700 Leoben, Austria
[c]Plansee Metall GmbH, A-6600 Reutte, Austria

Abstract

Tungsten and tungsten alloys show the typical change in fracture behavior from brittle at low temperatures to ductile at high temperatures. In order to improve the understanding of the effect of microstructure the fracture toughness of pure tungsten, potassium doped tungsten, tungsten with 1 wt.% La_2O_3 and tungsten rhenium alloys were investigated by means of 3-point bending, double cantilever beam and compact tension specimens. All these materials show the expected increase in fracture toughness with increasing temperature. The experiments demonstrate that grain size, texture, chemical composition, grain boundary segregation and dislocation density seem to have a large effect on fracture toughness below the DBTT. These influences can be seen in the fracture behavior and morphology, where two kinds of fracture occur: on the one hand transgranular and on the other hand intergranular fracture. Therefore, techniques like electron backscatter diffraction (EBSD), Auger electron spectroscopy (AES) and X-ray line profile analysis were used to improve the understanding of the parameters influencing fracture toughness.

A.1 Introduction

Most studies related to the ductility of tungsten and tungsten alloys were performed in the sixties and seventies. A good example is Raffo et al. [1]. As fracture mechanics was not well established at that time studies on fracture toughness were scarce. Riedle and Gumbsch [2–5] extensively studied the fracture toughness of tungsten single crystals in the nineties. The effects of crystallographic orientation, crack propagation direction, loading rate and temperature were investigated. Compared to the single crystal, the fracture toughness of polycrystalline tungsten is not yet well examined.
We started an extensive investigation of the fracture toughness of pure tungsten (W), potassium doped tungsten (AKS-W), tungsten with 1 wt.% La_2O_3 (WL10) and tungsten - 26 wt% - rhenium (WRe26). The results of a few selected microstructures are presented in this paper. A very large effect of the microstructure, especially below the ductile to brittle transition temperature, was observed. These investigations indicate that the change from transgranular to intergranular cleavage fracture plays an important role. Especially crystallographic analyzes are presented to improve understanding of the interaction of these fracture processes.
This paper was also presented at the 12th International Conference on Fracture - July 12–17, 2009.

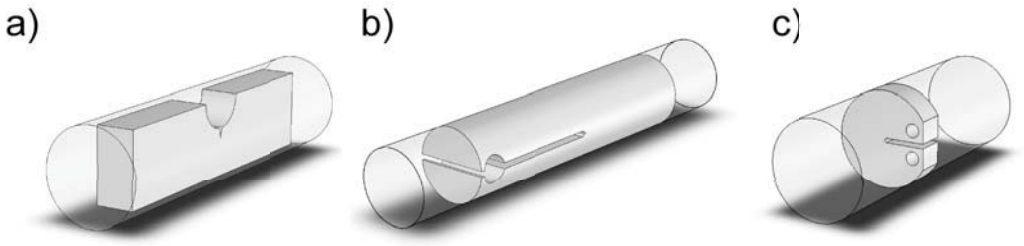

Figure A.1 Different specimen types manufactured out of tungsten rods. 3PB-specimen with crack direction in radial direction (a). DCB-specimen with crack direction in rolling direction (b). CT-specimen with crack direction in radial direction (c).

A.2 Experimental

The fracture toughness of W, AKS-W, WL10 and WRe26 were investigated by means of 3-point bending (3 PB – Fig. A.1-a), double cantilever beam (DCB – Fig. A.1-b) and compact tension specimens (CT – Fig. A.1-c). All specimens were manufactured out of rods at different stages of the processing route. Fig. A.1 shows specimens prepared to investigate the materials in rolling direction and radial direction. The experiments were performed in the range of -196°C to 1000°C.
In order to examine the local variation of the fracture resistance, DCB-specimens

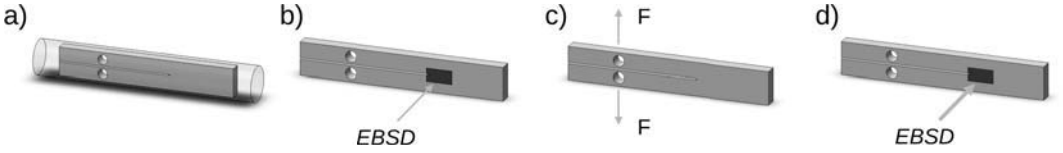

Figure A.2 Experimental setup to investigate the local variation of the fracture resistance: position of a DCB-specimen in a AKS-W rod (a). Scanning the area in front of the crack tip using EBSD (b). Apply a tensile load on the specimen (c). Scanning the previously scanned area again (d).

(Fig. A.2-a) with a length of 30 mm, a height of 3.5 mm and width of 7.5 mm and CT-specimens with a length of 7.5 mm, a height of 3 mm and a width of 6 mm were manufactured out of W, AKS-W, and WRe-rods. The notches were prepared with a diamond-saw, refined with a razor blade and fatigue-precracked under cyclic compression [6]. The areas in front of the crack-tips were scanned using electron backscatter diffraction (EBSD) after a heat treatment of 2000°C for an hour in hydrogen atmosphere (Fig. A.2-b). Some specimens were then loaded under tension within the range of stable crack growth (Fig. A.2-c). After that, the previously scanned areas were scanned again using EBSD (Fig. A.2-d) to quantify changes of the grain orientation in the obtained orientation imaging maps (OIM).

The tests performed at room temperature were done with a microtensile-testing machine from *Kammrath & Weiss*, while the tests at elevated temperatures were done by use of a *ZWICK* universal testing machine. The fractographic and crystallographic analyzes were made by use of a *Zeiss* 1525 scanning electron microscope equipped with an *EDAX* EBSD system.

Table A.1 Table of K_Q values of W, AKS-W, WL10 (sintered) and WRe26 (rolled and stress relieved) tested in the temperature range from room temperature to 800°C.

Temperature [°C]	Fracture toughness [MPa m$^{0.5}$]			
	W	AKS-W	WL10	WRe
RT	5.1	4.7	4.7	54.2
200	6.1	4.6	4.3	59.3
400	10.7	16.7	12.8	64.4
600	-	-	72.9[a]	-
700	-	-	86.3[a]	-
800	80.5[a]	93.0[a]	-	-

[a] These K_Q values have been estimated from the COD_C values using Eq. A.1.

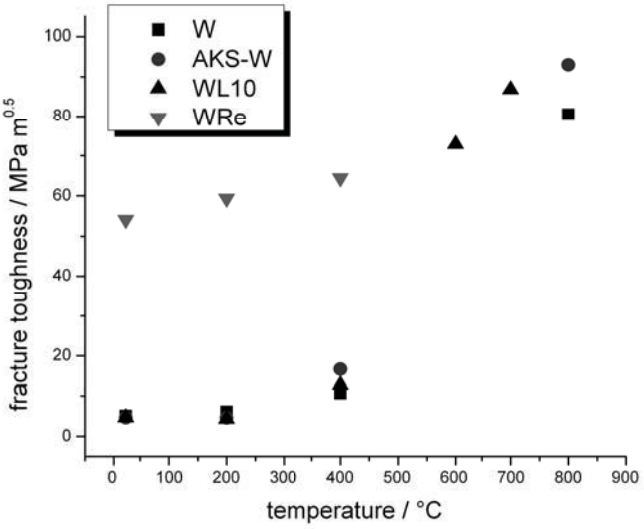

Figure A.3 Fracture toughness K_{Q} of W, AKS-W, WL10 (sintered) and WRe26 (rolled and stress relieved) as a function of temperature T. All values above 400°C have been calculated from their COD_{C} values using Eq. A.1.

A.3 Results and discussion

A.3.1 Fracture toughness investigations

All tested specimens showed the expected increase in fracture toughness with increasing temperature, examples are shown in Fig. A.3 with the associated values shown in Table A.1.

At low temperatures, the fracture toughness was determined by use of linear elastic fracture mechanics whereas at temperatures above 600°C the critical crack tip opening displacement $CTOD$ [7] was used to determine the critical stress intensity factor. The fracture toughness determined by stereophotogrammetric techniques is then calculated by

$$K_{\mathrm{IC}} = \sqrt{m \cdot \sigma_{\mathrm{y}} \cdot E \cdot COD_{\mathrm{C}}} \tag{A.1}$$

where σ_{y} represents the yield strength, E the Young's modulus and m a coefficient which depends on the work hardening factor n of the material. For low hardening m is about 1.5 [8, 9].
σ_{y} for recrystallized and stress relieved W as a function of the temperature are shown in Fig. A.4 as well as in Table A.2 which show the expected decrease of the yield strength with increasing temperature [10].

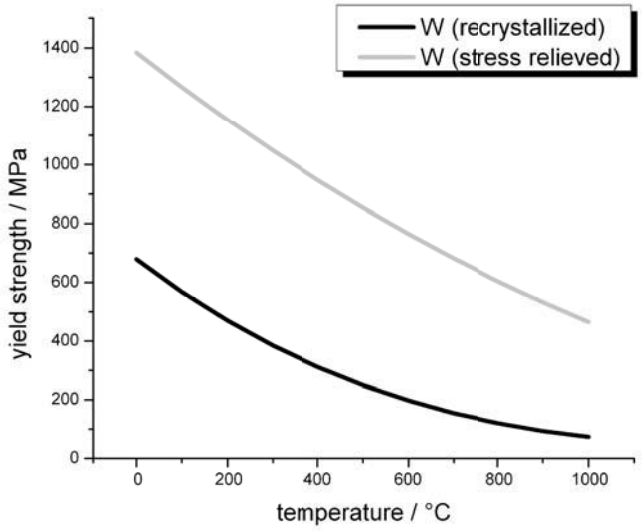

Figure A.4 Yield strength σ_y as $f(T)$ of recrystallized and stress relieved W [10].

Table A.3 shows fracture toughness values of CT and 3 PB specimens tested at room temperature. The two letter code in the brackets describes the crack plane orientation of different specimens with respect to the geometry of the manufactured material. The first letter designates the *direction normal* to the crack plane, and the second letter the *expected direction of crack propagation* [11]. φ is the technically degree of deformation, referring to a rolling process, given by $\Delta A/A_0$ where ΔA is the cross-sectional reduction in area and A_0 is the original area of the cross-section. Due to the extreme differences of the determined K_Q values, the processing route seems to have a great influence on the results as well as the direction the specimens have been manufactured out of the rods. While sintered materials have equiaxed

Table A.2 Yield strength σ_y of recrystallized and stress relieved tungsten as a function of the temperature in the range from room temperature to 1000°C [10].

Temperature [°C]	Yield strength [MPa]	
	W (recrystallized)	W (stress relieved)
0	680	1385
200	470	1154
400	311	948
600	197	765
800	120	604
1000	74	465

Table A.3 K_Q values of W and W-alloy specimens tested at room temperature.

Material	Condition	Rod ∅ [mm]	φ [%]	Tests performed	K_Q [MPa m$^{0.5}$]
W	As sintered	23	-	CT	5.1
	Rolled	9	84.7	CT (C-R)	4.7
	Forged	25	75.9	3PB (L-R)	8.0
	Rolled	9	84.7	3PB (L-R)	9.1
	Rolled	4	97.0	3PB (L-R)	5.4
	Rolled and drawn	1	99.8	3PB (L-R)	35.1
WL	As sintered	23	-	CT	4.7
	Rolled	9	84.7	CT (C-R)	6.0
	Forged	25	76.9	3PB (L-R)	16.6
	Rolled	9	84.7	3PB (L-R)	9.8
	Rolled	4	97.0	3PB (L-R)	9.7
AKS-W	As sintered	23	-	CT	6.4
	Rolled	9	84.7	CT (C-R)	4.5
	Rolled	9	84.7	3PB (L-R)	32.1
	Rolled	4	97.0	3PB (L-R)	13.5
	Rolled and drawn	1	99.8	3PB (L-R)	32.1
WRe (26%)	Forged	25		3PB (L-R)	54.2
	Recrystallized	18		CT (C-R)	22.8

grains and therefore the direction of the manufactured specimens does not play a role, especially rolled rods show very often large differences in K_Q for different crack propagation directions as a result of the elongated grains. An increasing degree of deformation leads to a stronger elongation of the grains. This makes it much easier for a crack to propagate along the axis of a rod than perpendicular to it. Additionally, it has to be mentioned that different specimens from the same rods and the same crack propagation direction sometimes show large differences. This is probably an effect of the location of the tested volume in the rod, as the texture changes from the center to the edge and also becomes more pronounced the thinner the rods are.

A.3.2 Examination of the local variation of fracture resistance

For a better understanding of the local variation of the fracture resistance, the DCB-specimens were tested with a microtensile-testing or a universal-testing machine as mentioned earlier. The crack path was recorded by EBSD. In the case of the potassium doped tungsten tested at *RT*, the inverse pole figures (IPF) and fracture surfaces show two types of fracture behavior (Fig. A.5). On the one hand the crack propagates intergranular (ig) and on the other hand also transgranular (tg), though the fraction of transgranular crack propagation prevails. Orientation changes within

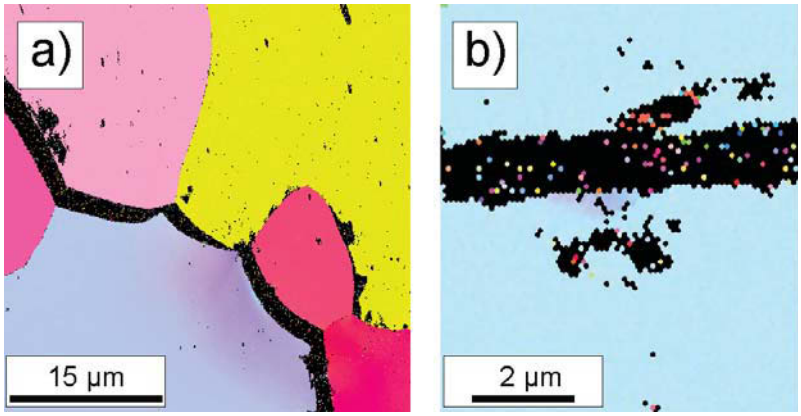

Figure A.5 Intergranular (a) and transgranular (b) propagated crack of a DCB-specimen manufactured out of an AKS-W-rod and tested at *RT*.

single grains in the interior of an intergranular propagated crack (Fig. A.5-a) as well as changes within grains in the case of a transgranular propagated crack (Fig. A.5-b) were observed and are clearly viewable due to the gradual change in color in both pictures of Fig. A.5. Such deformations are not frequently observable and are just very localized along the crack path of a *RT*-tested specimen.

Fig. A.6 shows the correlation between the change in orientation and plastic deformation. A narrow band of geometrically necessary dislocations (GND) - generated by the crack tip - is arranged one after the next in a small angle tilt boundary. The volume elements below the boundary are rotated with respect to the elements above. This rotation can be associated with a tilt of crystals and can be used to determine GNDs [12].
Measurements of the misorientation in the case of the intergranular propagated crack

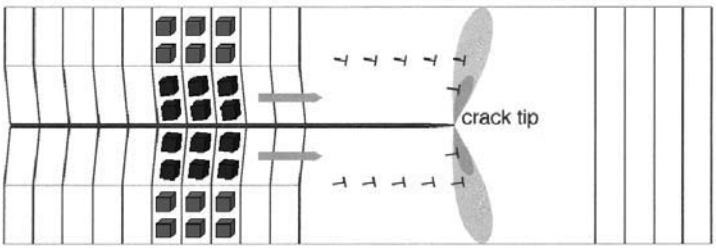

Figure A.6 The propagating crack generates a band of geometrically necessary dislocations (GND). These GNDs have an effect similar to a series of small angle boundaries. The rotation of the crystals can be used to determine the density of the GNDs and the size of the plastic zone. Additionally, they can be used to estimate the local plastic work spent during crack propagation.

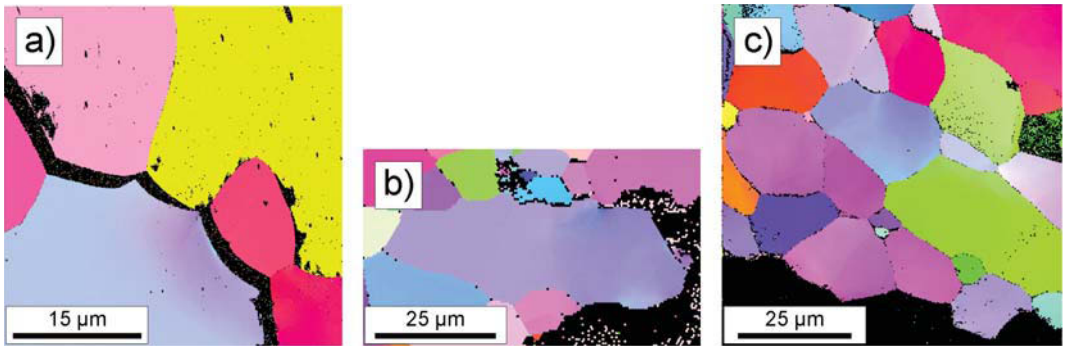

Figure A.7 Plastically deformed areas along the crack paths of potassium doped tungsten DCB-specimens tested at *RT* (a), 300°C (b) and 600°C (c).

show a maximum value of about 4° whereas the transgranular propagated crack leads to a maximum orientation change of about 5°.

The DCB-specimens tested at elevated temperatures are shown in Fig. A.7-b/-c and compared with the specimen tested at *RT* (Fig. A.7-a). It can be seen that the amount of plastically deformed areas within single grains does not significantly increase from a RT-tested specimen to a 300°C-tested specimen or a 600°C-tested specimen. Misorientation measurements within the grains also show that the values always are in the range between 4 and 6°. However, the frequency of deformed grains is increasing with increasing temperature. In the case of *RT* and 300°C-tested specimens the deformation was just observed directly along the crack path, whereas the 600°C tested specimen showed plastically deformed areas also in a wider vicinity of the propagated crack.

The compact tension specimens manufactured out of a WRe26 alloy were fractured at room temperature and at elevated temperatures. Fig. A.8 shows scans of all specimens after fracture. Compared to the AKS-W-specimens these IPF show many more plastically deformed areas. In the RT-tested specimens (Fig. A.8-a) plastically deformed grains were observed just in the direct vicinity of the propagated crack.

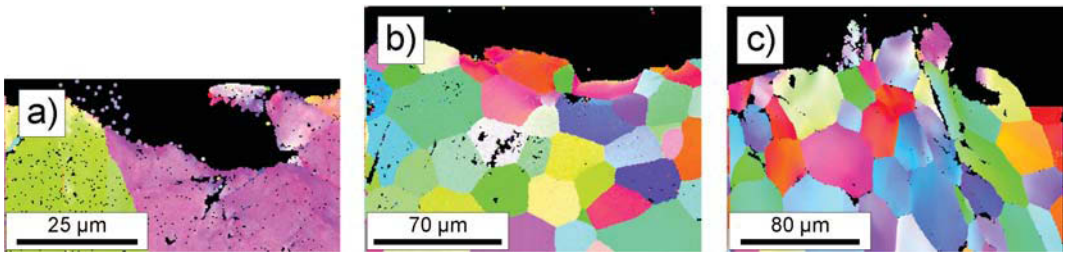

Figure A.8 Plastically deformed areas along the crack paths of tungsten rhenium CT-specimens tested at *RT* (a), 300°C (b) and 600°C (c).

The 300°C and 600°C-tested samples (Fig. A.8-b and -c) also show plasticity in the wider vicinity of the crack flanks. Measured misorientations of about 10 degrees for the 300°C and about 14° for the 600°C-tested specimens are much higher than the values obtained from the AKS-W-specimens.

In summary, a comparison of the EBSD analyzes shows that recrystallized tungsten and tungsten alloys mainly cleave intergranularly at room temperature. However, they have a small amount of transgranular cleavage as well. EBSD analyzes, taken along the crack path of the propagated crack, show plastic deformation close to the crack flanks only at selected places. This occurs in both transgranular and intergranular fracture. Most plasticity can be found at crack bridges which occur along the whole crack path. This indicates an extreme variability in deformation during cleavage processes at low temperatures. With increasing temperature the amount of plastic deformation rises which is clearly visible in the EBSD data. Plastic deformation can be seen along the whole crack path, in both intergranular and transgranular fractured grains. Grains neighboring the propagated crack show plastic deformation as well as grains in the wider surrounding of the crack path. This indicates a much higher amount of deformation during propagation of the crack, which can also be seen in the higher fracture toughness values. Compared to all other tungsten materials tungsten rhenium alloys show significantly higher amounts of plastic deformation, even at room temperature.
In order to quantify the effect of locally varying fracture resistances, further investigations on different microstructures will be performed and described in a forthcoming paper.

A.4 Conclusion and summary

The fracture toughness of pure polycrystalline tungsten, potassium doped tungsten, tungsten with 1 wt.% La_2O_3 and tungsten rhenium alloys were investigated by means of 3-point bending, double cantilever beam and compact tension specimens. Tests were performed in the temperature range of -196°C to 1000°C and the obtained values show the expected increase of fracture toughness with increasing temperature. However, the values obtained in the low temperature regime show a particularly strong dependence on the microstructure and therefore the production route.
Investigations of fracture surfaces, as well as EBSD-scans of propagated cracks, always show intergranular as well as transgranular fracture of all tested materials, although intergranular fracture behavior is dominant in most cases. Detailed EBSD investigations along the crack path show plastically deformed areas within single grains for both types of fracture. Tests performed at room temperature show such plasticity only locally while experiments at elevated temperatures lead to a greater amount of deformed areas in the grains neighboring the crack and also grains in the wider vicinity of the crack.

Fracture toughness tests of tungsten rhenium alloys show significantly higher values than all other tungsten materials. EBSD-scans along the crack path of the propagated crack show very pronounced plastic deformation even at room temperature.

Acknowledgements

The financial support by the "Christian Doppler Forschungsgesellschaft" is gratefully acknowledged.
A part of this work, supported by the European Communities under the Contract of Association between EURATOM and the Austrian Academy of Sciences, was carried out within the framework of the European Fusion Development Agreement. The views and opinions expressed herein do not necessarily reflect those of the European Commission.
The interesting discussions with Prof. R. Stickler and provided documents are thankfully acknowledged.

Bibliography to paper A

[1] Raffo PL. Yielding and fracture in tungsten and tungsten–rhenium alloys. J Less-Common Metals 1969;17:133–49.

[2] Riedle J. Bruchwiderstand in Wolfram-Einkristallen: Einfluss der kristallographischen Orientierung, der Temperatur und der Lastrate. Reihe 18 – Nr. 184: Düsseldorf: VDI Verlag; 1990.

[3] Riedle J, Gumbsch P, Fischmeister H. Cleavage anisotropy in tungsten single crystals. Phys Rev Lett 1996;76:3594–7.

[4] Gumbsch P. Brittle fracture and the brittle-to-ductile transition of tungsten. J Nucl Mater 2003;323:304–12.

[5] Gumbsch P. Modeling and simulation in materials science. Udine: Summer School of Fracture (lecture notes); 2005.

[6] Pippan R. The growth of short cracks under cyclic compression. Fatigue Fract Eng Mater 1987;9:319–28.

[7] Kolednik O, Stüwe HP. The stereophotogrammetric determination of the critical crack tip opening displacement. Eng Fract Mech 1985;21:145–55.

[8] Kolednik O, Stüwe HP. A proposal for estimating the slope of the blunting line. Int J Fracture 1987;33:R63–6.

[9] Shih CF. Relationship between the J-integral and the crack opening displacement for stationary and extending cracks. J Mech Phys Solids 1981;29:30526.

[10] University of California Los Angeles, ITER Material Properties Handbook, External link *http://fusionnet.seas.ucla.edu/fusionnetwork/iter_properties.php?mid=ST-M-RF-%23201&tid=0201P-0100* (accessed March 03, 2010).

[11] Annual Book of ASTM Standards–Standard Test Method for Plane-Strain Fracture Toughness of Metallic Materials (ASTM E 399-90), vol. 03.01. American Society for Testing and Materials; 1997. p. 413–43.

[12] Pippan R, Strobl G, Kreuzer H, Motz C. Asymmetric crack wake plasticity – a reason for roughness induced crack closure. Acta Mater 2004;52:4493–502.

B

Influence of impurities on the fracture behavior of tungsten

B. Gludovatz[a,b], S. Wurster[a], T. Weingärtner[c], A. Hoffmann[d], R. Pippan[a,b]

[a]Erich Schmid Institute of Materials Science, Austrian Academy of Sciences, A-8700 Leoben, Austria
[b]Christian Doppler Laboratory for Local Analysis of Deformation and Fracture, A-8700 Leoben, Austria
[c]Karlsruhe Institute of Technology, Institute for Material Research I, D-76344 Eggenstein-Leopoldshafen, Germany
[d]Plansee Metall GmbH, A-6600 Reutte, Austria

Abstract

Ten tungsten materials with different impurity concentrations and different microstructures have been investigated by Auger electron spectroscopy and scanning electron microscopy with respect to their fracture behavior. For almost all samples both inter- and transgranular fracture are observed, the proportion of each type varies. Due to the difference in their impurity content and grain boundary area, a large variation in the grain boundary impurities can be expected. By analyzing the fracture surfaces the effect of grain boundary impurities, especially phosphorous and oxygen, on the fracture resistance of the boundaries was determined. The results indicate that for the analyzed tungsten materials grain boundary impurities do not have a significant influence on the fracture resistance of the boundaries. Other factors such as the size and shape of the grains, the amount of deformation and therefore the density of dislocations within the grains have a greater impact on the fracture behavior of tungsten.

B.1 Introduction

Tungsten-based materials show the characteristic change in fracture behavior from brittle at low temperatures to ductile at high temperatures. Experiments indicate that grain size, texture, chemical composition, grain boundary (GB) segregation and dislocation density seem to have a large effect on the fracture toughness especially below the ductile to brittle transition temperature (DBTT) [1]. In contrary to many other bcc metals, in tungsten a combination of trans- and intergranular fracture is usually observed, although the area fraction of each type varies.
Over the last fifty years numerous investigations have been carried out with the aim of improving the understanding of the fracture behavior. Most studies relating to the ductility of tungsten materials were done in the fifties, sixties and few in the seventies [2–7]. GB impurities, which were thought to be one of the main causes of intergranular fracture, were investigated to determine the effect of particularly carbon (C), oxygen (O), potassium (K) and phosphorous (P) [8–10].
Joshi and Stein [9] investigated the segregation of O to the GBs of tungsten in the seventies. By adding various amounts of C they wanted to show an interaction of the two elements to better understand the brittle behavior of the material. As there was no direct reaction of C and O, they suggested that O is not the cause for the embrittlement of tungsten. However, Auger spectroscopy analyzes showed the segregation of P to the GBs which was thought to be the main cause for the brittle behavior of tungsten. The amount of segregation was dependent upon the grain-size - the larger the grain size, the greater the concentration of P at the GB and the higher the embrittlement. Values concerning the amounts of impurities contained in the investigated materials are not given in this study.
In the eighties Tran-Huu-Loi et al. [11] investigated three different tungsten materials with the main impurities as follows: material A) 20 ppm C, 3 ppm O, 60 ppm K / material B) 30 ppm C, 2 ppm K, 20 ppm P / material C) 30 ppm C, 30 ppm O, 10 ppm K, 50 ppm P. All materials had equiaxed microstructures and where investigated by impact tests, scanning electron microscopy and Auger spectroscopy in the temperature range -196°C to 1000°C. Below DBTT various proportions of inter- and transgranular fracture were observed while increasing temperature and increasing P concentration lead to an increasing amount of intergranular fracture.
Danninger et al. [12] carried out similar investigations on the role of P by secondary ion mass spectroscopy (SIMS). He concluded that an average content of 20-40 ppm P, like it was standard in technically produced tungsten heavy alloys at this time (W powders were mixed with Ni and Fe powders), does not influence the fracture behavior of tungsten and only higher concentrations can increase the embrittlement. Due to the improvement in industrial production nowadays W materials contain significantly lower P and O contents. Nevertheless, the frequently observed GB fracture is often associated with the impurity content. By discussing the limits of impurities it is important not only to relay on certain maxima of ppm, but to take into account the grain size or in other words the grain boundary area and how the impurities are distributed on the GBs.

Table B.1 Main impurity elements of the investigated technically pure tungsten (W > 99.97%).

Element	C	H	N	O	P	S	Si
Guaranteed analysis (max) / μg/g	30	5	5	20	20	5	20
Typical analysis / μg/g	10	2	<2	5	<10	<2	5

To better quantify the influence of impurities in W on grain boundary fracture, a standard technical W, a high purity W and a W material of high impurity content, with different grain sizes, grain shapes and dislocation structures are investigated with respect to grain boundary fracture.
Plansee Metall GmbH. manufactures tungsten materials with typical impurity concentrations as shown in table C.1. The first line shows the maximum concentration they guarantee not to exceed while the second line gives the average impurity concentrations.
Nowadays, Auger electron spectrometers with point resolutions of less than a micron can be much better focused on the areas of interest, however, the sensitivities of spectrometers did not improve as much as the ability to focus the electron beam. Nevertheless, the ability of Auger spectrometers to detect fractions of monolayers of elements on a surface, together with a good focused electron beam, is a useful tool to investigate GB impurities of large grained as well as the fine and ultra fine grained materials to improve the understanding of the effect of GB impurities like O or P in tungsten.

B.2 Materials and experimental methods

An investigation of the effect of impurity concentrations on the fracture behavior of tungsten materials was done by analyzes of fracture surfaces by Auger electron spectroscopy (AES) and scanning electron microscopy (SEM). The fracture behavior of materials purchased as-is was analyzed and compared with the fracture behavior of materials processed to different microstructures. Changing microstructures with an either higher or smaller area of grain boundaries (GBs) lead to a changing fraction of the impurity concentration on the GBs. If there is an influence of the impurities on the fracture behavior, this should become obvious by a changing amount of inter- and transgranular fracture.
A tungsten single crystal, with a significantly smaller impurity concentration, was severely plastically deformed (SPD) by a high pressure torsion (HPT) tool [13,14] to generate an ultra-fine grained (UFG) polycrystal and subsequent annealing resulted in a coarsening of the grain structure. Its fracture behavior was additionally taken into comparison.

Table B.2 Materials investigated by Auger electron spectroscopy, their fabrication conditions and their corresponding fracture toughness (FT) values. Additionally shown are the average grain sizes (diameter) of the materials with equiaxed grains. Materials with an elongated grain structure are described by the length of the major axes of the grains (l) together with its aspect ratios (UFG-W, UFG-W^{sc} and W^{sc}_{600}) or the average diameter (d) of the grains in the cross section (W_{rolled}). l_{GB} / A shows the sum of the length of high angle grain boundaries per $1\,\mu m^2$ grain boundary area while f_{ig} lists an average proportion of intergranular fracture obtained from the fracture surfaces. Most values are listed with their standard deviations. The superscript "sc" indicates that these samples were produced from a high purity single crystal.

Material	Condition	Av. grain size μm	Aspect ratio	l_{GB} / A $\mu m / \mu m^2$	f_{ig} %	FT MPa $m^{0.5}$
W_{rolled}	rolled	121.52 ± 35.55 (l) 31.0 ± 9.1 (d)	-	$1.09x10^{-1}$	68.4 ± 14.1 10.6 ± 5.0	(5 - 15)[b]
$W_{sintered}$	sintered	25.0 ± 9.9	-	$8.36x10^{-2}$	95.9 ± 2.0	~ 8
W_{hipped}	hipped	22.1 ± 6.4	-	$1.02x10^{-2}$	82.5 ± 4.2	~ 11
UFG-W^{sc}	ultra-fine grained	0.26 ± 0.09 (l)	0.43 ± 0.27	$1.86x10^{0}$	-[a]	-[c]
W^{sc}_{600}	SPD + 1h @ 600°C	0.31 ± 0.11 (l)	0.45 ± 0.27	$4.07x10^{0}$	92.0 ± 5.3	-[c]
W^{sc}_{800}	SPD + 1h @ 800°C	8.4 ± 2.7	-	$3.91x10^{-1}$	85.5 ± 7.2	-[c]
W^{sc}_{1200}	SPD + 1h @ 1200°C	92.4 ± 30.3	-	$1.38x10^{-2}$	66.1 ± 6.6	-[c]
UFG-W	ultra-fine grained	0.33 ± 0.13 (l)	0.49 ± 0.18	$6.22x10^{0}$	-[a]	(9 - 33)[d]
W_{1200}	SPD + 1h @ 1200°C	4.4 ± 1.5	-	$5.68x10^{-1}$	87.9 ± 2.1	-
$W_{recryst}$	1h @ 2000°C	95.2 ± 35.7	-	$3.79x10^{-2}$	72.4 ± 11.7	~ 5

[a] The amount of inter-/transgranular fracture could not be determined due to the extremely small grain sizes and also due to varying amounts in the different directions of a HPT sample [16]

[b] The fracture toughness range is mainly dependent on the crack orientation of the samples with respect to the rolling direction [17]

[c] Due to the their microstructures and fracture morphologies the fracture toughness values are similar to technically pure tungsten in the same conditions

[d] Values vary extremely depending on the direction of the crack propagation in a high pressure torsion sample [16]

Table B.2 summarizes the different tungsten samples investigated with their manufacturing condition and average grain size. Three of these samples were used as-is, purchased from Plansee Metall GmbH. They are described as follows: rolled tungsten rods (W_{rolled}) with an elongated grain structure - the grains have an average diameter of about 31 μm in the cross section (figure B.1-b) and an average length of about 121 μm (figure B.1-a) which gives an aspect ratio of d/l $\sim$ 0.26; sintered tungsten ($W_{sintered}$) with an average grain size of 25 μm (figure B.1-d) and hipped tungsten (W_{hipped}) with a slightly smaller grain size of 22 μm (figure B.1-e). The sintered and hipped materials have a porosity of about 16 %. The sintered tungsten has the same impurity concentration as the technically pure tungsten, while the hipped tungsten material has a higher concentration of impurities, in this case a significantly higher oxygen content, 118 μg/g.
In order to investigate the effect of impurities on grain boundary fracture, tungsten with different grain sizes was produced from the technically pure and single crystalline materials. This technical variation was achieved either by simply recrystallizing the pure material or by applying SPD to the materials. Two samples were used directly following SPD, all other samples were additionally heat treated. The technically pure tungsten was recrystallized at 2000°C for an hour leading to an average grain size of $\sim$ 95 μm referred to as $W_{recryst}$ (figure B.1-c). The ultra-fine grained (UFG) samples, both with an average grain size of $\sim$ 300 nm, were produced from a tungsten single crystal (UFG-W^{sc} / figure B.1-f) and a technically pure tungsten (UFG-W / figure B.1-j) using HPT. In each case, disc-shaped samples with a diameter of 8 mm and a thickness of 0.8 mm were deformed to 4 revolutions, corresponding to an equivalent von Mises strain, $\epsilon_{vm} \approx 64$, at a temperature of 400°C and a hydrostatic pressure of $\sim$ 8 GPa. Further UFG samples were subsequently heat treated at 600°C, 800°C or 1200°C in a vacuum furnace for one hour to produce coarser, recrystallized microstructures [15]. After recrystallization, the W_{1200} (figure B.1-k) had a grain size of $\sim$ 4 μm while the W^{sc}_{600} (figure B.1-g), W^{sc}_{800} (figure B.1-h) and W^{sc}_{1200} (figure B.1-i) had grain sizes of $\sim$ 300 nm, $\sim$ 8 μm and $\sim$ 92 μm, respectively. The significant effect of the impurities is clearly visible in the different recrystallization and grain growth behavior. Impurity contents of samples prepared from single crystals will be subsequently referred to as ultra low. Table B.2 additionally shows the sum of the length of high angle grain boundaries per 1 μm^2 area which is dependent on the size and shape of the grains.
For each sample, 3-point bending beam-like specimens were machined and fractured at room temperature in a ultra high vacuum (UHV) chamber of a PHI 680 Auger Nanoprobe, a field emission Auger microprobe. The fracture surface impurities were analyzed by Auger spectrometry immediately after fracturing the specimens at a vacuum between 1x10^{-9} mbar and 1x10^{-10} mbar and the fracture surface images were taken either with this microscope or with a Zeiss LEO 982 field-emission scanning electron microscope (FE-SEM).

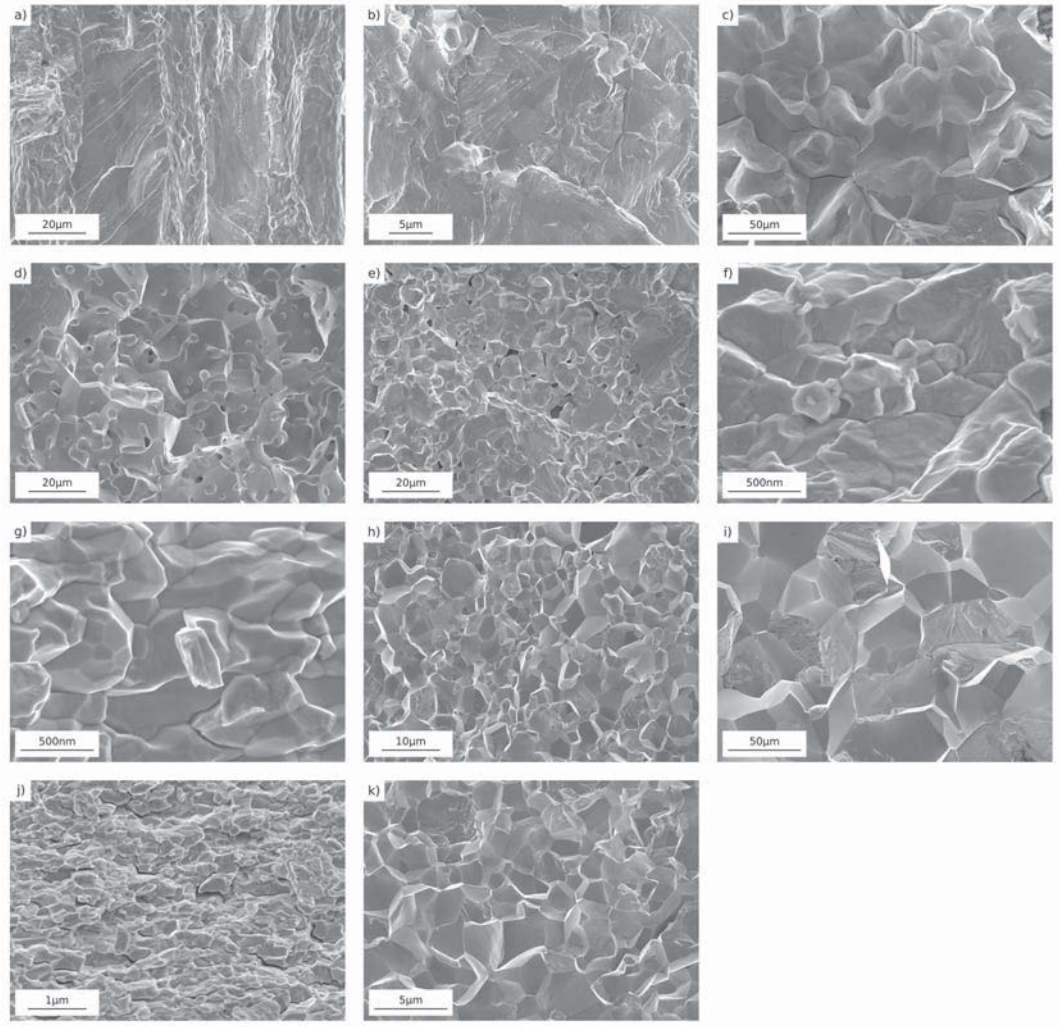

Figure B.1 Fracture surfaces of tungsten materials with different microstructures investigated by Auger electron spectroscopy (AES). Rolled tungsten rod (W_{rolled}) with crack propagation front parallel to the axis of the rod (a) and perpendicular to the axis of the rod (b), recrystallized tungsten ($W_{recryst}$) (c) and sintered tungsten ($W_{sintered}$) (d) are technically pure tungsten materials with the average impurity concentration shown in table C.1. Other technically pure tungsten materials are shown in (j) and (k), where (j) was just severe plastically deformed (SPD) by high pressure torsion (HPT) (UFG-W) and (k) was deformed and additionally heat treated at 1200°C for an hour in a vacuum furnace (W_{1200}). Figure (e) depicts the fracture surface of hipped tungsten (W_{hipped}) which contains a much higher amount of oxygen. Figure (f)-(i) show fracture surfaces of tungsten materials produced from a single crystal by HPT. While (f) was just severe plastically deformed (UFG-W^{sc}), the other materials were subsequently recrystallized at 600°C (W^{sc}_{600}) (g), 800°C (W^{sc}_{800}) (h) or 1200°C (W^{sc}_{1200}) (i).

B.3 Results

Microscopic observations of the fracture surfaces in figure B.1 show two types of brittle fracture: intergranular and transgranular fracture. While the ratio of intergranular to transgranular fracture varies significantly, every specimen shows fracture along the GBs as well as cleavage fracture.

B.3.1 Samples with an ultra low impurity concentration

The four materials produced from the tungsten single crystal (W-SC) exhibit no impurities at the GBs within the resolution limit of the used Auger electron spectroscopy (AES) device; namely UFG-W^{sc}, W^{sc}_{600}, W^{sc}_{800} and W^{sc}_{1200} (figure B.1f-i). The Auger-spectrum of one of these samples, W^{sc}_{1200}, can be seen in figure B.2a - a typical spectrum for tungsten [18] - where, other than a very small O-peak at $\sim 510\,\mathrm{eV}$, the spectra are clean and similar. The samples were cleaned before putting them on the fracture stage in the UHV chamber and fracturing them within the chamber. After that, the samples were moved from the fracture position to the analyze position and the spectra were recorded. As the time between fracturing and analyzing was relatively short, the detected O cannot be adsorbed on the new fracture surface from the remaining gas in the vacuum. Small O peaks like shown in figure B.2-a are sometimes visible on different samples and differ in their heights. If they appear, they are usually visible at GBs as well as on cleaved grains which can be found in the high purity W as in this case. Therefore, it can be concluded that this O peak (only when there is no difference in the peak height between the spectra of a GB and the cleaved grains) is a consequence of a desorption process from some other surfaces of

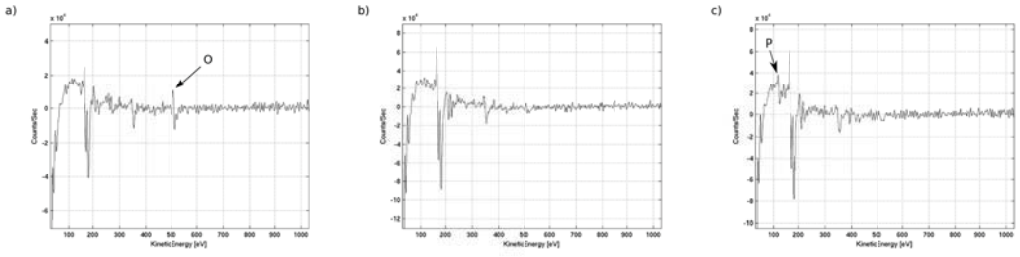

Figure B.2 Auger electron spectroscopy analyzes of investigated tungsten materials. (a) is showing the AES-spectrum of a severe plastically deformed tungsten single crystal which was subsequently recrystallized at 1200°C for an hour in a vacuum furnace. The O-peak at 510eV represents the adsorbed oxygen after fracturing the sample in the analysis chamber. (b) is showing the AES-spectrum of technically pure tungsten which was just severe plastically deformed. The spectrum shown in (c) represents technically pure tungsten rods where after a rolling deformation mainly phosphorous (123eV) was found at the grain boundaries. All spectra were taken at grain boundaries.

the sample or the sample holder during fracture or the sample manipulation and an adsorption process on the newly generated fracture surface which has a high sticking coefficient.
While the percentage of fracture that is intergranular is almost 100% for the UFG-W^{sc} and the W^{sc}_{600} (crack propagation front tangential to the axis of the HPT specimen [16]), the other recrystallized samples, W^{sc}_{800} and W^{sc}_{1200}, show increasing transgranular fracture with increasing recrystallization temperature as shown in table B.2.

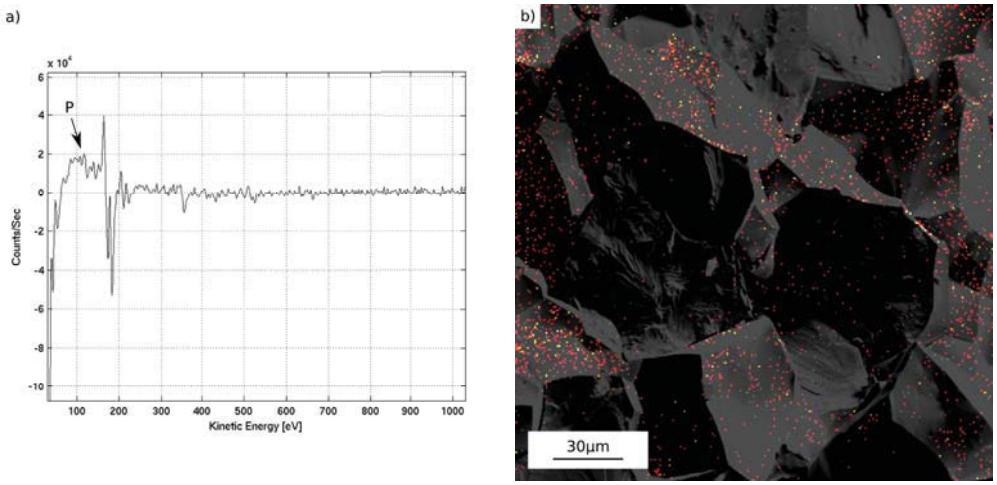

Figure B.3 (a) is showing the AES spectrum of the grain boundary of $W_{recryst}$ indicating P as the only impurity. (b) depicts the fracture surface of recrystallized tungsten with a P-mapping as an overlay showing P covering several grain boundaries.

B.3.2 Technically pure tungsten samples

Compared to the nearly impurity-free materials, $W_{sintered}$, W_{rolled} and $W_{recryst}$ as well as UFG-W and W^{1200} contain the typical impurities shown in table C.1. While $W_{sintered}$, W_{1200} and UFG-W (in tangential direction) are dominated by intergranular fracture, $W_{recryst}$, with an average grain size of $95.2 \pm 35.7\,\mu$m, shows an increased amount of transgranular fracture. W_{rolled} has a mixture of both fracture types with a higher amount of grain boundary fracture along the axis and cleavage fracture is dominating the cross section of the rods.
Figure B.2-b shows the AES-spectrum of UFG-W. Except for the difference in the O-peak, the spectrum is basically the same like the W^{sc}_{1200} spectrum in figure B.2-a. P (peak at $\sim 123\,$eV), the only detected impurity of W_{rolled}, was found on almost all GBs which can clearly be seen in the AES-spectrum of figure B.2-c. $W_{recryst}$ and W_{1200} are materials with quite different grain sizes, however in both cases most GBs are covered with phosphorous. This can be seen for example in figure B.3-b, an

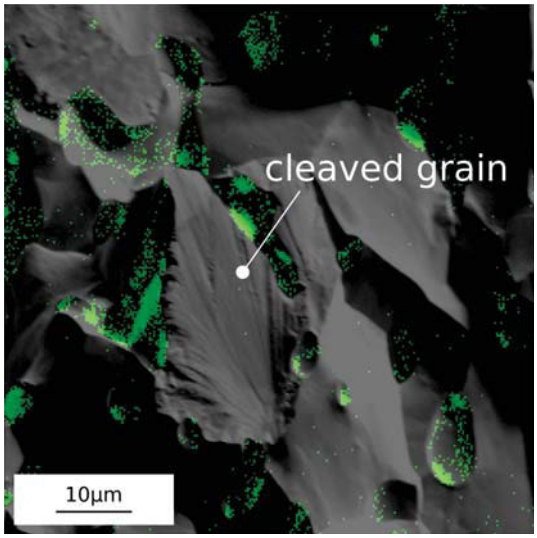

Figure B.4 Fracture surface of $W_{sintered}$ with a P-mapping as an overlay showing P concentrated in the sinter pores.

overlay of a P-mapping over the corresponding fracture surface of $W_{recryst}$. Figure B.3-a shows the additional AES spectrum of a GB, indicating P as the only impurity. Another P-mapping as an overlay on the SEM image of the fracture surface of $W_{sintered}$ can be seen in figure B.4. Clearly visible is the P concentrated in the sinter pores.
Despite most GBs of W_{rolled}, $W_{recryst}$ and W_{1200} being covered with P, the highest fraction of cleavage fracture is found in W_{rolled}. $W_{recryst}$ and W_{1200} show a higher fraction of intergranular fracture, while $W_{sintered}$ and UFG-W (in tangential direction), materials with a relatively low impurity concentration at the GBs, show most intergranular fracture.

B.3.3 Samples with a high impurity concentration

W_{hipped} contains a much higher amount of impurities, as already described in section B.2. An O-mapping as an overlay on the corresponding SEM image of the fracture surface is shown in figure B.5, showing that oxygen covers almost all GBs. The dominant fracture type is intergranular fracture which is clear in figure B.1-e, however, the amount of fracture along the GBs is smaller than for $W_{sintered}$ as shown in table B.2.

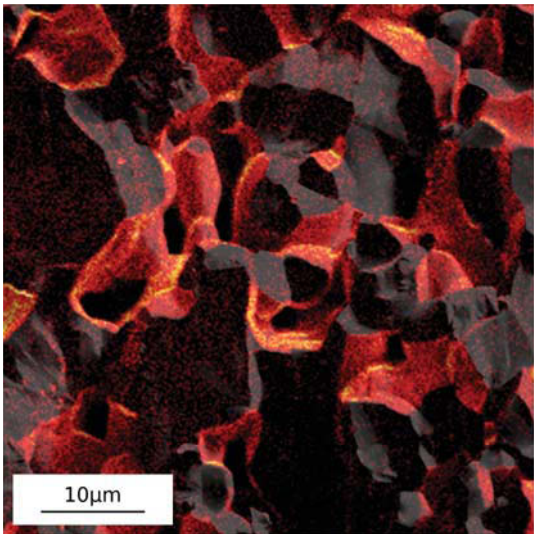

Figure B.5 Fracture surface of W_{hipped} with an overlaying O-mapping showing O covering most grain boundaries.

B.4 Discussion

B.4.1 Influence of impurities

Impurities like O, P or C generally cover high angle GBs as they are not soluble in tungsten [19]. A varying amount of GBs obtained by either just recrystallizing a pre-deformed material or a combination of SPD and recrystallization, as it was applied in this study, leads to a varying impurity concentration on the GBs. The shear deformation during HPT distributes the impurities on the increasing density of high angle GBs and as a result the concentration of impurities per GB area should decrease. Materials produced from the single crystal have very low impurity concentrations and the density of GBs does hardly influence the material with respect to the impurity concentration per GB area especially at smaller grain sizes. Technically pure tungsten materials are changing their impurity concentrations per GB area with their GB proportions. This can also be seen in figure B.2-b, the AES data of UFG-W. The material has a very high density of GBs, impurities are extremely wide distributed and therefore the spectrum looks very similar to UFG-W^{sc} (figure B.2-a). Although impurities were not found at the GBs of these materials, cracks propagate inter- and transgranularly which is more dependent on the size and shape of the grains than on the concentration of impurities on the grain boundaries. Similar effects have also been seen in iron [16].
Most samples were recrystallized after the HPT deformation, thus having a lower density of GBs and therefore a higher concentration of impurities on the GBs compared to the UFG samples. Despite the smaller grain size and the lower GB impurity concentration of W_{1200} compared to $W_{recryst}$, both materials with a recrystallized

microstructure (figure B.1-c and B.1-k, respectively), W_{1200} shows the higher fraction of intergranular fracture which can be seen in table B.2. This is contrary to the expected fracture behavior as a lower GB impurity concentration is assumed to have a larger GB fracture toughness and therefore transgranular fracture should happen more often. Figure B.3-b shows the SEM image of a recrystallized tungsten material with an overlay of a P mapping. The mapping shows clearly that P is covering most of the GBs, however, the weakening-effect on the GB is not as pronounced as to just obtain intergranular fracture. The corresponding spectrum in figure B.3-a indicates P as the only impurity at the GBs. As the recrystallized materials produced from the former single crystal show different fractions of inter- and transgranular fracture and impurities do not play a role in these cases, it is obvious that factors like size and shape of the grains, which will be discussed in the following section B.4.2, play a more significant role for the cleavage of GBs or grains.
Another material with a relatively high number of GBs, depending on the degree of deformation, is W_{rolled}. The rolling deformation of the material leads to elongated grains and therefore a high density of GBs, although far fewer than for the UFG-materials. The impurities are widely distributed on the relatively high density of GBs, which decreases their weakening-effect and therefore transgranular fracture should be preferred. While cleavage fracture was found beside $\sim 70\,\%$ intergranular fracture along the axis of the rod, transgranular fracture is the dominant type in the case of crack propagation perpendicular to rolling direction. Although P was found on several GBs, which can be seen in the spectrum of figure B.2-c, its weakening-effect on the GBs is rather limited and does not force a crack to propagate just intergranularly although a lot of GBs are available due to the elongated grain structure. However, instead of propagating just along the GBs, it seems much easier for a crack to cleave grains too.
The crack path is governed by the local driving force in the different propagation directions and the corresponding crack propagation resistances. The local driving force is determined by the global driving force and the local geometry of the crack. The possible crack propagation directions for cleavage crack propagation are given by the possible cleavage planes and the geometry of the grain boundaries. The resistance for cleaving the grain boundary and the resistance for cleaving the grain can depend on many parameters, for example the dislocation density. It is important to note that both crack propagation resistances depend on temperature in a different manner. This results in a change of the ratio between transgranular and intergranular fracture at different temperatures [11]. For the crack propagation perpendicular to rolling direction an almost transgranular fracture behavior is observed (figure B.1-b). Due to the heavily elongated grains the crack encounters predominately GB's which are perpendicular to the macro crack propagation direction. The driving force for a 90° kinked crack is significantly smaller than for the unkinked one [20]. Only for the case that the fracture resistance for the intergranular fracture is less than $\frac{1}{2}$ of the fracture resistance for transgranular fracture (in terms of stress intensity factor), a crack deflection along the grain boundaries should occur. That is obviously not the case. The weakening due to the impurities is not sufficient in the

present case. The fracture experiments for the crack propagation in rolling direction indicate that the fracture resistance at room temperature is only somewhat smaller than the resistance to cleave grains, because both fracture modes are present.
$W_{sintered}$ is a technically pure tungsten material with an average grain size of $\sim 25\,\mu$m. Although P, the only detected impurity, can mainly be found in the sinter pores and is not covering the GBs (figure B.4), intergranular fracture is the dominant fracture type for this material. Compared to that, W_{hipped}, the only material with a significantly higher O concentration, where most of the GBs are covered by O as shown in figure B.5, shows a lower fraction of intergranular fracture than $W_{sintered}$. Although both materials have the same porosity and a similar grain size their fracture behavior is quite different. This cannot be caused just by impurities especially since W_{hipped}, the material with the higher impurity concentration, has a higher fraction of cleavage fracture as shown in table B.2. The reason for such a behavior is probably the grain size distribution as well as the morphology which will be discussed in section B.4.2.
The investigations show that an increased number of GBs by e.g. a very fine grain structure or elongated grains, is able to distribute GB impurities widely enough to avoid an effect on the boundaries. However, the typical grain boundary impurities like O or P, as they are present in the small amounts in these technically used materials or in the W_{hipped}, do not seem to influence the crack path significantly.

B.4.2 Influence of grain size

Due to the high density of GBs in UFG-W and UFG-W^{sc}, impurities have no effect on the crack path. The varying fractions of inter- and transgranular fracture in the different directions of a HPT sample [16] demonstrate an effect of the shape of the grains. Such an effect can also be seen in the case of the rolled material. Most of the GBs are partly covered with P, hence a decrease in the fracture resistance of the GBs is expected. Obviously that is not the case in the investigated material, the effect of impurities seems to be to small compared to other parameters. Compared to these materials all other investigated samples have equiaxed grains except for the W^{sc}_{600}. After recrystallizing at 600°C an aspect ratio and therefore a dependency on the testing direction of the sample remains. However, the samples with equiaxed grains, especially W^{sc}_{800} and W^{sc}_{1200} with low impurity concentrations and also W_{1200} and $W_{recryst}$ demonstrate a very pronounced dependency of the fracture characteristic on the grain size. Table B.2 clearly shows a decreasing fraction of intergranular fracture with increasing grain size. While in the case of fine grained W materials crack propagation along grain boundaries is favored, in the coarse grained recrystallized materials cleaved grains are more frequently observed. The difference might be explained by the different crystal texture as the probability to find cleavage planes parallel to the macroscopic crack propagation plane is determined by the texture. Another possibility could be an intrinsic effect of the grain size on the resistances to fracture grain boundary or grain. For ideal brittle fracture such behavior is not expected however in the cleaving process of tungsten a certain plasticity is involved

hence such effect might be possible especially for very small grains. However, in the present case we believe that the variation of the ratio of transgranular fracture to intergranular fracture is not dominated by the mentioned effect, it is more related to the grain size distribution. In the fine grained materials there is a more sharp grain size distribution than in the coarse grained materials. In a material with equiaxed grains and small variation in grain size the crack can follow without large deviation the macroscopic crack plane along the grain boundary. In the case of a bimodal distribution of grain size, the crack has to deviate sometimes more from the crack propagation plane. To avoid this the larger grains are sometimes cleaved.
$W_{sintered}$ is a material with a relatively large grain size of $\sim 25\,\mu$m and almost 100 % intergranular fracture. The materials has the highest fraction of intergranular fracture while most impurities are in the pores and the GB impurity concentration is relatively low. W_{hipped}, a material with the same porosity of 16 %, has a slightly smaller grain size and a much higher O concentration at the GBs. It is also dominated by GB fracture but has a higher amount of cleaved grains. From the production history one may imagine that $W_{sintered}$ and W_{hipped} have a very similar microstructure. However, that is not the case, $W_{sintered}$ exhibits a well developed polycrystalline microstructure with a relatively unique grain size and a prososity of 16 %. W_{hipped} has a similar porosity, however, the grains contain a higher dislocation density as a result of the HIP process and the grain size shows a larger variation. Furthermore it is interesting to note that despite the higher impurity content of W_{hipped}, the fracture toughness is larger than of $W_{sintered}$ ($K_Q^{hipped} = 11.0\,\mathrm{MPa\,m^{0.5}}$ $> K_Q^{sintered} = 7.9\,\mathrm{MPa\,m^{0.5}}$). The reason for this surprising behavior is not obvious, it seems that the higher roughness of the fracture surface which might be caused by the larger variation in grain size, is responsible for both, the increase of transgranular fracture and the increased fracture toughness of W_{hipped}. The observations indicate that grain boundary impurities do not influence the fracture behavior of technically pure tungsten as strongly as other factors. An increased dislocation density due to an elongated grain structure, like the microstructure of W_{rolled}, seems to have more of a positive effect on the fracture toughness than grain boundary impurities can influence it in a negative way.

B.5 Concluding remarks

The fracture surfaces of ten tungsten materials differing in grain size, microstructure and impurity concentration were investigated by Auger electron spectroscopy and scanning electron microscopy.
1. All samples were fractured in the low temperature regime (room temperature) where the expected brittle fracture behavior was observed with varying proportions of intergranular and transgranular fracture.
2. A strong dependence of the grain size and microstructure on the fracture behavior was observed for materials with a low impurity concentration, technically pure

tungsten materials and materials with a high impurity concentration.
3. Auger electron spectroscopy measurements show that a decreasing grain size, and hence an increasing density of grain boundaries, leads to a reduction of grain boundary impurities.
4. Fracture surface analyzes of recrystallized materials with larger grain sizes and a relatively low density of grain boundaries show that certain amounts of transgranular fracture can be found for such materials despite most grain boundaries being covered with phosphorous. The same behavior can be found for rolled tungsten with elongated grains and a relatively high amount of grain boundaries.

The experiments clearly indicate that the occurrence of intergranular fracture cannot be correlated with the difference in grain boundary impurities. The fraction of transgranular to intergranular fracture is controlled by other effects, like the shape of grains, the grains size distribution, texture, dislocation density and temperature. The fracture resistance of even impurity free grain boundaries in tungsten at room temperature is somewhat lower than the resistance to cleave the grain. The observed differences in impurities do not seem to change this relation significantly. A transgranular fracture therefore only occurs when the propagation of the crack along the grain boundary is sufficiently unfavorable due to geometrical reasons. The statement that the grain boundary impurities do not effect the ratio of intergranular to transgranular fracture does not mean that the impurities do not have any impact on the ductility. It might be that in the ductile regime or in deformation experiments with crack free samples the impurities which occur sometimes in islands on the grain boundaries may be responsible for a crack initiation or formation of pores on this islands. The crack propagation resistance is not affected by a small quantity of such assumed islands, as shown in this study. Therefore, only the simple occurrence of grain boundary fracture in tungsten is not a hint for impurity induced embrittlement.

Bibliography to paper B

[1] B. Gludovatz, S. Wurster, A. Hoffmann and R. Pippan, Int. J. Refract. Met. Hard Mater. (2010) *in press*.

[2] P.L. Raffo, J. Less-Common Met. 17 (1969) p. 133.

[3] A. Wronski and A. Fourdeux, J. Less-Common Met 6 (1964) p. 413.

[4] G.A. Geach and J.E.Hughes, 2^{nd} Plansee Seminar (1955) p. 245.

[5] R.I. Jaffee, C.T. Sims and J.J. Harwood, 3^{rd} Plansee Seminar (1958) p. 380.

[6] G.L. Davis, Nature 181 (1958) p. 1198.

[7] P.J. Burdon and G.L. Davis, Nature 185 (1960) p. 455.

[8] A.W. Funkenbusch, F. Bacon and D. Lee, Met. Trans. A 10A (1979) p. 1085.

[9] A. Joshi and D.F. Stein, Met. Trans. 1 (1970) p. 2543.

[10] J.M. Liu and B.W. Shen, Acta Met. 30 (1982) p. 1197.

[11] Tran-Huu-Loi, J.P. Morniroli, M. Gantois and M. Lahaye, J. Mater. Sci. 20 (1985) p. 199.

[12] H. Danninger, F. Knoll, B. Lux, P. Wilhartitz and M. Grasserbauer, Int. J. Refract. Met. Hard Mater. 4 (1985) p. 92.

[13] A. Vorhauer and R. Pippan, Scr. Mater. 51 (2004) p. 921.

[14] A.P. Zhilyaev and T.G. Langdon, Prog. Mater. Sci. 53 (2008) p. 893.

[15] M. Faleschini, H. Kreuzer, D. Kiener and R. Pippan, J. Nucl. Mater. 367 (2007) p. 800.

[16] A. Hohenwarter and R. Pippan, Mater. Sci. Eng., A 527 (2010) p. 2649.

[17] R.W. Margevicius, J. Riedle and P. Gumbsch, Mater. Sci. Eng., A 270 (1999) p. 197.

[18] K.D. Childs, B.A. Charlson, L.A. LaVanier, J.F. Moulder, D.F. Paul, W.F. Stickle and D.G. Watson, *Handbook of Auger Electron Spectroscopy*, Third Edition, Physical Electronics, Inc., Eden Prairie, Minnesota, 1995.

[19] B. Predel, *Landolt-Börnstein - Numerical Data and Functional Relationships in Science and Technology*; Group IV: Physical Chemistry; Thermodynamic Properties - Phase Equilibria, Crystallographic and Thermodynamic Data of Binary Alloys, vol. 5i, Springer-Verlag, Berlin Heidelberg, 1998.

[20] R. Pippan, Eng. Fract. Mech 44 (1993) p. 821.

C

A study into the crack propagation resistance of pure tungsten

B. Gludovatz[a,b], S. Wurster[a], A. Hoffmann[c], R. Pippan[a,b]

[a]Erich Schmid Institute of Materials Science, Austrian Academy of Sciences, A-8700 Leoben, Austria
[b]Christian Doppler Laboratory for Local Analysis of Deformation and Fracture, A-8700 Leoben, Austria
[c]Plansee Metall GmbH, A-6600 Reutte, Austria

Abstract

Recrystallized and deformed tungsten have been investigated with respect to the crack resistance as a function of crack extension. The compact tension specimens were manufactured with different crack plane orientations with respect to the axis of a rod. All recrystallized samples fractured predominantly intergranularly, whereas the deformed samples fractured transgranularly in certain crack propagation directions. Both showed an increase in the fracture resistance with crack extension, i.e. they exhibit an R-curve behavior. It was determined in this study that the consolidation of the various fracture planes and crack bridging causes R-curve behavior in tungsten.

C.1 Introduction

Fracture toughness is an important parameter when characterizing the mechanical behavior of materials and describes the resistance of a material against crack propagation. For ductile materials it is usually assumed that the fracture resistance is independent of the crack extension, based on the concept of Irwin [1]. The energy to generate a fracture surface under linear elastic fracture mechanic conditions is the specific surface energy plus the specific plastic work to extend the crack, both are assumed to be independent of the absolute crack length. As a consequence the critical energy release rate and therefore also the critical stress intensity factor should not depend on crack extension. In the case of ceramics it is well known that the fracture resistance increases with crack extension until it reaches a steady state value, see for example [2]. This increase of the fracture resistance is called R-curve behavior. To characterize the resistance against fracture, a curve, for example the critical stress intensity versus crack extension, is required instead of a single parameter like the plane strain fracture toughness, K_{IC}, or the critical energy release rate G_{IC}. Due to their ductile behavior the fracture toughness of metals and alloys is usually characterized by a single parameter determined according to a certain standard, for example the ASTM standard E399 [3]. Bcc metals show a ductile to brittle transition with a relatively high fracture resistance at high temperatures caused by the microductile fracture process and a low fracture resistance at low temperatures induced by a cleavage like crack propagation. Despite the different fracture process, the fracture toughness below as well as above the ductile transition temperature is usually determined by the same procedure.
The aim of this paper is to show that for tungsten at low temperatures the fracture resistance shows R-curve behavior similar to ceramics despite the plasticity which is involved in the fracture process. Microstructures which exhibit predominantly intergranular and transgranular cleavage fracture are analyzed. Furthermore, special attention is paid to the effect of the pre-crack on the resulting R-curve.

C.2 Experimental methods

The crack propagation behavior under monotonic loading of a technically pure tungsten in the recrystallized and deformed state were used in this investigation. The chemical composition is given in table C.1 and the two investigated microstructures are presented in figure C.1. Both microstructures exhibit an elongated grain structure. The substructure of dislocations in the deformed material is clearly reflected in the orientation micrographs by the changes of the crystal orientation. The experimental procedure is first described for the recrystallized material and then the deformed one.

Compact tension, C(T), specimens (width 6 mm; thickness 3 mm), with different crack propagation directions according to ASTM standard E399 [3], were manu-

Table C.1 Main impurity elements of the technically pure tungsten (W > 99.97%) investigated.

Element	C	H	N	O	P	S	Si
Guaranteed analysis (max) / μg/g	30	5	5	20	20	5	20
Typical analysis / μg/g	10	2	< 2	5	< 10	< 2	5

factured out of a technically pure tungsten rod. Because of the elongated grain structure due to the rolling process of the rod, the crack plane orientations of the manufactured samples play an important role on the crack propagation direction. Consistent with ASTM standard E399, the position of a sample is identified by a two letter crack plane orientation code. The *first* letter designates the direction normal to the crack plane and the *second* letter the expected direction of the crack propagation with respect to the axis of the rod. *C* stands for *circumferential*, *R* for *radial* and *L* for *longitudinal*. After notching with a diamond wire saw and polishing by razor blade, the samples were recrystallized at 2000°C for one hour leading to a slightly elongated grain structure, as shown in figure C.1-a. The specimens were subsequently fatigue pre-cracked under cyclic compression (R = 20). In this case - recrystallization *before* pre-cracking - the crack-tip is generally in the interior of the grain. For recrystallization *after* pre-cracking the crack-tip is expected to lie at a grain boundary. To investigate this in more detail, C(T) samples of the same specification but recrystallized *after* pre-cracking were also manufactured. Furthermore, a part of the tungsten rod was deformed to 110 % at 650°C in compression leading to pronounced elongated grains (figure C.1-b). C(T) specimens were again manufactured and pre-cracked afterwards. Samples were loaded monotonically at $\sim 0.5\,\mu$m/sec with a "Kammrath & Weiss" tensile-compression testing machine mounted in a Zeiss LEO 1525 field-emission scanning electron microscope (FE-SEM). Load and crack extension on the surface of the samples were recorded simultaneously.

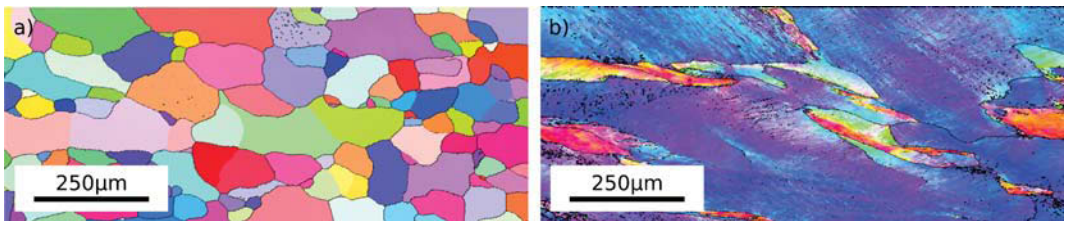

Figure C.1 Microstructures of the tungsten samples investigated. The inverse pole figure (IPF) maps show that both materials, the recrystallized (a) and the deformed tungsten (b), have an elongated grain structure. Compared to the recrystallized material the deformed sample shows a pronounced substructure, obvious from the changes of the crystal orientation.

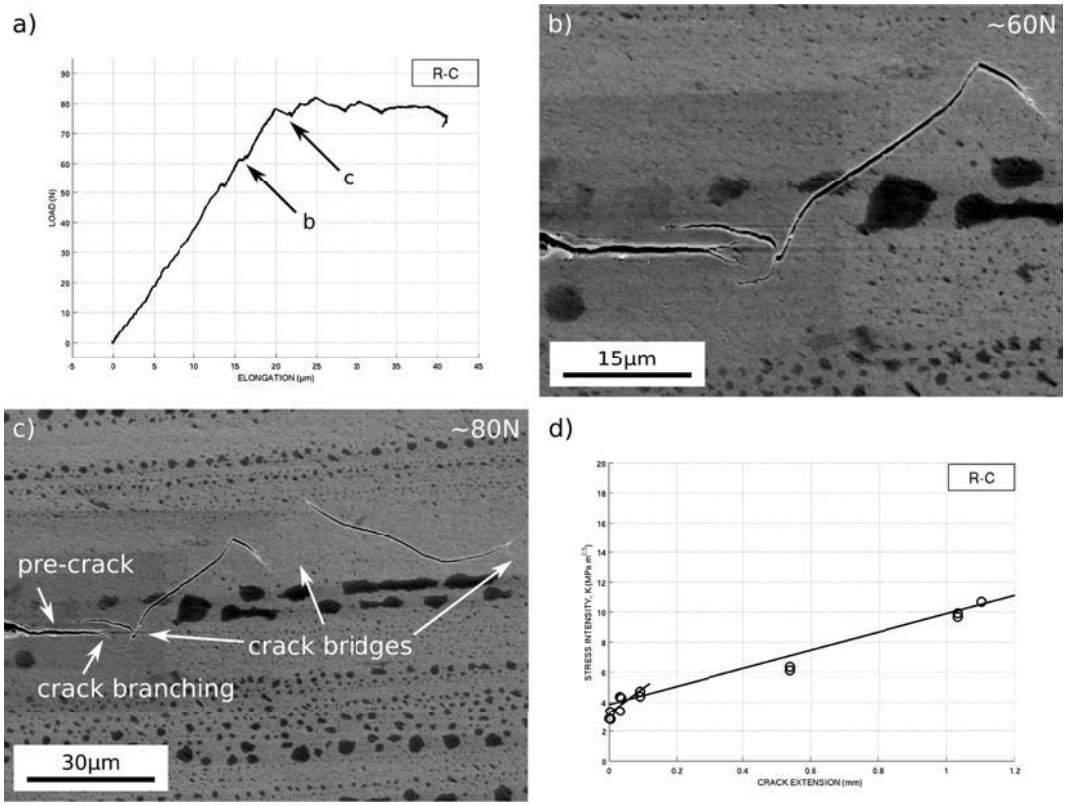

Figure C.2 R-curve behavior of intergranular fractured tungsten. The sample was manufactured in *R-C* crack plane orientation out of a rod according to ASTM standard E399 [3]. The load displacement curve (a) shows a linear elastic increase without significant plastic deformation before the first load drop occurs. The crack propagates straight from the root of the pre-crack, (b), before the crack front deviates in two directions resulting in several crack bridges, (c). (d) shows the increasing stress intensity K as a function of the crack extension Δa. (The regularly distributed dark areas on the surface stem from cleaning with ethanol.)

C.3 Results

Figure C.2 shows the load displacement curve (a), some micrographs of the crack tip at different loads, (b) and (c), and the resulting stress intensity versus crack extension behavior (d) of a typical experiment. The samples show a linear elastic increase of the load followed by load drops corresponding to crack extensions. Plastic deformation prior to the first crack extension was not observed. Further increase of the load led to further load drops corresponding to crack propagation. Since the crack extensions do not occur along the whole crack front not every load drop could be seen on the surface as a crack extension, for example at 52 N. Figures C.2-b and C.2-c show SEM pictures from the crack extensions at the second and third load drop ($K \approx 3\text{-}5\,\mathrm{MPa\,m^{0.5}}$), this is close to the transition from the initial

to the extended part of the R-curve. The crack propagates straight from the root of the pre-crack followed by crack branching. Branching often leads to crack bridges, such bridges are observed on the surface, see figure C.2-c. Figure C.2-d depicts the stress intensity K as a function of the crack extension Δa calculated *before* and *after* each crack propagation. A steep increase in K with increasing Δa, starting at about $3\,\mathrm{MPa\,m^{0.5}}$, is clearly visible for this sample with R-C crack plane orientation. The following flattening of the crack resistance curve leads to a K of approximately $10\,\mathrm{MPa\,m^{0.5}}$ at a crack extension of 1 mm.

Figure C.3 shows two R-curves of recrystallized tungsten with L-R crack plane orientation. The sample with higher fracture resistance (square and diamond symbols) was manufactured, then recrystallized and finally fatigue pre-cracked - this sample will be subsquently referred to as fatigue pre-cracked in this section. The specimen with the lower stress intensities (triangle symbols) was manufactured in a similar way but recrystallized *after* the fatigue pre-cracking - this sample will be subsequently referred to as recrystallized within this section. The recrystallized sample starts at a stress intensity of about $3.5\,\mathrm{MPa\,m^{0.5}}$ compared to about $6.5\,\mathrm{MPa\,m^{0.5}}$ of the fatigue pre-cracked sample. Both show a similar increase of the observed R-curve. After a macroscopically straight crack propagation the cracks of the two

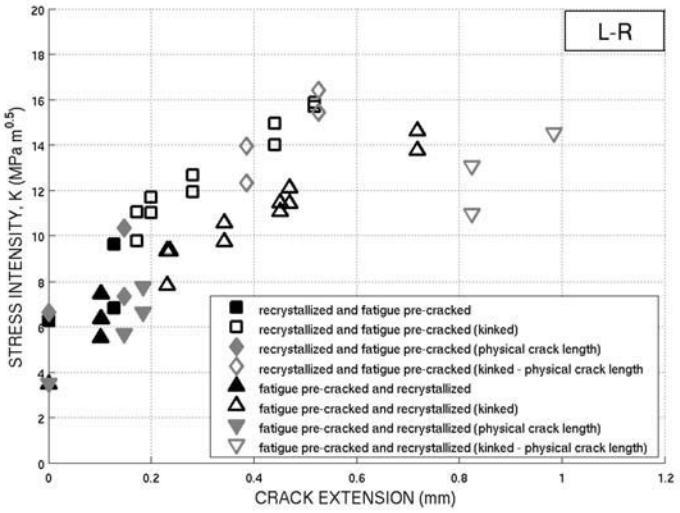

Figure C.3 R-curves of recrystallized tungsten in the L-R crack plane orientation. One sample was manufactured, recrystallized and finally fatigue pre-cracked in cyclic compression (square and diamond symbols). The other sample was fatigue pre-cracked and finally recrystallized (triangle symbols). Pure mode I cracks are depicted with solid symbols, while kinked cracks have empty symbols. For these kinked cracks the projected crack length and the physical crack length are both plotted where these values differ. R-curve behavior is observed for both samples.

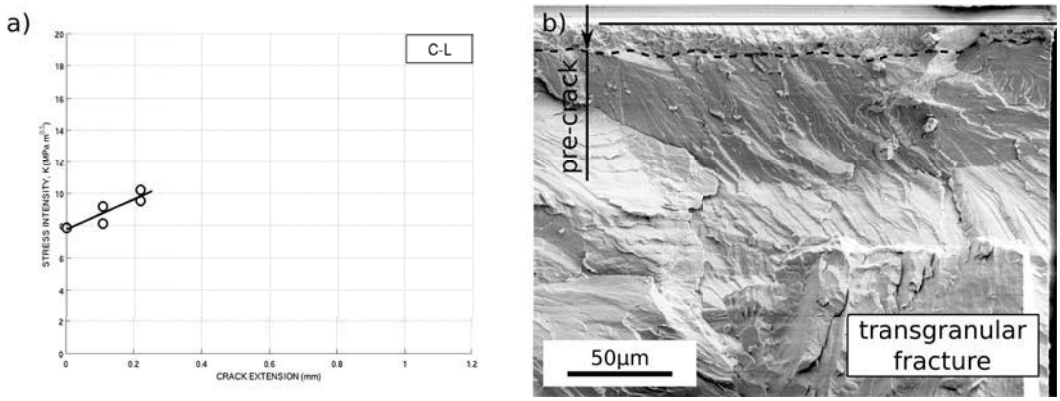

Figure C.4 Fracture resistance as a function of crack extension in deformed tungsten. The sample was manufactured with *C-L* crack plane orientation according to ASTM standard E399 [3]. Stable crack propagation starts at $8\,\mathrm{MPa\,m^{0.5}}$ until the stress intensity reaches about $10\,\mathrm{MPa\,m^{0.5}}$, $200\,\mu\mathrm{m}$ crack extension, at this point failure is catastrophic, (a). Cleavage of grains was observed as the predominant fracture mechanism, starting from the uneven front of the fatigue pre-crack, (b).

samples kink into the direction of the elongated grains. The filled symbols are valid mode I stress intensities. The empty symbols represent values of kinked cracks. However, they were calculated as mode I cracks with both, the projected *and* the physical crack lengths. This way of calculating the stress intensities leads to values of up to $16\,\mathrm{MPa\,m^{0.5}}$ before catastrophic failure occured.
The heavily deformed samples, manufactured with *C-L* crack plane orientation, do not show measurable plastic deformation prior to first crack propagation at stress intensities of about $8\,\mathrm{MPa\,m^{0.5}}$ either. The fracture resistance, shown in figure C.4-a, increases to $10\,\mathrm{MPa\,m^{0.5}}$ at 0.2 mm crack extension before catastrophic failure. Starting from the fatigue pre-crack, grain cleavage is predominantly found on the fracture surface (figure C.4-b). Crack bridges, as depicted in figure C.2-b, were not observed for these samples.

C.4 Discussion

The experiments have shown that in recrystallized as well as deformed tungsten, independent of the crack propagation direction, the fracture resistance at room temperature increases with crack extension. This is usually called R-curve behavior. Depending on the type of microstructure - deformed or recrystallized - transgranular or intergranular fracture is dominant. Hence for both types of fracture R-curve behavior is observed.
The initial part of the R-curve for the recrystallized and fatigue pre-cracked samples (figure C.2-d) originates from the primarily transgranular arrested fatigue pre-crack cleaving the encountered grains. Hereafter, the crack switches to mainly intergran-

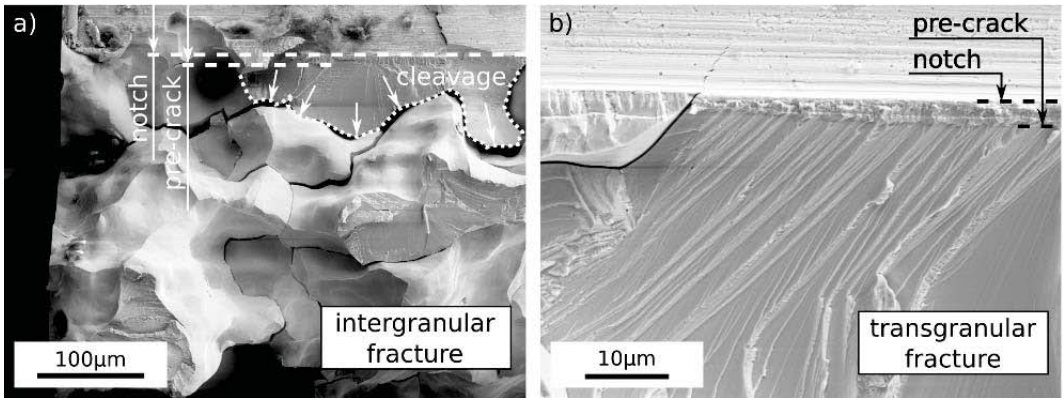

Figure C.5 Crack propagation of transgranularly arrested fatigue pre-cracks. In recrystallized materials cracks switch to mainly intergranular fracture after cleaving those grains penetrated by the pre-cracks, (a). Processes necessary to combine the different cleavage planes determine the initial part of the R-curve (b).

ular crack propagation. This indicates that the crack propagation resistance of the grain boundaries is somewhat smaller than the resistance to cleave grains. Such a transition can be seen in figure C.5-a, where the notch, the pre-crack and the intergranular fractured ligament are indicated. The initial part of the R-curve should be mainly caused by processes which are necessary to connect the different cleavage planes (figure C.5-b). The remaining part of the R-curve is dominated by larger crack bridges which are formed by connecting grains. Bridging is often a result of crack branching, which might occur as a combination of geometrical reasons and small differences in the local crack propagation resistance of the grain boundaries. Such bridges are shown in figure C.2-b, close to the pre-crack, and along the whole crack path in figure C.6. The inverse pole figure (IPF) maps of a C(T) specimen with a crack in the *R-L* plane orientation show intergranular fracture with no signs of extensive plastic deformation around the crack. Limited plastic deformation is observed a few micrometers from the crack faces even at room temperature, shown as details in figure C.6. More plastic deformation can sometimes be found at grains which form crack bridges or along the crack flanks at elevated temperatures [5].

C.4.1 Influence of crack propagation direction

The sample in figure C.2 was manufactured with *R-C* crack plane orientation resulting in a fatigue pre-crack parallel to the longer axis of the grains. The crack can therefore propagate relatively directly along the grain boundaries without major global deviations. Figure C.7-b depicts a sample with *L-R* crack propagation orientation where the fatigue pre-crack was perpendicular to the major axis of the grains. The crack starts intergranularly and propagates along the grain boundary before crack branching occurs. After bridging the crack kinks about 90° to the for-

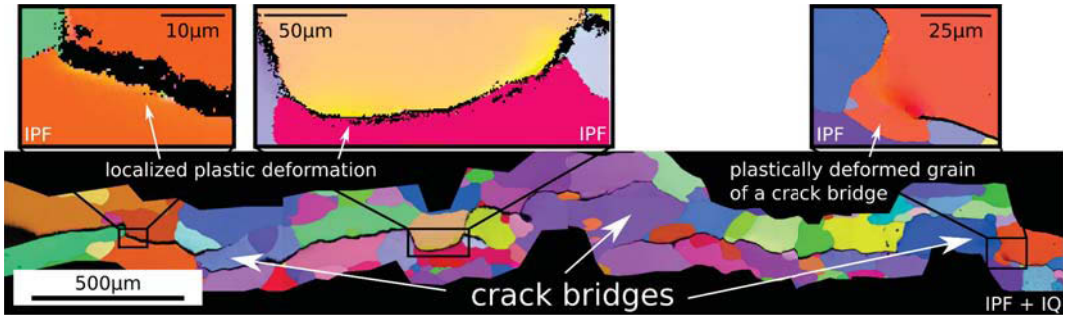

Figure C.6 Electron backscatter diffraction (EBSD) scan of the crack path in a recrystallized C(T) specimen with *R-L* crack plane orientation. The IPF map is depicted as an overlay on the image quality (IQ) map, showing that the crack propagates predominantly along the grain boundaries. (The IQ describes the quality of EBSD pattern and is dependent on the material and its condition [4].) The propagated crack exhibits a lot of crack bridges. Plastic deformation, i.e. a change in the color, is only very localized along the crack path and at grains which form crack bridges, shown in the IPF maps.

mer direction and propagates along the grain boundaries parallel to the longer axis of the grains. A possible reason for this behavior might be a significantly higher fracture resistance in this direction resulting from the orientation of the elongated grains. This forces a crack to change to the longitudinal direction with the lower fracture resistance along the grain boundaries.
The discussed recrystallized microstructures fractured predominantly intergranularly whereas the deformed material fractured mainly transgranularly. This microstructure exhibits R-curve behavior as shown in figure C.4-a. Starting from the fatigue pre-crack, the initial crack propagation is controlled by connecting the different cleavage planes. Further crack propagation occurs in the same global direction which can also be seen in the transgranularly dominated fracture surface (figure C.4-b). Despite the lower resistance of the grain boundaries, cleavage seems to be the preferred fracture type for deformed tungsten in this direction. A possible reason for this behavior could be the significantly increased dislocation density, which causes a pronounced subgrainstructure (figure C.1-b). This might lead to a slightly textured microstructure which decreases the fracture resistance in this direction. Therefore, transgranular crack propagation occurs rather than major crack deviations to intergranular fracture. Hence the R-curve is just dependent on the cleavage process in this case. Influences like the dislocation densities, the grain orientation or texture were not taken into account in these investigations and have to be examined in further studies.

C.5 Concluding remarks

Compact tension specimens of tungsten were investigated with respect to its crack resistance behavior. The tests were performed at room temperature and the crack extension was measured in-situ in a scanning electron microscope.

1. Tungsten shows R-curve behavior of the fracture resistance for most investigated specimens.
2. Transgranular dominated fracture shows a relatively steep increase of the R-curve over short crack extensions until catastrophic failure occurs.
3. Fracture along the grain boundaries often results in a continuous increase in the stress intensities over long crack extensions.
4. As discussed, the crack initiation might play an important role on the initial part of the crack propagation behavior (for details see Appendix).
5. In the present experiments, no significant influence of a heat treatment subsequently to fatigue pre-cracking was observed (for further details also see Appendix).
6. The initial part of the R-curve is dominated by connecting different cleavage planes in the near crack tip region. Crack bridges somewhat further from the pre-crack tip govern the further increase of the fracture resistance.

The investigations show that tungsten, despite its brittle behavior at low temperature, cannot be described with a single fracture toughness value. The crack propagation starts at relatively low stress intensities, the increasing fracture resistance with increasing crack length leads to significant larger toughness values. Both, the microstructure and the crack propagation direction significantly affects fracture toughness R-curve of tungsten.

Appendix

The generation of pre-cracks in fracture mechanics samples of brittle materials is not a straight forward task, especially when the R-curve behavior of the fracture resistance should be determined. The increase of the fracture resistance with crack extension is mainly caused by extrinsic toughening mechanisms [6]. In the present case these are geometrical effects due to crack deflection, crack branching and crack bridging. Furthermore, residual stresses may introduce shielding or anti-shielding effects. Therefore, the resulting R-curve might be affected significantly by the pre-cracking procedure used. In the following the used technique and different alternative procedures are discussed.

Crack initiation by cyclic compression

Fatigue pre-cracking in cyclic compression initiates a crack which arrests in the plastic zone ahead of the crack tip [7–10]. The maximum length of the crack depends on the size of the plastic zone and the load ratio. Cyclic compression leads to tensile stresses ahead of the crack tip, causing an anti-shielding effect. Such stresses normally decrease the fracture resistance and should therefore be removed by a subsequent heat treatment of the sample. However, in the case of the tested tungsten samples an influence on the R-curve could not be observed, as shown in figure C.7-a. The sample pre-cracked *after* recrystallization started with an even higher fracture resistance than the one with recrystallization as the final step. This indicates a rather limited effect of the cyclic compression on the fracture resistance compared to the influence of other factors. However, it should be noted that the applied cyclic compression load was always as small as possible, cracks were generated only somewhat larger than $10\,\mu$m.
The significantly different starting values may partially result from the initial crack propagation by cleavage compared to crack propagation along the grain boundary. In the case of recrystallization as the final step, grain boundaries move to the tip of the pre-crack leading to a predominantly intergranular starting crack. This could lead to lower starting values of the R-curve due to a slightly lower fracture resistance of the grain boundary. Additionally, the deviation along the grain boundary away from to the global crack propagation direction should be taken into account when discussing the difference in the starting values of the two sample. Cyclic compression after recrystallizing leads to transgranular pre-cracks instead. Beside influences like, for example, the position of the crack plane with respect to the cleavage plane, residual stresses might also influence the R-curve. However, their effect seems rather limited compared to other influences on the fracture resistance, as shown in figure C.3. Nevertheless, such residual stresses should be kept to a minimum by using small loads in cyclic compression. This also leads to short fatigue pre-cracks, this is important in studying the initial part of the R-curve. However, a minimum pre-crack length of $\Delta l > 2\,R$, where Δl is the length of the pre-crack measured from the notch root and R is the notch root radius, should be taken into account, to avoid an influence of the notch geometry [11].
To discount the influence of residual stresses on the fracture resistance of tungsten after fatigue pre-cracking, annealing should be sufficient enough to remove these stresses. However, a subsequent recrystallization after the cyclic compression is an easy way to get a predominantly intergranular pre-crack for this material. It is possible that residual stresses might alter the recrystallization of tungsten, however, this was not observed in the investigated microstructures.

Although pre-cracks should be kept short, some investigated samples had relatively long starting cracks of up to $100\,\mu$m on the surface. In recrystallized tungsten such long pre-cracks normally arrest at a grain boundary. Further crack extensions do not occur along the whole crack front, especially since the front of a crack is

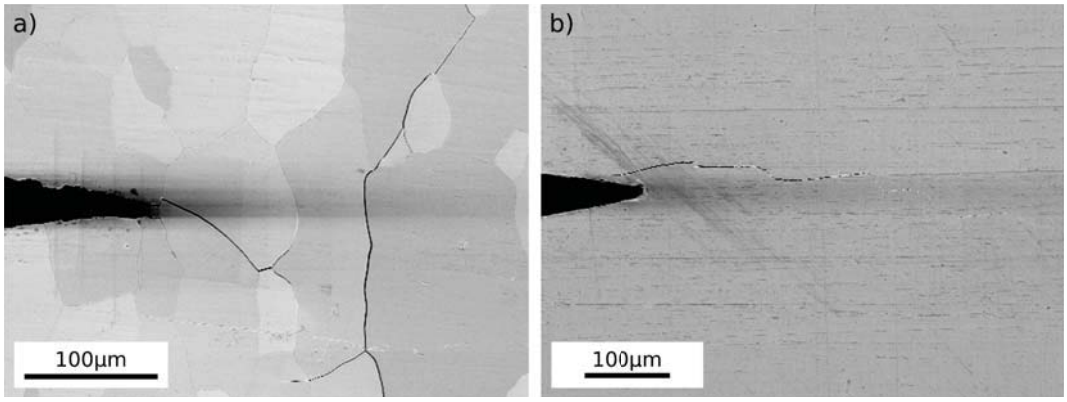

Figure C.7 Crack propagation starting from pre-cracks in recrystallized tungsten. A sample with *L-R* crack plane orientation [3] leads to a change in the global crack propagation direction, now perpendicular to the pre-crack along the longer axis of the slightly elongated grains (a). A crack bridge directly at the pre-crack causes a crack starting from a flank of the notch at the surface (b).

naturally uneven. This might cause crack bridges due to geometrical reasons, also occuring directly at the pre-crack as shown in figure C.7-b. The crack at the surface started from a flank of the notch behind the pre-crack. Such bridging shields the crack-tip which raises the materials initial crack resistance behavior. Therefore, short starting cracks might be a good way to prevent this toughening at the initial stage of the R-curve, as already discussed for bridging ceramics [12].
Aside from the initial part of the fracture resistance curve, the stress intensities of both samples in figure C.3 increase with crack extension. Differences in the R-curve might result from the amount and size of bridges along the crack path. Both samples exhibit crack propagation starting from the pre-crack.

Cracks machined with the focused ion beam (FIB)

Although fatigue pre-cracking works relatively well for brittle materials decreasing specimen sizes often cause problems in this step, particularly for the production of short cracks. This leads to either a very time consuming process or, in the worst case, to catastrophic failure of the sample in the manufacturing stage. Therefore some groups [13,14] use a focused ion beam (FIB) for cutting very fine notches working as pre-cracks. This is a useful method, especially for extremely small specimens, where fatigue pre-cracking is hardly possible [15, 16].
The same principle, just with larger samples, is shown in figure C.8-a. The FIB-notch is cut into a tungsten alloy, has a length of about 100 μm and a width of about 1 μm on top. Such FIB cuts have a depth of about 10 μm and an estimated root radius of 0.01 μm. This leads to a crack like defect. Therefore, crack propagation mainly starts from the notch root, which can also be seen in figure C.8-c. The

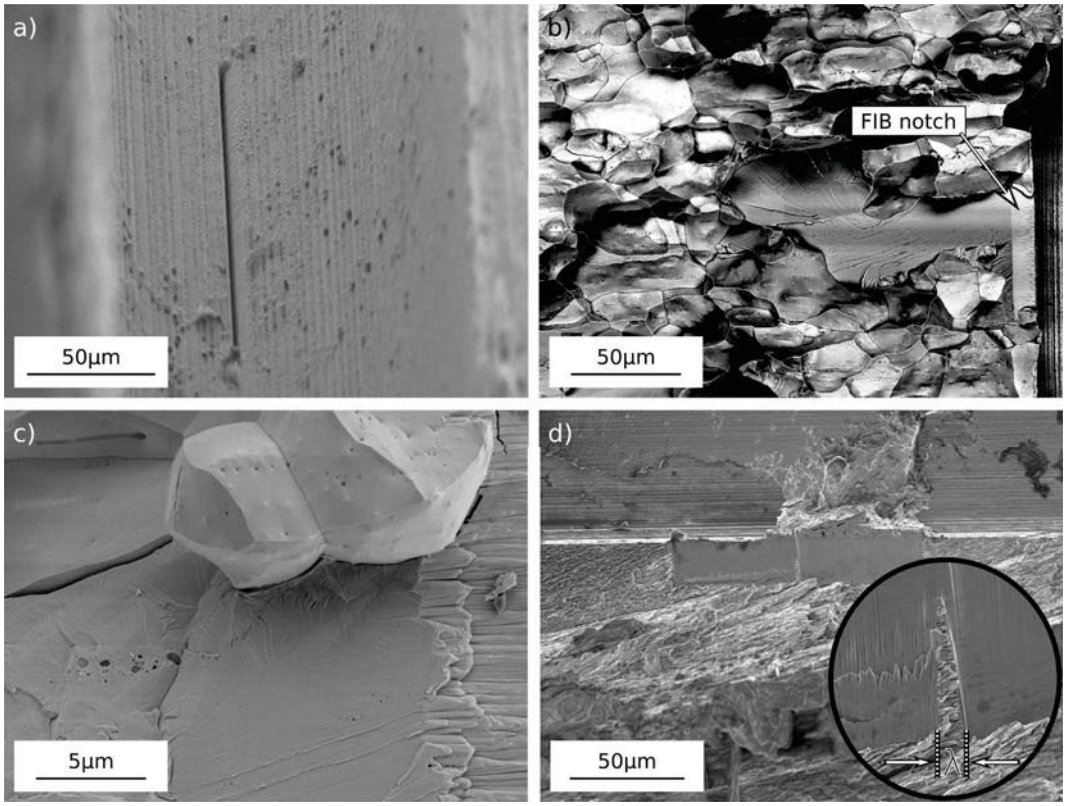

Figure C.8 SEM fractographs showing pre-cracks generated with a focused ion beam (FIB). A single FIB cut at the root of a razor blade polished notch (a). SEM fractograph of a fracture mechanic tungsten alloy sample where the generation of the crack from the FIB notch is depicted (b). The crack starts mainly transgranularly before it switches to fracture along the grain boundaries (b, c). A remaining bridge between two FIB cuts is used as a stress concentrator to initiate a crack at the notch root (d).

fracture resistance for this initial stage is controlled by cleavage, as the notches are predominantly cut into the grains. After first crack propagation the crack switches to grain boundary fracture due to its lower fracture resistance (figure C.8-b/C.8-c). One may argue that such a notch is not atomistically sharp. A possibility to overcome this problem is to cut notches with a FIB as shown in figure C.8-d. The two neighboring notches are cut into ultra-fine grained (UFG) tungsten and each has a length of about 50 μm and a width of about 2 μm on top. The depth of about 20 μm is necessary for the remaining bridge between the notches, as shown in the detail of figure C.8-d. Such a bridge causes a stress concentration. At the notch root a crack initiates at the maximum of the stress intensity, this is directly dependent on the width, λ, of the bridge.
Although such artificial cracks, with root radii of estimated 0.01 μm, are not as sharp as for fatigue pre-cracked specimens, they are very useful. This is particularly true

for brittle materials and small samples where the time required is relatively low and the sample cannot be destroyed, as it is possible with fatigue pre-cracking.

Compound bending technique

Another possibility for making atomistically sharp cracks in a brittle metals was used by Riedle for pre-cracking tungsten single-crystals [17–19]. The technique uses a combination of two or three beams which allows an overlap of compressive stress fields ahead of a notch of a 3-point bending specimen. A beam, underneath the tungsten specimen to be pre-cracked, moves the neutral axis of the whole setup to the vicinity of the notch. When loading the specimen a crack initiates, propagates and arrests in the compressive stress field ahead of the crack tip. Sharp cracks with final lengths of about $500\,\mu$m are produced which are ideal for fracture toughness measurements. However, such cracks are too long for the measurement of an R-curve as all toughening mechanisms are fully developed.

Electrical-discharge machining

Electrical-discharge machining is a common method for manufacturing fracture toughness specimens as well as notches in metallic materials, see for example [20–22]. The roots of such notches often have cracks which are ideal for further crack propagation investigations. However, generally more than a single crack initiates, leading to complicate stress intensity profiles along the crack front and no through thickness crack is usually generated. Furthermore, one has to take into account that the crack is a result of a thermal shock loading and is therefore not free of residual stresses.

Summary of the effect of pre-cracking

It is evident from the discussion that each technique used to generate a pre-crack for the measurement of the R-curve of fracture resistance in the brittle regime of bcc metals has advantages and disadvantages. The most important advantages and disadvantages and related consequences for the R-curve are summarized in table C.2. An important fact which has to be taken into account, is that the crack path with the lowest fracture resistance can be the grain boundaries or the cleavage planes of grains. Furthermore, it should be noted that the crack tip plasticity might be significantly affected by the crack path.

Table C.2 Techniques to generate pre-cracks for the measurement of the R-curve of fracture resistance in the brittle regime of bcc metals. Listed are advantages, disadvantages and consequences for the R-curve of each method.

Pre-cracking technique	Advantage	Disadvantage	Consequences for the R-curve
Tension - tension fatigue	- well established	- difficult to apply in brittle metals - very short through thickness crack can not be generated	- pre-crack is often impossible to generate or is too long
Cyclic compression	- easy to apply - well defined, short crack	- residual stresses	- the residual stresses may reduce the stress intensity in the initial part of the R-curve - the change in crack path may increase the initial part of the R-curve
Cyclic compression and thermal heat treatment	- well defined, short crack	- fatigue crack path often differs from the overload fracture crack path - can only be applied in cases where the heat treatment does not affect the mechanical properties	- if the crack path a pre-crack do not agree with the overload crack path an increase of the initial part of the R-curve can be expected
FIB machining	applicable to - all materials - small sample sizes	- notch front does not agree with the low energy crack path - for large samples it is too expensive to generate a through thickness notch	- the transition to the low energy crack path should increase the initial part of the R-curve
Compound bending	- crack path of pre-crack is identical to the overload fracture crack path	- too long for R-curve measurement	- not applicable to determine the interesting initial phase of an R-curve
Electrical discharge	- relatively easy to apply to very brittle metals	- no through thickness crack - multi-cracks - residual stresses are present	- initial coalescence may increase the initial part of the R-curve - residual stresses may reduce the initiation toughness

Bibliography to paper C

[1] G.R. Irwin: *J. Appl. Mech.*, 1957, vol. 1957, pp. 361–364.

[2] R.O. Ritchie: *Int. J. Fract.*, 1999, vol. 100, pp. 55–83.

[3] American Society for Testing and Materials: *E 399 - 90: Standard Test Method for Plane-Strain Fracture Toughness of Metallic Materials - Annual Book of ASTM Standards*, 1997, vol. 03.01., pp. 413–443.

[4] EDAX: Orientation Image Microscopy - Analysis Software v5.31

[5] B. Gludovatz, S. Wurster, A. Hoffmann, and R. Pippan: *Int. J. Refract. Metals Hard Materials*, 2010, *in press.*

[6] R.O. Ritchie: *Mater. Sci. Eng. A*, 1988, vol. 103 (1), pp. 15–28.

[7] C.N. Reid, K. Williams, and R. Hermann: *Fatigue Engng. Mater. Struct.*, 1979, vol. 1, pp. 267–270.

[8] W.Y. Chu, C.M. Hsiao, L.J. Jin, and T.H. Liu: *Scripta Metall.*, 1983, vol. 17 (8), pp. 993–96.

[9] S. Suresh: *Engng. Fract. Mech.*, 1985, vol. 21 (3), pp. 453–63.

[10] R. Pippan: *Fatigue Fract. Engng. Mater Struct.*, 1987, vol. 9 (5), pp. 319–28.

[11] T. Fett, S. Fünfschilling, M.J. Hoffmann, R. Oberacker, H. Jelitto, and G.A. Schneider: *J. Am. Ceram. Soc.*, 2008, vol. 91 (11), pp. 3638–42.

[12] J.J. Kruzic, R.L. Satet, M.J. Hoffmann, R.M. Cannon, and R.O. Ritchie: J. Am. Ceram. Soc., 2008, vol. 91 (6), pp. 1986–94.

[13] M. Faleschini, H. Kreuzer, D. Kiener, and R. Pippan: *J. Nucl. Mater.*, 2007, vol. 367–370 (1), pp. 800–05.

[14] B. Gludovatz: Diploma Thesis, University of Leoben, Austria, 2006.

[15] K. Matoy, H. Schönherr, T. Detzel, T. Schöberl, R. Pippan, C. Motz, and G. Dehm, *Thin Solid Films*, 2009, vol. 518 (1), pp. 247–56.

[16] D. Di Maio and S.G. Roberts: *J. Mater. Res.*, 2005, vol. 20 (2), pp. 299–302.

[17] J. Riedle, P. Gumbsch, H.F. Fischmeister, V.G. Glebovsky, and V.N. Semenov: *Mat. Res. Soc. Symp. Proc.*, 1996, vol. 409, pp. 23–28.

[18] J. Riedle, P. Gumbsch, and H.F. Fischmeister: *Phys. Rev. Let.*, 1996, vol. 76 (19), pp. 3594–97.

[19] G. Bergmann and H. Vehoff: *Scripta Metall. Mater.*, 1994, vol. 30 (8), pp. 969–74.

[20] A.S. Booth and S.G. Roberts: *Acta Mater.*, 1997, vol. 45 (3), pp. 1045–53.

[21] T.D. Joseph, M. Tanaka, A.J. Wilkinson, and S.G. Roberts: *J. Nucl. Mater.*, 2007, vol. 367–70 (1), pp. 637–43.

[22] M. Tanaka, A.J. Wilkinson, and S.G. Roberts: *J. Nucl. Mater.*, 2008, vol. 378 (3), pp. 305–11

D

Influence of deformation, microstructure and temperature on the fracture resistance of tungsten

B. Gludovatz[a,b], S. Wurster[a], A. Hoffmann[c], R. Pippan[a,b]

[a]Erich Schmid Institute of Materials Science, Austrian Academy of Sciences, A-8700 Leoben, Austria
[b]Christian Doppler Laboratory for Local Analysis of Deformation and Fracture, A-8700 Leoben, Austria
[c]Plansee Metall GmbH, A-6600 Reutte, Austria

Abstract

Technically pure tungsten has been investigated with respect to its fracture resistance. Compact tension and disc compact tension specimens were tested, taking into account the influence of deformation, microstructure and temperature. Samples were taken from three different directions of a rod and tests were performed in-situ in a scanning electron microscope (SEM) and in a vacuum chamber equipped with a radiation furnace. Crack extensions were measured either on the surface of the samples with the SEM or by the standard DC potential drop method. Elongated grains show the most pronounced effect on the fracture resistance and lead to a strong dependence of the R-curve of fracture resistance on the crack propagation direction of the sample. Deformation increases the fracture resistance but leads to reduced R-curve behavior while elevated temperatures result in a more pronounced and improved R-curve behavior.

D.1 Introduction

The relatively low ductility of tungsten and most tungsten alloys at room temperature is the main drawback in the application of these materials. Extensive research to improve these properties was performed in the sixties, see for example [1–4]. These activities were driven by the potential for application as high temperature materials for aircraft engines. With the introduction of the Ni-based super alloys most research activities on this topic stopped. Due to its excellent combination of properties for several high temperature applications in future fusion reactors, the interest on the structural application of W or W alloys has substantially increased. The fracture toughness is one of the most important parameters in characterizing the ductility. However, the investigations on these properties in W are very scarce [5,6]. Even in the 1950s and 1960s no attention was devoted to this property, this was mainly due to fracture mechanics at that time being not well developed. In a recent study we have shown that the fracture toughness of polycrystalline W at room temperature can exhibit a pronounced increase of the fracture resistance with crack extension, this is called R-curve behavior. It is well known that the ductility in tension or bending experiments of tungsten and its alloys is significantly affected by the microstructure, see for example [7]. However, the knowledge of microstructure effects on fracture toughness is limited, as already mentioned, and nothing is known - to the knowledge of authors - with respect of the effect of microstructure on the R-curve behavior of tungsten.
The following study is a first attempt to quantify the effect of grain shape, dislocation substructure and temperature on the R-curve of the crack growth resistance.

D.2 Experimental

Four technically pure tungsten cylinders with a diameter of 20 mm and a height of 30 mm were recrystallized at 2700°C for one hour. The achieved microstructure after recrystallization had slightly elongated grains remaining from the rolling production of the rods with a grain diameter d of about 240 μm in the cross section and a length l of about 280 μm, giving an aspect ratio of $d/l \sim 0.86$. To study the influence of deformation on the fracture resistance, two cylinders were compressed at room temperature to 2 % and 20 %, while the others were compressed to 2 % and 110 % at 350°C and 650°C, respectively (figure D.1-a). Deformation was more pronounced in the middle part of the cylinders which became obvious due to barreling (figure D.1-b). Therefore, they were cut in three sections and the effect of deformation on the crystal structure was analyzed by electron backscatter diffraction (EBSD) scans on top of every section. Compact tension, C(T), specimens were manufactured with different crack propagation directions, with respect to the axis of the cylinders. The position of each sample is identified by a two letter crack plane orientation code, consistant with ASTM standard E399. The first letter designates the direction normal to the crack plane and the second letter the expected direction of the crack

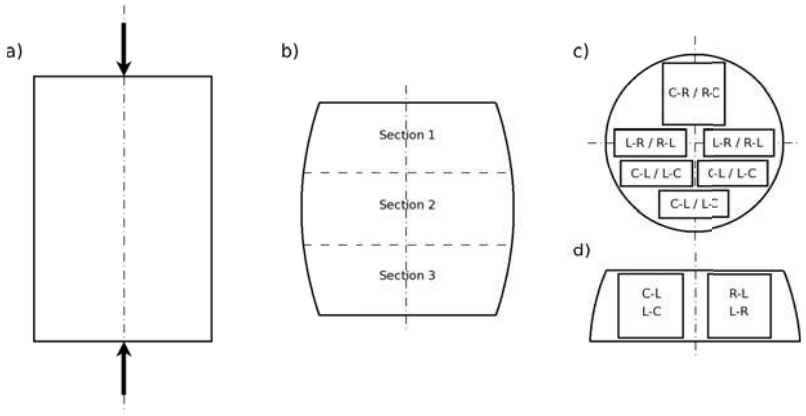

Figure D.1 Deformation of tungsten and manufacturing of compact tension samples. Undeformed tungsten cylinders (a) were compressed at room temperature or elevated temperatures. The deformed cylinders were cut in three sections (b) and compact tension with different crack plane orientations, with respect to the axis of the cylinder, were manufactured (c, d) according to ASTM standard E399 [8].

propagation with respect to the axis of the cylinder. C stands for circumferential, R for radial and L for longitudinal. The samples (width 6 mm; thickness 3 mm), in accordance with ASTM standard E399 [8], were taken from all sections of the room temperature deformed cylinders as well as the cylinder deformed at 350°C, as shown in figure D.1-c/-d. The height, about 10 mm, allowed manufacture of samples from just one section of the 110 % deformed material. Some of these specimens were stress relieved at 1000°C for one hour to investigate if there are residual stresses and how they affect the toughness. An additional set of specimens with the same dimensions were machined from recrystallized tungsten for comparison. All samples were fatigue pre-cracked under cyclic compression [9,10] leading to an average crack length of about xx μm.
The specimens were loaded monotonically at $\sim 0.5\,\mu$m/sec with a "Kammrath & Weiss" tensile-compression testing machine mounted in a "Zeiss LEO 1525" field-emission scanning electron microscope (FE-SEM). The load and the crack mouth opening displacement were recorded together with the crack extension measured on the surface of the samples.

According to ASTM standard E399 [8], disc-shaped compact tension, DC(T), specimens (width 14.8 mm; thickness 7.4 mm) were manufactured in the C-R direction out of a 20 mm tungsten rod to investigate the fracture resistance of rolled and recrystallized tungsten at elevated temperatures. Both microstructures are shown in figure D.2. The material with the rolled microstructure had grains with a diameter of 40 μm in the cross section (a) and a length of 150 μm (b). The grain aspect ratio d/l is about 0.27. Subsequent fatigue pre-cracking under cyclic compression resulted in crack lengths, measured from the notch root, of 10 - 100 μm. To perform tests on

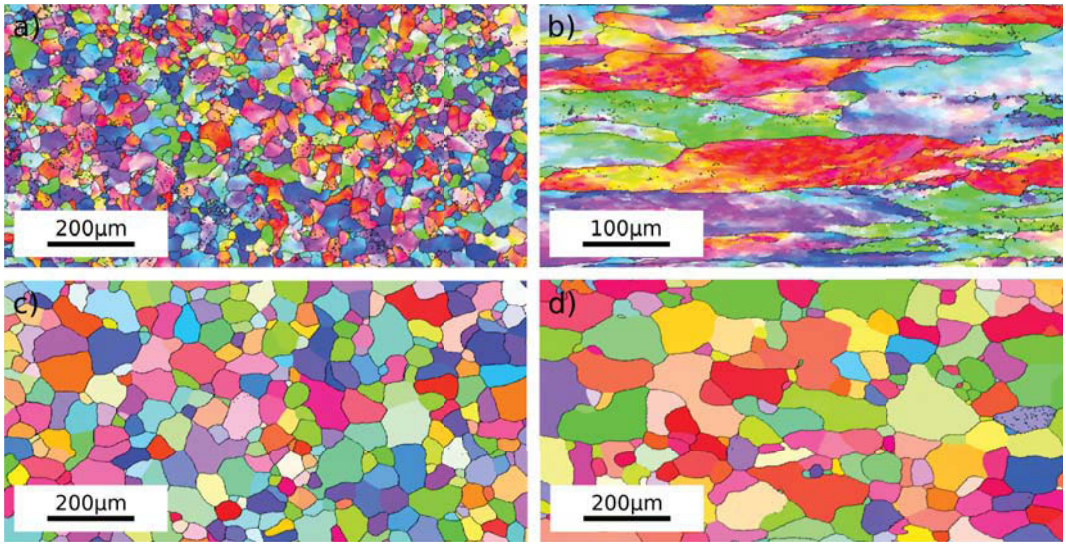

Figure D.2 Microstructures of rolled (a, b) and recrystallized (c, d) tungsten. From the IPF maps of the elongated grains (b, d) and the cross section scans (a, c), it is obvious that both materials exhibit an elongated grain structure, whereas just the rolled tungsten has a pronounced subgrain structure. This can be seen in the changes of the crystal orientation.

recrystallized tungsten some samples were subsequently recrystallized at 2000°C for one hour leading to grains with a diameter d of about 80 μm in the cross section (c) and a length l of about 115 μm (d). This gives a grain aspect ratio d/l of about 0.70.
Tests were performed with a "ZWICK" universal testing machine equipped with a vacuum chamber and a radiation heater capable of heating to 700°C. The samples were monotonically loaded at 6.67 μm/sec and the load was monitored together with the crack propagation using the standard DC potential-drop method [11]. The tested samples were analyzed in the SEM and evidence of plastic deformation along the crack path was recorded by electron backscatter diffraction (EBSD) measurements.

D.3 Results

Figure D.3 shows EBSD scans from the top surface of each middle section of the four deformed cylinders. While 2% deformation at room temperature (a) does not show development of a pronounced substructure in the grains, the same degree of deformation at 350°C causes clearly visible changes in the orientation, which are induced by the stored dislocations, as shown in (b). Significantly higher grain misorientation can be found after 20% deformation at room temperature (c). However, such heavy deformation at low temperatures also results in a decohesion of some of the grain boundaries, which is obvious in (c). Figure D.3-d shows the sample

Figure D.3 Electron backscatter diffraction (EBSD) scans from the upper surface of each middle section of the four deformed cylinders; 2% @ RT (a), 2% @ 350°C (b), 20% @ RT (c) and 110% @ 650°C (d).

deformed to 110% at 650°C. In this case very high misorientation in the grains was generated but no degradation of grain boundaries is visible.
Table D.1 shows the corresponding Vickers hardness of the deformed materials and of recrystallized tungsten. Starting from the lowest values for the recrystallized material, 2% deformation at elevated temperature leads to a more pronounced increase in the hardness than both room temperature deformations. The highest values can be found for the 110% deformed tungsten, as expected.

C(T) samples with different crack plane orientations tested at room temperature

The compression did not cause a homogeneous deformation of the four tungsten cylinders. The mid sections exhibited higher degrees of deformation compared to the top and the bottom of each of the cylinders. Therefore, the fracture toughness of samples taken from the top or bottom region and the mid section were distinguished. Despite their differences in microstructure, most experiments exhibited an increase in the fracture resistance with increasing crack extension. This can be seen in figure D.4 for the 2% deformed tungsten cylinders and in figure D.8 for the higher deformations. Figure D.11 depicts a similar behavior for samples of the recrystallized

Table D.1 Vickers hardness of deformed and recrystallized tungsten.

Deformation grade	2% @ RT	2% @ 350°C	20% @ RT	110% @ 650°C	recrystallized
Vickers hardness (-)	409.2	483.1	459.6	519.5	374.8

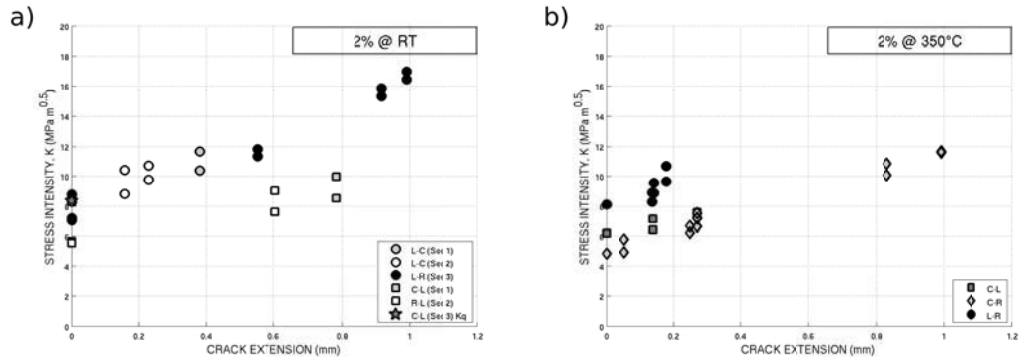

Figure D.4 R-curves of the fracture resistance of tungsten deformed 2% in compression at room temperature (a) and 350°C (b), tested at room temperature. Samples with *L-R* crack propagation direction show first crack extensions at about 8 MPa $m^{0.5}$. *C-L* samples start at lower values of about 5 - 6 MPa $m^{0.5}$. *C-R* specimens are similar to *C-L* specimens with starting values of about 5 MPa $m^{0.5}$ in the case of the material deformed at elevated temperatures.

tungsten. The increase in the fracture resistance with increasing crack extension for samples from all three sections is similar, as long as they have the same crack propagation direction. As an example, figure D.4-a shows samples from all sections of the material deformed to 2% at room temperature. It is obvious that samples with *L-C* crack plane orientation of section 1 and section 2 show similar R-curve behavior as the sample with *L-R* crack plane orientation of section 3, which has the same crack propagation direction. Additionally shown are samples with another crack propagation direction, a "*C-L* - sample" of section 1 and an "*R-L* - sample" of

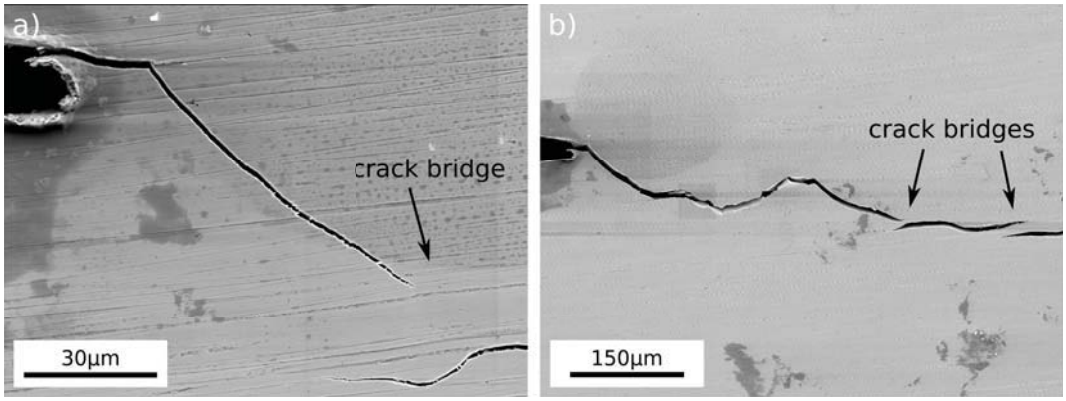

Figure D.5 Samples with *C-L* - crack plane orientation manufactured from section 3 after 2% deformation at 350°C. Crack bridges govern the whole crack path, near the notch root (a) and along the propagated crack (b).

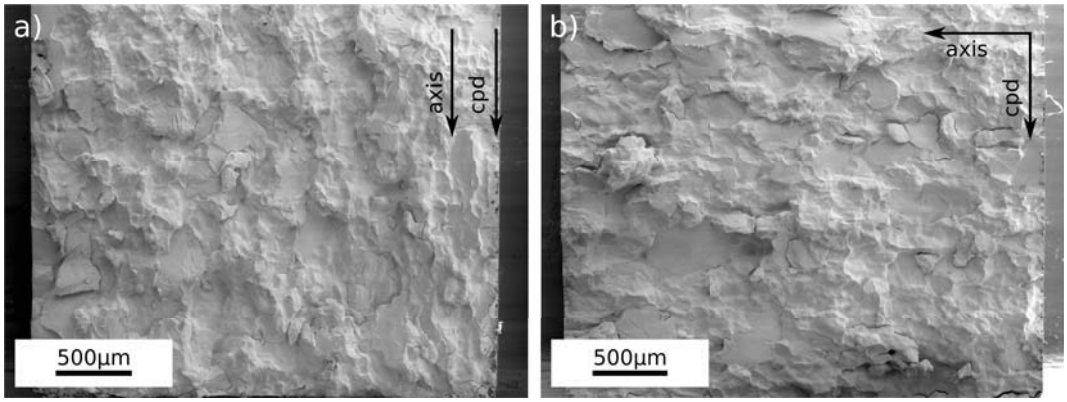

Figure D.6 Samples with different crack propagation directions from the 2% at 350°C deformed tungsten. The fracture surface of the "*C-L* - sample" (a) as well as of the "*R-C* - sample" (b) show both grain boundary dominated fracture with some cleaved grains. (In all fractographs the direction of crack propagation and the axis of the cylinder are indicated.)

section 2. Both have a somewhat different R-curve behavior compared to the other crack propagation direction, they do not however differ relative to each other. Microstructural differences between the different sections seem to be too small to have an effect on the R-curve of fracture resistance. Therefore, for each crack propagation direction one representative sample is shown for the other deformation grades and for the recrystallized material.

Figure D.4-a also shows that crack propagation of the "*R-L*" and the "*C-L* - samples" 2% deformed at room temperature starts at about $6\,\mathrm{MPa\,m^{0.5}}$, which is

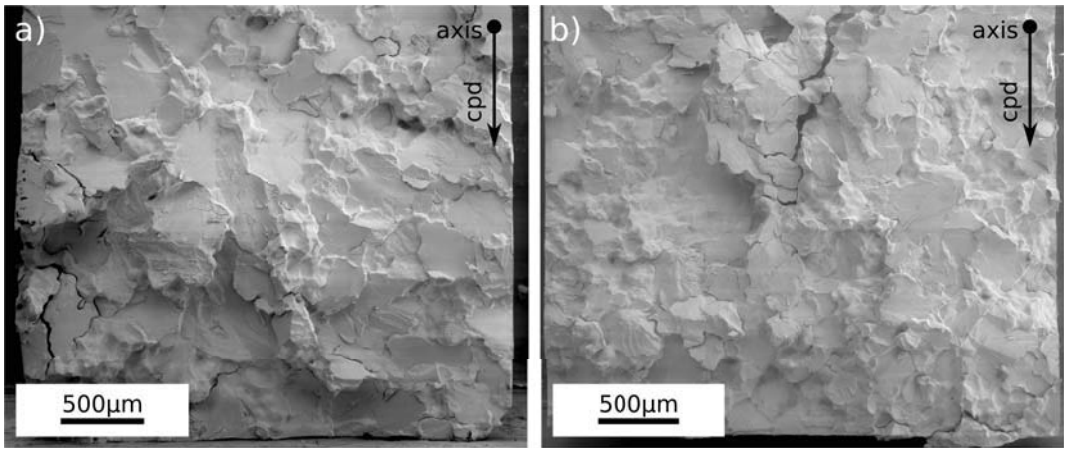

Figure D.7 Fracture surfaces of 2% deformed tungsten materials. (a) depicts an *L-C* - sample deformed at room temperature dominated by cleavage fracture. The *L-R* - sample in (b) was deformed at 350°C and shows also cleavage as the main fracture type.

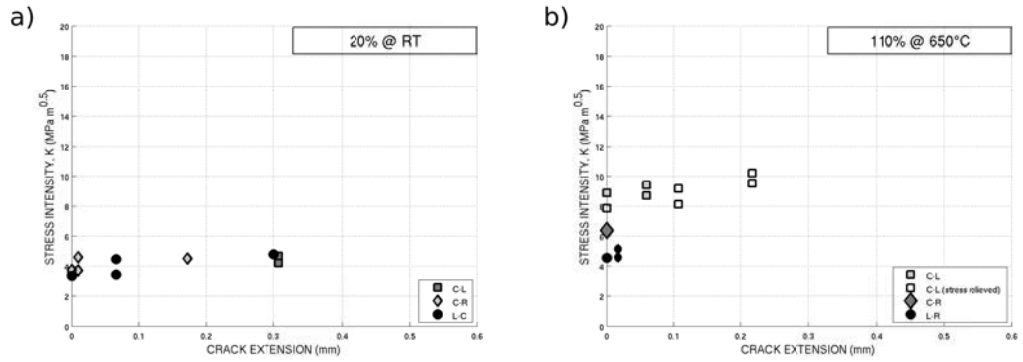

Figure D.8 R-curves of the fracture resistance of tungsten deformed 20% at room temperature (a) and 110% at 650°C (b) in compression, tested at room temperature. For all crack propagation directions the R-curves of the 20% deformed material start at about 4 MPa $m^{0.5}$. Crack propagation of the 110% deformed tungsten samples starts at higher values followed by a more pronounced R-curve behavior.

the same for the samples deformed at elevated temperatures (figure D.4-b). The increase of fracture resistance with crack extension is caused mainly by crack bridges which can be found along the intergranular propagated crack (figure D.5). The fracture surface of a sample with this crack propagation direction can be seen in figure D.6-a, which shows grain boundary fracture as the dominant fracture type and some cleaved grains.
Figure D.6-b depicts a sample with *R-C* crack propagation direction which also shows grain boundary dominated fracture. The R-curve of fracture resistance of a "*C-R* - sample" with the same crack propagation direction can be seen in figure D.4-b. The stress intensity at first crack extension of 5 MPa $m^{0.5}$ is slightly lower compared to the "*C-L* - sample", however, the fracture resistance increases up to 12 MPa $m^{0.5}$ at 1 mm crack extension. The crack propagates mainly intergranularly and the R-curve is governed by bridges along the crack path, as for the *C-L* crack propagation direction.
"*L-C*" and "*L-R* - samples" start crack propagation at about 8 MPa $m^{0.5}$ (figure D.4) and the fracture surface shows a relatively large amount of cleaved grains, as shown in figure D.7. Figure D.7-a depicts the fracture surface of an "*L-C* - sample" deformed 2% at room temperature while the fracture surface of an "*L-R* - sample" deformed at 350°C can be seen in figure D.7-b. The surfaces are similar and exhibit a relatively high fraction of cleavage. However, except for the higher starting values, the crack resistance increases with crack extension as for the other directions.
Some samples failed catastrophically without any visible, stabile crack extension. One of them, the "*C-L* - sample" of section 3 from the 2% at room temperature deformed material, is additionally shown in figure D.4-a. The fracture toughness of about 8.5 MPa $m^{0.5}$ is higher than the stress intensity at first crack extensions of samples with the same crack propagation direction which exhibited an R-curve behavior.

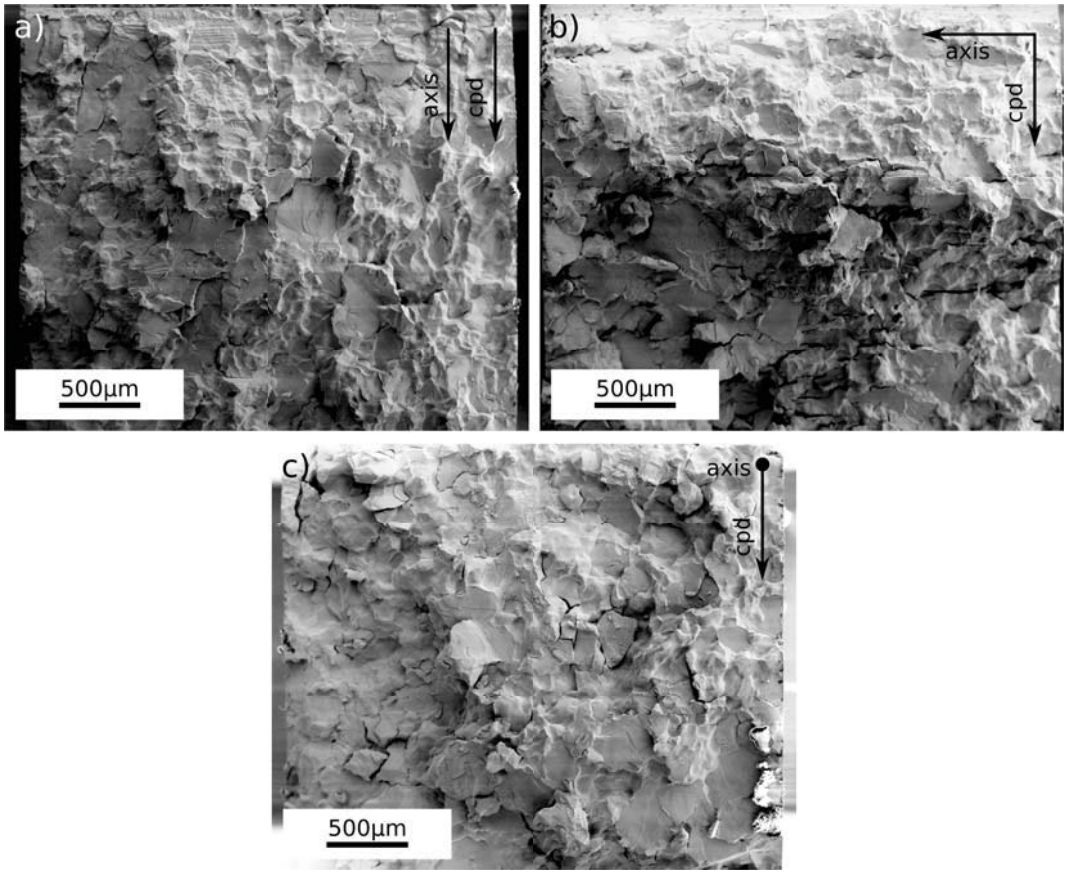

Figure D.9 Fracture surfaces of samples 20% deformed and tested at room temperature. Samples with *C-L* (a) and *R-C* (b) crack propagation direction are dominated by grain boundary fracture with some cleaved grains. The "*L-R* - sample" has a similar fracture surface to the other two samples but a significantly lower amount of transgranular fracture compared to the less deformed samples with the same crack propagation direction.

Compared to the samples of the slightly deformed materials, figure D.8 shows the influence of higher deformations on the crack resistance. Figure D.8-a depicts the results of the samples manufactured out of the room temperature deformed cylinder. All tested specimens exhibit first crack propagation at about $4\,\mathrm{MPa\,m^{0.5}}$. The fracture resistance shows a slight increase with crack extension leading to a very flat R-curve. Samples of all three crack propagation directions are dominated by grain boundary fracture but have a certain fraction of cleaved grains, as shown in figure D.9. The fracture surfaces of the *C-L* (a) and *R-C* (b) crack propagation directions can be compared to the less deformed materials whereas the "*L-R* - sample" (c) shows a higher amount of fracture along the grain boundaries.
Samples from the material deformed to 110% at 650°C show less pronounced R-

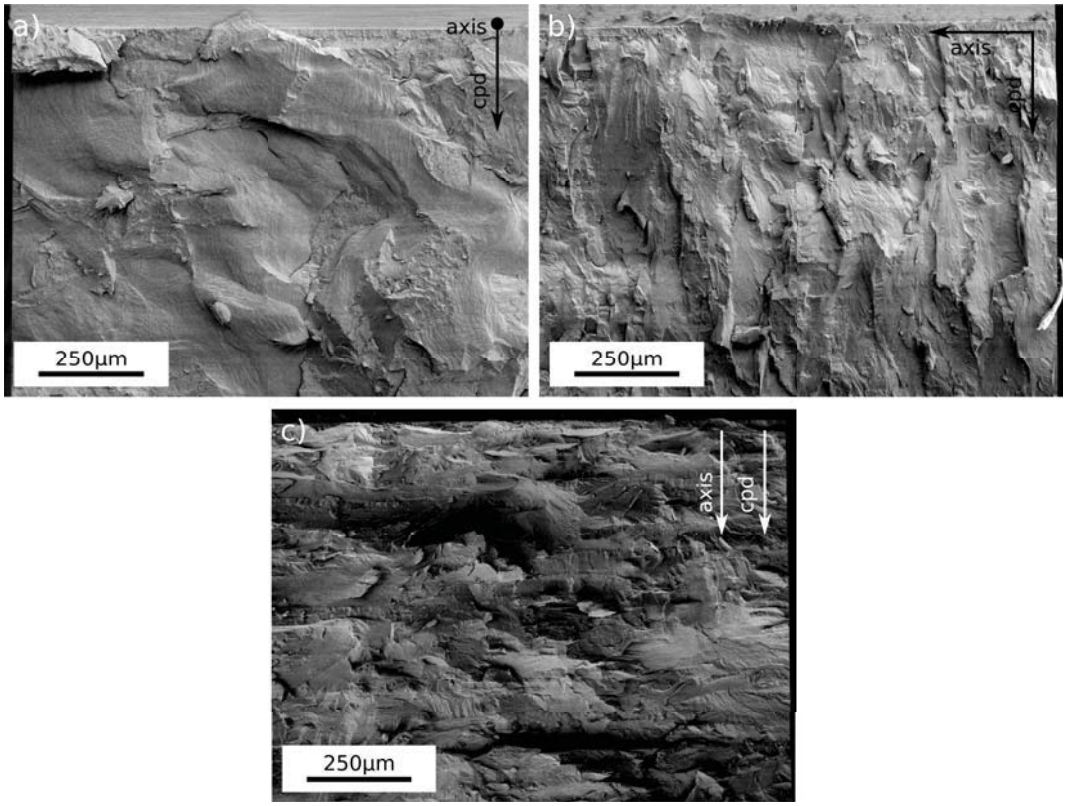

Figure D.10 SEM fractographs of tungsten deformed to 110% at 650°C. The fracture surface of a sample with *L*-*R* crack plane orientation is shown in (a), whereas (b) depicts the fracture surface of a sample with *C*-*R* crack propagation direction. The "*C*-*L* - sample" is shown in (c).

curve behavior compared to all other materials (figure D.8-b). In this case the "*L*-*R* - samples" have the lowest starting values, somewhat above $4\,\mathrm{MPa\,m^{0.5}}$. The crack propagates less than $50\,\mu$m before catastrophic failure occurs. Grain boundary fracture is dominant in this propagation direction (figure D.10-a). The samples with *C*-*R* crack plane orientation did not show R-curve behavior. Unstable crack growth occurred predominantly by cleavage (figure D.10-b) at a fracture toughness of about $6\,\mathrm{MPa\,m^{0.5}}$. The "*C*-*L* - samples" exhibit the highest stress intensities at initial crack extensions, about $9\,\mathrm{MPa\,m^{0.5}}$, followed by a slight increase of the fracture resistance. Failure occurred mainly by cleavage at about $9.5\,\mathrm{MPa\,m^{0.5}}$, as shown in figure D.10-c. Compared to that, the stress relieved sample started crack propagation at a lower stress intensity but showed a more pronounced increase in the fracture resistance, up to $10\,\mathrm{MPa\,m^{0.5}}$, until reaching about $200\,\mu$m crack extension.

Initial crack extensions of the samples from the recrystallized material start at lower stress intensities compared to the deformed tungsten materials, as shown in

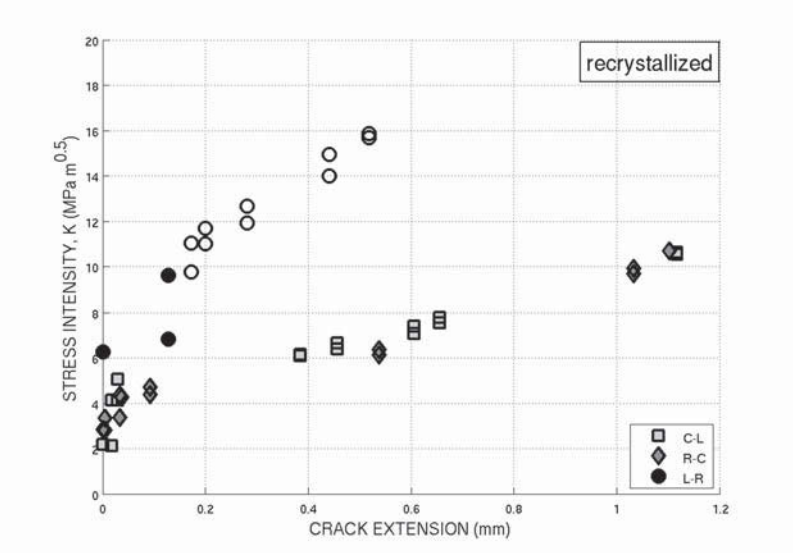

Figure D.11 R-curves of recrystallized tungsten in different crack propagation directions with respect to the axis of the rod.

figure D.11. The "*C-L* - samples" and the "*R-C* - samples" have very low stress intensities at initial crack extensions between 2 and 3 MPa $m^{0.5}$. The steep increase of the fracture resistance flattens after about 100 μm crack extension. However, the fracture resistance increases over a much longer distance compared to all other sample types. The samples with *L-R* crack plane orientation had a resistance curve starting at about 6 MPa $m^{0.5}$ followed by an increase up to 10 MPa $m^{0.5}$ before the crack kinked 90° to the original crack propagation direction. Further data points were calculated with the projected crack length and are shown as non-filled symbols. The fracture surfaces of all three crack propagation directions are shown in figure D.12. The "*C-L*", (a), and the "*C-R*" direction, (b), show almost pure intergranular fracture while the "*L-R*" direction (c) has a slightly increased fraction of cleavage.

DC(T) samples with *C-R* crack plane orientation tested at elevated temperatures

DC(T) samples of rolled and recrystallized tungsten were tested up to 700°C. R-curve behavior could not be observed for samples with rolled microstructure in the *C-R* crack propagation direction. The fracture toughness increases with temperature, as expected. Starting from about 10 MPa $m^{0.5}$ at room temperature, the materials fracture toughness is about doubled at 700°C (figure D.13-a). All values were calculated by use of linear elastic fracture mechanics (LEFM), this is only applicable if the size of the plastic zone ahead of the crack tip is small compared to the sample geometry. This is true at room temperature but may be inaccurate at elevated temperatures. The yield strength, σ_y, of stress relieved tungsten is about

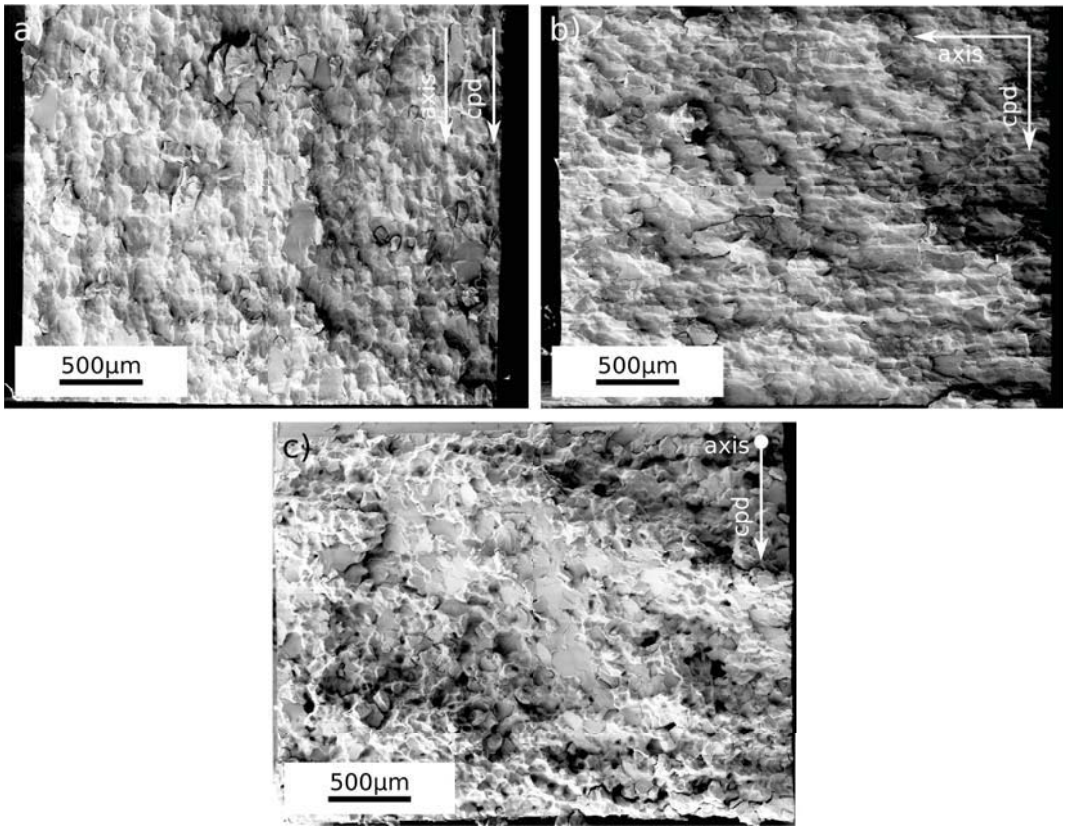

Figure D.12 SEM fractographs of the recrystallized tungsten material. The sample with *C*-*L* crack plane orientation is shown in (a), the "*C*-*R* - sample" in (b) and the "*L*-*R* - sample" in (c).

700 MPa at 700°C, as shown in figure D.13-b [12]. The size of the plastic zone, r_{pl}, is calculated as a first approximation with

$$r_{\mathrm{pl}} = \frac{1}{6\pi}\left(\frac{K_{\mathrm{I}}}{\sigma_{\mathrm{y}}}\right)^2 \tag{D.1}$$

assuming plane strain conditions [13]. Using a K_{I} of 20 MPa m$^{0.5}$ gives a plastic zone size r_{pl} of about 40 μm, therefore making the LEFM approximation applicable. Figure D.14 shows the fracture surfaces of the investigated samples tested at room temperature (a), 300°C (b), 500°C (c) and 700°C (d). All specimens exhibit grain boundary dominated fracture while plastically deformed crack bridges lead to a slightly rougher fracture surface at elevated temperatures.

Compared to rolled tungsten, tungsten with a recrystallized microstructure exhibits R-curve behavior, as shown in figure D.15. Crack propagation starts at room temperature at about 4 MPa m$^{0.5}$, this is similar to the recrystallized "*R*-*C* - sample"

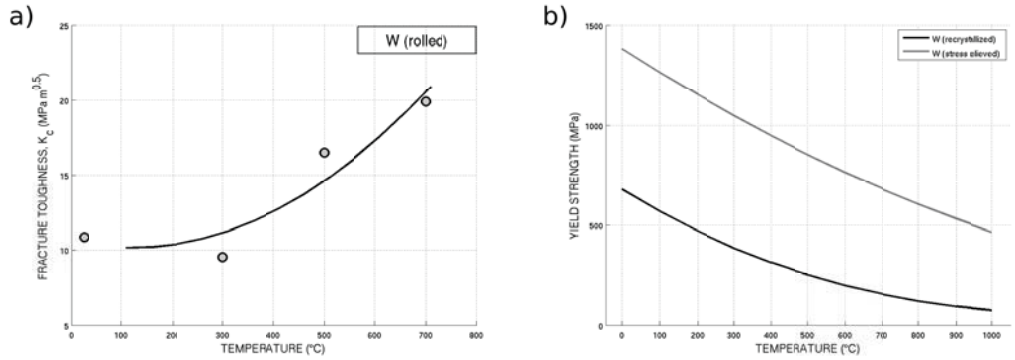

Figure D.13 The fracture toughness of rolled tungsten with C-R crack plane orientation increases with increasing temperature (a). (b) shows the yield strength σ_y as $f(T)$ of recrystallized and stress relieved tungsten in the range of room temperature to 1000°C [12].

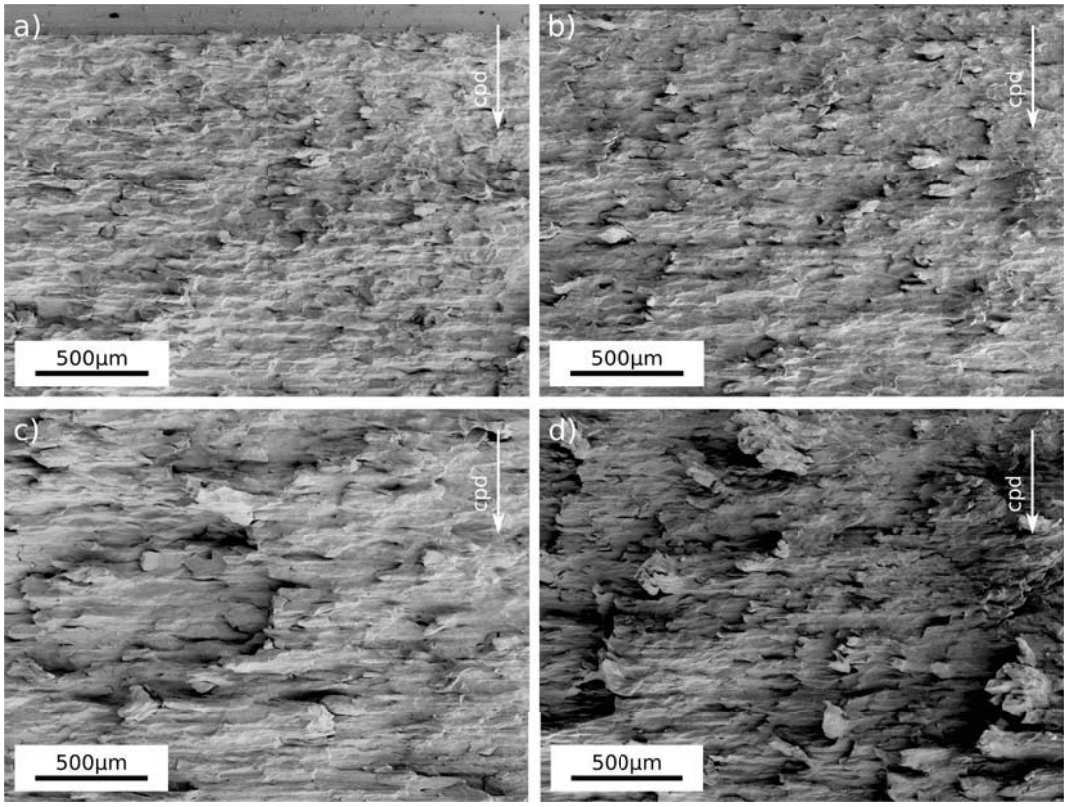

Figure D.14 DC(T) samples of rolled tungsten tested at room temperature (a), 300°C (b), 500°C (c) and 700°C (d). The samples were manufactured with C-R crack propagation direction and show a slightly rougher fracture surface with increasing testing temperature.

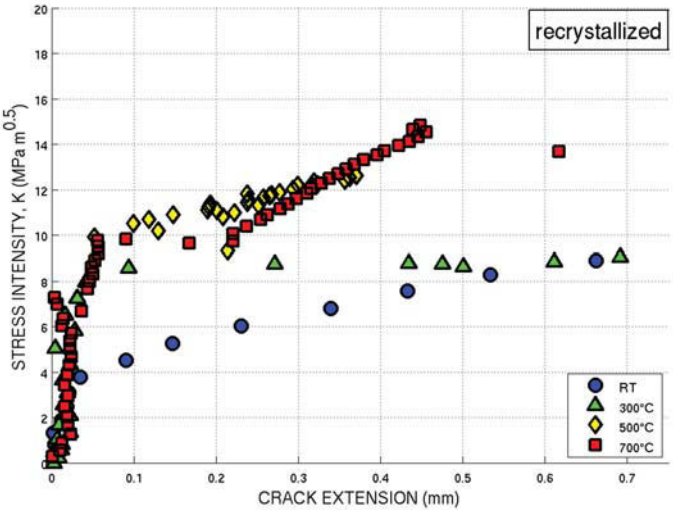

Figure D.15 Fracture resistance of recrystallized tungsten as a function of the crack extension tested in the temperature range room temperature to 700°C. Crack extensions are determined by the DC potential drop method.

in figure D.11 which has the same crack propagation direction. However, the fracture resistance increases to about 9 MPa $m^{0.5}$ at a crack extension of 700 μm. Crack propagation of the sample tested at 300°C starts somewhat higher at about 6 MPa $m^{0.5}$ and increases to 9 MPa $m^{0.5}$ within 100 μm. After that the R-curve reaches a plateau and no further increase in the fracture resistance was observed. The specimen tested at 500°C starts even higher at 10 MPa $m^{0.5}$. The fracture resistance increases relatively steep to 13 MPa $m^{0.5}$ before crack extension to 700 μm occurs. After that, the R-curve rises just slightly from 7 MPa $m^{0.5}$ with increasing crack length. First crack extensions were observed at about 8 MPa $m^{0.5}$ for the sample tested at 700°C, before at 10 MPa $m^{0.5}$ the crack extended about 200 μm. After that the fracture resistance increased rapidly to about 15 MPa $m^{0.5}$ at almost 0.5 mm crack extension. This was followed by a significant crack extension of about 1 mm to 6 MPa $m^{0.5}$.
The fracture surfaces of the investigated samples are shown in figure D.16. Intergranular fracture is dominant for all samples, however, lower testing temperatures - room temperature (a) and 300°C (b) - show more cleavage, while elevated temperatures - 500°C and 700° - cause a larger deviation of the global crack path from an even crack front.
Tests were stopped after the first long crack extension occurred, indicated by a big load drop. This was done to measure the crack length on the surface after the test and also to investigate the crack path by means of EBSD. Compared to the crack lengths calculated from the monitored potential, the measured crack lengths were always larger. This discrepancy arises from remaining crack bridges which can be

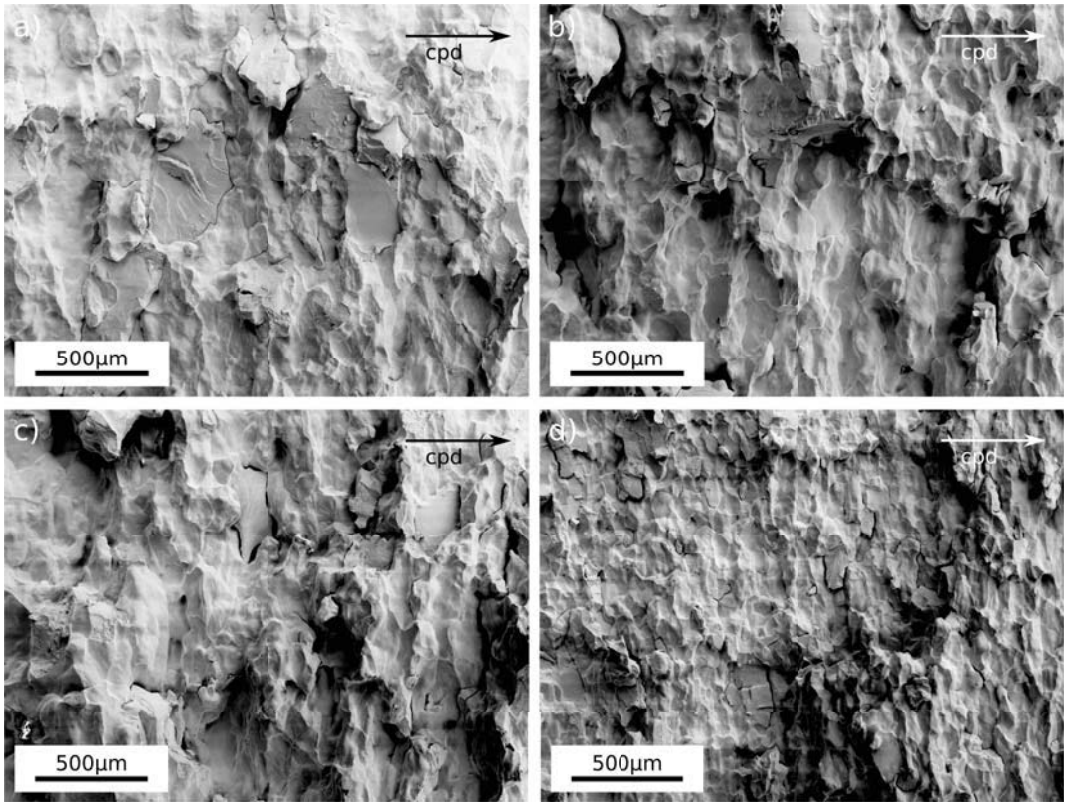

Figure D.16 Recrystallized tungsten DC(T) samples with C-R crack propagation direction, tested at room temperature (a), 300°C (b), 500°C (c) and 700°C (d). The fracture surfaces show more cleaved grains at room temperature while elevated temperatures seem to cause more deviations from an even crack front.

found along the whole crack path [14] and which are present along the propagated crack across the whole sample. Such crack bridges have a significant effect on the measured potential and furthermore on the crack length. Due to the electrical contact of both crack flanks, the crack length is normally underestimated, this effect increases with the number of bridges [15].

D.4 Discussion

Most of the tested C(T) samples exhibit R-curve behavior, this is most clear for the recrystallized material (figure D.11). Pre-deformation of tungsten increases the R-curves with respect to their starting values (figure D.4 and figure D.8). Higher starting values result in increased stress intensities which cause longer crack extensions and furthermore seem to cause less pronounced R-curve behavior before catastrophic failure (figure D.8-b). However, this may be an effect of the sample

size. The investigated samples (W = 6 mm) are relatively small, the sample has usually a ligament of 3 mm. The increase in K with crack extension is relatively high, therefore it is difficult to obtain stabile crack extension. The R-curve behavior of a material can only be measured if the increase of the crack driving force due to crack extension in the used system - sample plus testing machine - is smaller than the increase of the fracture resistance of the material. Hence the resistance curve of the microstructures with a low initial fracture resistance and a pronounced increase of the resistance can easily be measured, even in this small samples. The microstructures which exhibit a relatively large resistance for the first crack propagation and only a small increase in fracture resistance are more difficult or impossible to measure with such small samples.

Influence of deformation on the fracture resistance

Samples of the less deformed materials show R-curve behavior similar to the recrystallized material. The material with the lowest degree of deformation is tungsten deformed to 2% at room temperature (figure D.3-a). Compared to tungsten deformed at 350°C to 2% (figure D.3-b), misorientations within the grains are barely visible. This might be a result of different relative amounts of edge and screw dislocations. Many more edge dislocations can be produced at room temperature due to the low mobility of screw dislocations, at elevated temperatures the proportions are probably more equal. However, screw dislocations normally contribute a higher degree of misorientation to the global deformation, which could be a reason for the observed differences in figure D.3-a and D.3-b. Nevertheless, samples with the same crack propagation directions of both 2% deformed materials show similar fracture resistances at the initial crack propagation (figure D.4). They are slightly increased compared to recrystallized tungsten (figure D.11), which indicates an effect of the deformation of both microstructures.

Although the samples deformed 20% at room temperature show longer crack extensions (figure D.8-a) than the samples deformed 2% at 350°C (figure D.4-b), the observed R-curves are very flat and not valid. The high deformation at low temperature causes a decohesion of a significant proportion of the grain boundaries, as shown in figure D.3-c. Therefore, on one hand fatigue pre-cracking sometimes results in an undefined network of cracks ahead of the notch (figure D.17), and on the other hand the crack propagates mainly along the already separated grain boundaries. Furthermore, the fracture resistance is governed by intergranular fracture of these parts of the grain boundaries which remain combined after deformation. This makes those samples deformed 20% at room temperature not comparable to the other materials. Figure D.8-b shows R-curves of 110% deformed tungsten. Despite the higher degree of deformation, a degradation of the grain boundaries was not observed for deformation at 650°C. The higher temperature allows a significant amount of plasticity which can be seen in the large misorientations in figure D.3-d. Furthermore, the higher deformation results in increased stress intensities at first crack extensions

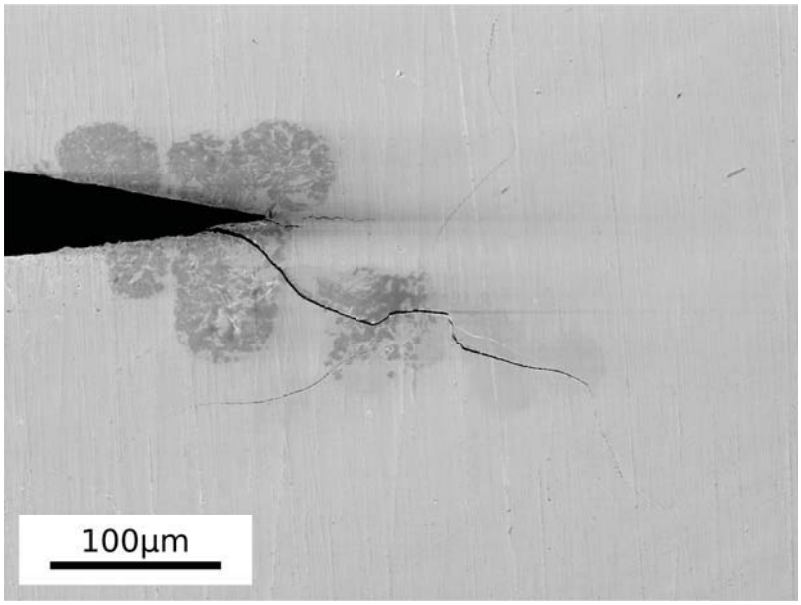

Figure D.17 Network of pre-cracks ahead of a notch polished by a razor blade. The 20% at room temperature deformed tungsten material was pre-cracked by cyclic compression.

compared to all other tested samples. However, this causes longer crack extensions which can hardly be measured with the C(T) samples used. This leads to a less pronounced R-curve of the fracture resistance for the tungsten deformed to 110%. The stress relieving of the sample with C-L crack plane orientation leads to a decreased fracture resistance at the first crack propagation. Hence more steps of shorter crack extensions at the beginning of the R-curve were observed before catastrophic failure occurred. However, beside this effect on the first part of the fracture resistance curve, larger samples should be tested to investigate an influence of such heat treatment on further crack extensions.

Deformation applied to tungsten seems to have a positive effect on the fracture resistance of the material. Compared to a recrystallized microstructure, deformation causes an increasing dislocation density leading to a substructure within the grains which results in higher stress intensities at first crack propagations starting from the pre-crack.

Influence of grain shape

Aside from the influence of deformation on the fracture resistance of tungsten materials, figures D.4, D.8 and D.11 also show a strong dependency of the R-curve on the crack propagation direction of each sample. The microstructure, and furthermore the shape of the grains plus a possible subgrain structure, play a significant role on

the propagating crack. It is important to know whether the pre-crack is produced parallel or perpendicular to the axis of the cylinder, and therefore to the mainly elongated grains. This has a large influence for K at the first crack extension and also if crack propagation occurs mainly intergranular or rather by cleavage of grains. Fracture toughness investigations on rods of technically pure tungsten as well as on tungsten alloys additionally show this strong dependency on the relative position of the samples with respect to elongated grains [16–18].
The fracture resistances of the recrystallized (figure D.11) and the 2% deformed materials (figure D.4) are similar with respect to their first crack extension, their increase in K and also relative to each other, as long as samples of the same crack propagation direction are compared. Samples of the 110% deformed tungsten do not follow this trend. The heavy deformation caused disc-shape like grains with their longer axes perpendicular to the axis of the former cylinder. This can be seen for example in figure D.12. The fracture surface of the "*L*-*R* - sample" (figure D.12-a), where crack propagation occurred perpendicular to the axis of the former cylinder, shows mainly intergranular fracture. Compared to that, the "*L*-*R* - sample" of the 2% deformed tungsten material is dominated by transgranular fracture, as shown in figure D.7. Therefore, samples of the 110% deformed material with the same denotation as the other tungsten materials cannot be used for comparison and have to be exchanged by samples with other crack plane orientations, like for example *C*-*L* instead of *L*-*R*, to follow the trend of the lower deformed materials.
Except for samples from the 110% deformed tungsten, all other specimens with the front of the fatigue pre-crack parallel to the longer axis of elongated grains exhibit relatively low stress intensities at first crack extensions. This can be seen for example in figure D.4-b for the "*C*-*R* - sample" of the 2% at 350°C deformed material, where first crack extension occurs at about $5\,\mathrm{MPa\,m^{0.5}}$. Due to the slightly elongated grains (figure D.6-b) a relatively high density of grain boundaries, which are parallel to the crack propagation direction, can be found ahead of the crack tip. As the fracture resistance along the grain boundary is somewhat smaller than the resistance to cleave grains, intergranular crack propagation is the preferred fracture mode and occurs at relatively low stress intensities in this direction. A similar behavior can be found for the 110% deformed material, just perpendicular to the axis of the former cylinder due to the disc-shaped grains. As a result of the large fraction of grain boundaries in this direction intergranular fracture is preferred, this can be seen in figure D.10-a. This causes the lowest K values of all three crack propagation directions, which is clear in figure D.8.
Samples with the pre-crack front perpendicular to the axis of the cylinder and therefore perpendicular to the longer axis of the elongated grains, like for example the "*L*-*C*" or "*L*-*R* - samples"of the 2% deformed materials (figure D.7), exhibit the highest values of all three crack propagation directions. Due to the limited number of grain boundaries in this direction crack propagation normally starts by cleavage. Even intergranularly initiated cracks often switch to transgranular fracture as the resistance to cleave grains is somewhat smaller than the resistance to propagate along the grain boundaries in this direction. This causes the higher stress intensities

compared to all other directions.
The third direction, where the crack propagates along the axis of the cylinder, is similar to the direction with the crack propagation front parallel to the axis, at least for the recrystallized and the 2% deformed materials. The high number of grain boundaries favors intergranular crack propagation which can be seen for example in figure D.6-a. This results in relatively low stress intensities as shown in figure D.4-b, where the "*C-L* - sample" has a stress intensity of about $6\,\mathrm{MPa\,m^{0.5}}$ at first crack extension. Although intergranular fracture is the preferred fracture mode, cleaved grains can often be found as well as crack bridges.

Influence of temperature on the fracture resistance

Elevated temperatures normally have a positive effect on the fracture resistance of bcc materials. The experiments with recrystallized and rolled tungsten were performed in the range of room temperature to 700°C. The rolled material exhibts a room temperature fracture toughness of about $10\,\mathrm{MPa\,m^{0.5}}$ in the *C-R* crack propagation direction (figure D.13-a). However, R-curve behavior of the fracture resistance could not be observed. The examined fracture toughness exceeds all other measurements in this direction, which is probably a result of the much higher deformed grains due to the rolling process. Due to the heavily elongated grains (figure D.14), crack deviation occurs much more often as a result of the large number of grain boundaries. This increases the fracture resistance significantly and prevents the measurement of the R-curve with the used setup. Tests at elevated temperatures show the expected increase in the fracture toughness (figure D.13-a). The improved plasticity causes deformation of the grains which increases with temperature (figure D.14) and leads to a rougher fracture surface.

In the case of recrystallized tungsten, the DC(T) sample tested at room temperature starts crack propagation in the *C-R* direction between $2 - 4\,\mathrm{MPa\,m^{0.5}}$ (figure D.15), which is about the same as for the C(T) sample in the *R-C* crack propagation direction (figure D.11). The fracture resistance increases with crack extension and the fracture surface shows a large number of cleaved grains (figure D.16-a) compared to the rolled material (figure D.14-a) or compared to the fracture surfaces of samples tested at elevated temperatures (figure D.16-b/-d). This is a result of the relatively straight crack propagation through the material.
However, the sample tested at 300°C starts crack propagation at about $6\,\mathrm{MPa\,m^{0.5}}$ and reaches a plateau at $9\,\mathrm{MPa\,m^{0.5}}$ after short crack extension, as shown in figure D.11. Due to the slightly increased temperature, which is at the lower end of the brittle-to-ductile transition, the crack can easily propagate along the grain boundaries - the path of the lowest fracture resistance - through the sample. The constant fracture resistance might be a result of deviations from the global crack propagation direction which is possible because of the elevated temperature.
The testing temperatures of 500°C and 700°C are in the more ductile regime of the

material. Both show a relatively steep increase in the fracture resistance with crack extension. Aside from major deviations along the direct crack path (figure D.16), the used testing temperatures already cause significant plasticity along the propagated crack [16]. The crack deviation significantly contributes to the increasing fracture resistance with crack extension, however, the increasing plasticity with temperature rises the load for crack propagation.
It needs to be noted that the calculated crack extensions are lower limits due to crack bridges which have a significant influence on the DC potential drop method. Furthermore, the validity of LEFM of recrystallized tungsten is probably not given for higher fracture resistances at 700°C testing temperature.

D.5 Concluding remarks

Compact tension specimens and disc compact tension specimens have been investigated with respect to their fracture resistance. Samples with different crack plane orientations, with respect to the axis of the rod, were manufactured and tests were performed in the temperature range from room temperature to 700°C.

1. Most samples show an increasing fracture resistance with crack extension, i.e. they exhibit R-curve behavior of the fracture resistance.

2. Elongated grains exhibit a significant influence on the observed R-curves depending on the crack propagation direction with respect to the grains.

3. Deformed tungsten shows an improved fracture resistance compared to recrystallized microstructures.

4. Temperature has the expected positive effect on the fracture resistance and leads to a more pronounced R-curve behavior in the ductile to brittle transition regime.

An increasing dislocation density due to plastic deformation of tungsten either by compression or rolling at elevated temperatures obviously has a positive effect on the materials fracture resistance. However, it is evident from the experiments that most improvements are possible by the microstructure, for example by elongated grains. Such grain structure significantly increases the fracture resistance at least in one crack propagation direction. Considering the brittle nature of the material, the only chance to enhance the fracture resistance in a second direction might be the deformation to plate-like shaped grains. However, microstructures such as this pose a serious challenge for production.

Bibliography to paper D

[1] P. Beardmore, D. Hull, J. Less Common Met. 9 (1965) p. 168.

[2] D. Hull, P. Beardmore, A.P. Valintine, Phil. Mag. 12 (1965) p. 1021.

[3] P.L. Raffo, J. Less Common Met. 17 (1969) p. 133.

[4] J. Liu, J.C. Bilello, Phil. Mag. 35 (1977) p. 1453.

[5] D. Rupp and S.M. Weygand, J. Nucl. Mater. 386–388 (2009) p. 591.

[6] E. Tarleton and S.G. Roberts, Phil. Mag. 89 (2009) p. 2759.

[7] E. Pink and L. Bartha, *The Metallurgy of doped/non-sag Tungsten*, Elsevier Applied Science, London and New York, 1989.

[8] American Society for Testing and Materials, *E 399 - 90: Standard Test Method for Plane-Strain Fracture Toughness of Metallic Materials - Annual Book of ASTM Standards*, Vol 03.01., 1997, pp. 413–443.

[9] S. Suresh, Engng. Fract. Mech. 21 (1985) p. 453.

[10] R. Pippan, Fatigue Fract. Engng. Mater Struct. 9 (1987) p. 319.

[11] G.H. Aronson and R.O. Ritchie, J. Test. Eval. 7 (1979) p. 208.

[12] University of California Los Angeles, *ITER Material Properties Handbook*, http://fusionnet.seas.ucla.edu/fusionnetwork/iter_properties.php?mid=ST-M-RF-%23201&tid=0202P-1100 (accessed September 17, 2010).

[13] T.L. Anderson, *Fracture Mechanics: Fundamentals and Applications*, 2nd ed., 1995.

[14] B. Gludovatz, S. Wurster, A. Hoffmann, R. Pippan, *submitted to Met. Trans. A* (2010).

[15] F.O. Riemelmoser, R. Pippan, H. Weinhandl and O. Kolednik, J. Test. Eval. 27 (1999) p. 42.

[16] B. Gludovatz, S. Wurster, A. Hoffmann and R. Pippan, Int. J. Refract. Met. Hard Mater. 28 (2010) p. 674.

[17] D. Rupp, R. Mönig, P. Gruber and S.M. Weygand, Int. J. Refract. Met. Hard Mater. 28 (2010) p. 669.

[18] D. Rupp and S. Weygand, Phil. Mag. 90 (2010) p. 4055.